



## **Packaging of Microfluidicsystem: A microfluidic motherboard integrating fluidic and optical interconnections**

**Perozziello, Gerardo; Geschke, Oliver**

*Publication date:*  
2006

*Document Version*  
Publisher's PDF, also known as Version of record

[Link back to DTU Orbit](#)

*Citation (APA):*  
Perozziello, G., & Geschke, O. (2006). Packaging of Microfluidicsystem: A microfluidic motherboard integrating fluidic and optical interconnections.

## **DTU Library** Technical Information Center of Denmark

---

### **General rights**

Copyright and moral rights for the publications made accessible in the public portal are retained by the authors and/or other copyright owners and it is a condition of accessing publications that users recognise and abide by the legal requirements associated with these rights.

- Users may download and print one copy of any publication from the public portal for the purpose of private study or research.
- You may not further distribute the material or use it for any profit-making activity or commercial gain
- You may freely distribute the URL identifying the publication in the public portal

If you believe that this document breaches copyright please contact us providing details, and we will remove access to the work immediately and investigate your claim.

Packaging of Microfluidic systems:  
A microfluidic Motherboard Integrating Fluidic and  
Optical Interconnections

Gerardo Perozziello

Ph.D. thesis

MIC – Department of Micro and Nanotechnology  
Technical University of Denmark

January 2006

Supervisor:  
Associate professor Oliver Geschke



## **Abstract**

The field related to the development of microfluidic systems performing bio-chemical analysis is continuously growing.

Careful packaging of microsystems is vital to ensure efficient work of the device, especially at the interface between the system and the environment, where fluidic electrical and optical interconnections must be provided in a reliable manner, ease of use and low cost.

The objective of this project was to investigate, design and modeling new packaging solutions to interface the microfluidic systems with the outer world and finally to design, fabricate and test a fluidic motherboard for microfluidic devices. This project can be divided in three parts:

- Specifying the definition of packaging: what characterizes it, the weak points and difficulties and all the parameters involved and important to fulfill a successful protection and interface of a system.
- Developing models regarding the critical parameters in packaging for ease the design and dimensioning of fluidic interconnection and optical external couplers and experiments have been performed to validate those.
- Design, fabricate and testing a new polymer-based microfluidic motherboard that integrates polymer-based waveguides, external optical connector plugs and fluidic networks providing an interface between microfluidic systems and the outer world.

The motherboard, on one hand, facilitates interconnections of several microfluidic systems for multiplexed and simultaneous analysis. On the other hand, it offers a modular network for microfluidic chips, allowing complex microfluidic processes, where each microchip has a particular function. The motherboard shows a robust design allowing an easy interconnection of several microsystems alleviating critical issues as optic alignment and fluidic interfacing.

A novel procedure for integrating polymer waveguides into the motherboard has been developed.

It consists of spinning a thin layer of doped polymer (doped PMMA  $n=1.499$ ) onto a polymer substrate with a lower refractive index (native PMMA  $n=1.485$ ).

The refractive index of doped PMMA was increased to by ‘doping’ the PMMA with styrene-acrylonitrile copolymer. This gave waveguiding properties to one side of the polymer substrate which is then machined by using micromilling technology, in order to fabricate the motherboard.

The motherboard includes:

- Fluidic network to drive liquids from outside into the chips;
- Pockets to house polymer microfluidicsystems;
- Waveguides to guide light inside the chips;
- PDMS sockets to establish high density microfluidic interconnections between the motherboard and external tubes.
- PDMS optical connector plugs for interconnecting the polymer waveguides to the light source and to the detection system, which integrates spherical lenses aligned to several optical fibers to the other side have been fabricated. The optical connector plugs allow focusing of the light from an optical fiber to a waveguide and vice versa.

Testing polymer-based microfluidic systems have been developed to demonstrate the performance of the motherboard. The chips contain:

- Fluidic network;
- waveguides;
- integrated fluidic interconnections consisting of custom made o-rings allowing alignment to the connection pins of the motherboard.

The single chips were attached to the motherboard by just pressing them onto the alignment pins. A sealed fluidic connection between chip and motherboard is ensured by the deliberate mismatch in diameter between the o-rings of the chip and the pins of the motherboard.

Experiments have shown constant propagation losses around 1 dB/cm between 400 nm and 850 nm for the waveguides. Regarding the optical connector plugs, the measurements of the propagation of the light show a maximum light intensity for the plugs, which is ~50% higher than for the cleaved fiber itself and more focused with respect to lateral distribution. Induced misalignments showed less measured insertion losses for the optical plugs than a coupled cleaved fiber. Finally, the fluidic interconnections were tested reaching 3.5 bars without detection any leakage.

Coupling efficiency was tested on the motherboard with the chip mounted onto it, sending a light signal having a power of 300  $\mu\text{W}$  and a power of 4  $\mu\text{W}$  has been detected in output.

## Resume (in Danish)

Udvikling af mikrofluide systemer til biokemiske analyser er et stadig voksende felt.

Til at mikrosystemet virker effektivt, er nænsom indkapsling vital, især i grænsefladen mellem system og omgivelser, hvor sikre elektriske og optiske sammenkoblinger skal foreligge og som skal være billige og nemme i brug.

Projektets hovedindsatsområde var at undersøge, designe og modellere nye løsninger til indkapsling på grænsefladen imellem mikrofluide systemer og omverdenen, og til sidst designe, fremstille og teste et fluide motherboard for mikrofluide systemer. Dette projekt kan inddrages i tre dele:

- Definitionen af indkapsling: hvad karakteriserer den, de svage punkter og besværligheder og alle de parametre som er involverede og vigtige til at opnå en vellykket beskyttelse og en effektiv grænseflade til et system.
- Udvikling af modeller over de kritiske parametre i indkapsling til at gøre design og dimensionering af væske tilkoblinger og ydre optiske koblinger nemmere, og udføre eksperimenter til at validere dem.
- Designe, fremstille og teste et nyt polymer baseret mikrofluid motherboard, som integrerer polymer baserede bølgeledere, ydre optiske stikkontakter og væske netværk som giver grænsefladen imellem det mikrofluide system og omgivelsen.

Motherboardet indeholder forbindelse for adskillige mikrofluide systemer for mangfoldige og simultane analyser. Ligeledes giver det et modul opbygget netværk for mikrofluide chips, som giver mulighed for komplekse mikrofluide processer, hvor hver mikrochip har en bestemt funktion. Motherboardet har en robust design som tillader en nem tilkobling af adskillige mikrosystemer og letter kritiske parametre som optisk alignment og væske tilkoblinger.

En ny metode til at integrere bølgeledere i motherboardet er blevet udviklet.

Den foregår ved at spinde et tyndt lag af dopet polymer (dopet PMMA  $n=1.499$ ) på et polymersubstrat som har en lavere brydningsindeks (naturlig PMMA  $n=1.485$ ).

Brydningsindekset for dopet PMMA blev forøget ved at ”dope” PMMA med styren-acrylonitril copolymer. Dette gav den ene side af polymersubstratet bølgeleder egenskaber, motherboardet blev siden fremstillet ved hjælp af mikro fræser teknik.

Motherboardet inkluderer:

- Fluide netværk til at drive væske udefra og ind i chippen.
- Lommer som kan huse polymer mikrofluide systemer.
- Bølgeledere til at lede lyset ind i chippene
- PDMS sokkel til at danne en høj viskos mikrofluide forbindelse imellem motherboardet og eksterne slanger.
- PDMS optiske stikkontakter til forbindelse af polymer bølgelederne til lyskilden og detektoren. Dette inkluderer fremstilling af sfæriske linser som er alignet til adskillige optiske fibre. De optiske stikkontakter tillader fokusering af lys fra en optisk fiber over til en bølgeleder og omvendt.

Polymer baserede mikrofluide systemer er udviklet til at demonstrere hvordan motherboardet arbejder. Chippen indeholder

- Fluide netværk:
- Bølgeledere
- Integreerede væske tilkoblinger som består af O-ringe lavet efter mål, som tillader alignment til forbindelses pindene på motherboardet.

De enkelte chips blev fastgjort på motherboardet ved at trykke dem oven på alignment pindene. Forsegling af væskeforbindelsen imellem chip og motherboard er sikret ved den tilsligtede forskel på diameteren af O-ringene på chippen og pindene på motherboardet.

Eksperimenter har påvist tab ved konstant udbredelse på 1dB/cm imellem 400 nm og 850 nm for bølgelederne. Målinger for udbredelsen af lys for de optiske stikkontakter viser maksimal lys intensitet i stikkene, hvilket er ~50% højere end for den kløvede fiber og lyset er bedre fokuseret med hensyn til sidelæns distribution. Induceret misalignment viste mindre indførelses tab for den optiske stikkontakt, end for koblet kløvet fiber. Til sidst blev væske koblingerne testet til at kunne holde 3.5 bar uden lækage.



## **Preface**

This thesis has been written as a partial fulfillment of the requirements for obtaining the Ph.D. degree at the Technical University of Denmark (DTU). This work has been carried out at MIC-Department of Micro and Nanotechnology at DTU in the period from 1<sup>st</sup> January 2002 to 31<sup>st</sup> December 2005.

The Ph.D. project has been supervised by the associate Professor Oliver Geschke, leader of the POEM group at MIC.

The Ph.D program included an external period of research to the Prof. Klavs Jensen group at the department of Chemical Engineering of the Massachusetts Institute of Technology (MIT), Boston, MA, US.

## **Acknowledgments**

During these three years at MIC, I met a lot of persons, wonderful persons I would say. I would like to thank all of them for making me feeling so comfortable with their kindness. I have really felt like in a big family.

I must sincerely thank my supervisor Oliver Geschke for giving me the opportunity to do my Ph.D. at MIC, for guiding me during these years and for his friendship.

I would like to thank also my roommates Frederik Bundgaard and Christian Bergenstof Nielsen for the nice time we have spent together, Thrastardottir Gudrun for helping me to translate the abstract in Danish, and all POEM group for the interesting discussions we had.

I want to thank Anders M. Jørgensen, for training me to the cleanroom facilities with an original interactive project he set-up for me for fabricating my microfluidic chips.

A particular thank goes to Detlef Snakenborg, Jörg P. Kutter, Lars Göesman and Henning Klank who gave to me not only their scientific and technical support, which was great, but especially their friendship, and they supported me a lot.

I have to thank Prof. Klavs Jensen of MIT for giving me the opportunity to visit their department, his group in general for their friendship and scientific and technical support, and in particular Zhiyu “Ben” Zheng who is the Ph.D student I worked with.

Finally, I would like to dedicate this thesis to my parents and my brother that, from Italy and during their visits, supported me during my staying here.

## Index

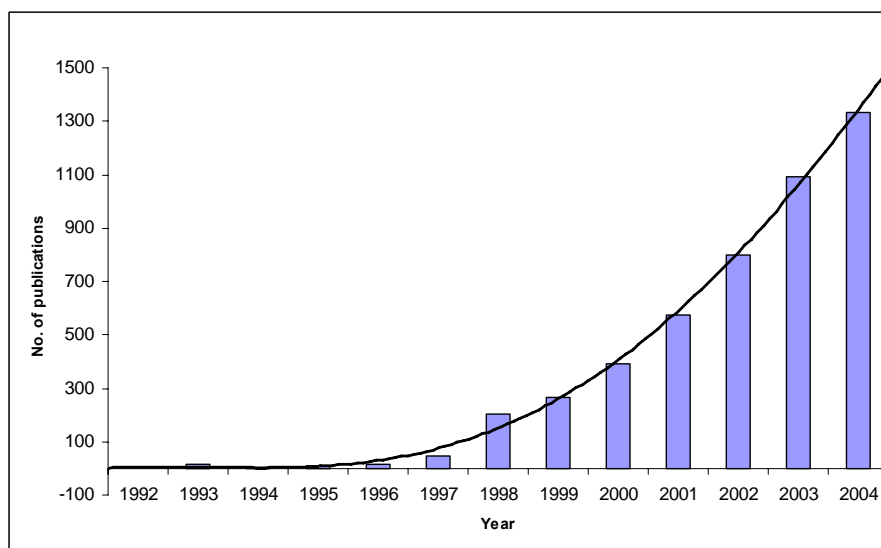
Abstract.....	I
Resume (in Danish).....	IV
Preface.....	VI
Acknowledgments.....	VII
1. Introduction.....	1
1.1. State of the art.....	3
1.2. Goal.....	4
1.3. Outline.....	5
2. Packaging of Microfluidicsystems.....	6
2.1. Levels of packaging.....	7
2.1.1. Substrate Level Packaging.....	8
2.1.2. Multichip Packages.....	9
2.1.3. Unconventional packages.....	10
2.2. Factors influencing the packaging design and reliability.....	12
2.3. Materials.....	14
3. Theory.....	16
3.1. Fluid Dynamics.....	16
3.1.1. Navier-Stokes equations.....	17
3.1.2. Continuity equation.....	18
3.1.3. Analytical solutions.....	18
3.2. Optical waveguiding.....	20
3.2.1. Tapers and light concentration.....	22
3.2.2. Bends.....	24
3.2.3. Power attenuation.....	25
3.3. Lenses.....	26
3.3.1. Diffraction.....	27
3.3.2. Surface roughness.....	28
3.3.3. Aberration due to a spherical lens.....	28
3.3.4. Limits of coupling from a lens to a waveguiding structure.....	29
4. Interconnections.....	30
4.1. Fluidic interconnections.....	31
4.2. Electrical Interconnections.....	35
4.3. Optical interconnections.....	38
5. Modeling.....	44
5.1. Fluidic interconnections.....	44
5.1.1. External interconnections modeling.....	45
5.1.2. Integrated interconnection modeling.....	55
5.2. Optical connector plugs.....	62
6. Microfluidic motherboard.....	64
6.1. Fabrication.....	66
6.2. Main body.....	67

---

6.3.	Waveguides.....	69
6.3.1.	Fabrication .....	69
6.3.2.	Characterization and experiments.....	72
6.4.	Optical plug.....	74
6.4.1.	Fabrication .....	75
6.4.2.	Characterization and experiments.....	77
6.5.	Chip.....	83
6.6.	Fluidic interconnections.....	85
6.6.1.	Plug'n'pump fluidic interconnection .....	85
6.6.2.	PDMS fluidic socket.....	87
6.6.3.	Experiments .....	89
6.7.	Coupling experiments on the motherboard.....	90
6.8.	Discussion.....	91
7.	Conclusion .....	93
A.	List of Fluidic interconnections .....	96
	Permanent fluidic interconnections.....	97
	MCM fluidic interconnections.....	98
	Reversible fluidic interconnections: integrated interconnections .....	99
	Reversible fluidic interconnections: Gaskets.....	100
	Reversible fluidic interconnections: O-rings .....	101
	Reversible fluidic interconnections: Silicone tubes.....	102
B.	List of Optical interconnections .....	103
C.	List of publications.....	105
	Bibliography .....	108

# 1. Introduction

In the last years, the developing of microfluidic systems performing bio-chemical analysis has expanded very fast [1,2,3,4,5].



**Figure 1-1: Trend of number of publications on microfluidics in the last 13 years**

The success of these tiny systems is due to several advantages in comparison to conventional analysis and includes high processing speed, high throughput capabilities,

minimal sample or reagent consumption, integration of different functions in one system, and potentially low manufacturing costs [6, 7, 8,9].

Careful packaging of microsystems is vital to ensure efficient work of the device. Successful packaging design requires a detailed knowledge of packaging, materials, device behavior, reliability and an understanding of the limits of current packaging technology.

Microfluidic interconnections between device to device and for interfacing the environment to the device, electrical connections, designed in a way that isolation is maintained between electronics and fluidics, and optical interconnections are critical and challenging packaging issues to be considered. Finally, housing devices should be provided for the appropriate interface to the other devices or the external environment.

It is also important to consider the costs of the used packaging technologies, since they contribute most to the overall cost of the system

Much attention has been given to integrated circuit (IC) packaging technologies where advanced approaches have been developed. However, for microfluidic systems, the techniques used are still in its infancy and not standardized due to the fact that more issues come into play.

The problems are accentuated especially at the interface between the system and the environment, where fluidic electrical and optical interconnections must be provided in a reliable manner, ease of use and low cost.

A solution to the above mentioned problems would be the use of a motherboard allowing an easy plug'n'play functionality of one or more systems.

The motherboard can provide an interface to the microfluidic systems to perform single or multiplexed, simultaneous or modular bio-chemical analysis. It can integrate fluidic, electrical, and optical interconnections and ensure auto-alignment of those to the system.

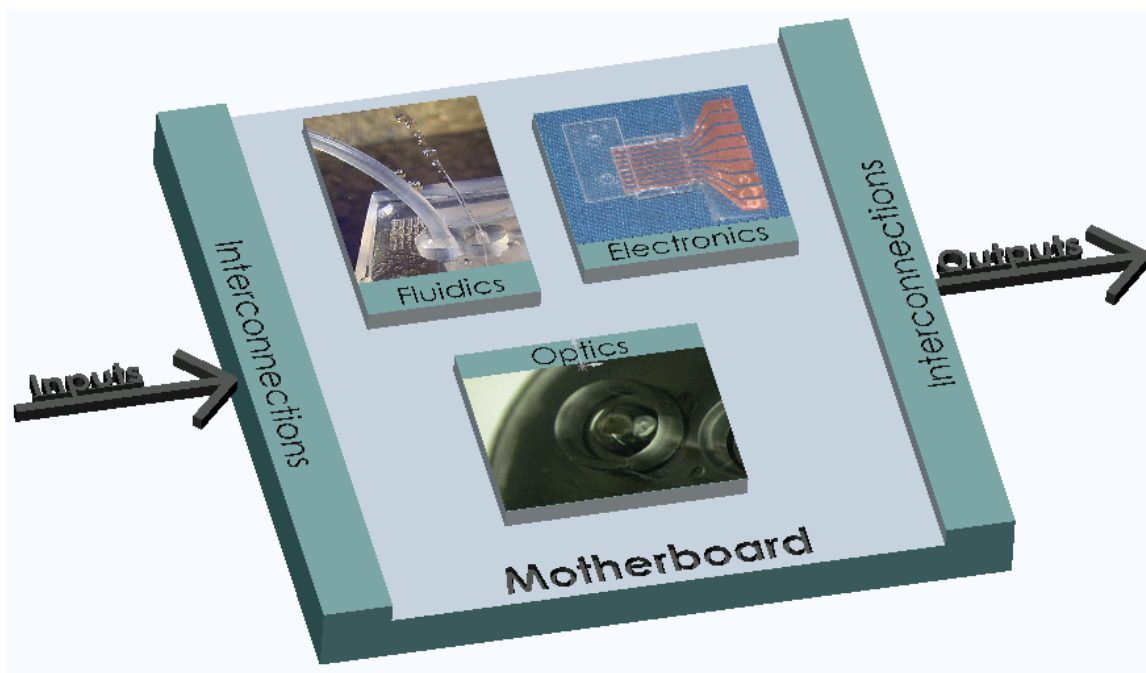


Figure 1-2: Schematic representation of the fluidic motherboard

### 1.1. State of the art

Several groups have proposed different solutions to achieve multiplexed or modular interface between microfluidic systems and to macro-scale tools.

Yang and Maed [10] developed a socket for connecting fluidic devices to the macroworld. This module incorporates both fluidic and electrical interconnections. Fluidic interconnections are provided by pressing silicone tubes on the inlet and outlet of the system. While, electrical interconnections are provided by metal springs arranged in a way to match with the electrical contacts of the device. They also integrate built-in valves in their socket.

A similar solution has been proposed by Galambos et al. [11]. They developed a manifold for fluid distribution. The interface between the device and the outer world is reached in two levels of packaging. The first level interconnects the outerworld and the manifold which does not require a particular precision of assembling and a second level to interface the manifold to the device. For the second level of packaging a PDMS gasket has been used to seal the inlet and outlet of the system.

Gonzalez et al. [12] have developed an interlocking structure to auto-align and assembly modularly fluidic systems to a silicon-glass bread board, having- plug functionality. In particular interlocking fingers ensure mechanical connection while o-rings ensure a sealed fluidic connection.

Similarly, Gray et al. [13] developed an interlocking hole and notched cylinder pins which accomplish mechanical and fluidic interconnect for modular analysis. The cylinder side wall are gasketed for ensuring sealed connections.

Lammerlink et al. [14] proposed a modular concept for fluid handling systems. The concept is based on a planar mixed circuit board with electrical and fluidic interconnections acting as a substrate for sensors and actators modules. The mixed circuit board consists of an epoxy printed circuit board attached to a transparent polycarbonate substrate. They use techniques like glue and soldering to ensure interconnections.

Man et al. [15] developed a flexible plastic fluidic connectors suitable for assembling of non planar microfluidic systems. In this case micro channels are etched into polyimide and poly-p-xylylene layers glued to the modules using epoxy.

Flexible films have been used by Hikita et al. [16] having waveguiding properties. These films are used to interconnect modularly different devices.

Cho et al. [17] have developed a board to board optical interconnection system using optical slots to interconnect optoelectronic devices. Cho integrates also mirrors to drive the light allowing flexibility of slot-layouts avoiding propagation of stray light into the system.

Finally, Debaes et al. [18] propose an MCM-level optical interconnection consisting of a prism ending with spherical lenses to direct the light from one system to another. The structure is aligned by passive self-alignment features.

## **1.2. Goal**

The objective of this project is to design, fabricate and test a fluidic motherboard for microfluidic systems. The motherboard, for the first time, will allow an easy *plug'n'play* functionality of one or more systems integrating, at the same time, fluidic and optical interconnections and ensure autoalignment of those to the system. The motherboard will



be able to connect in an easy way different type of microfluidic systems performing bio-chemical analysis.

The aim is not to create a standard for every kind of microfluidic systems, quite improbable due to the diversity of the same systems and the vast number of applications they have. The thesis concentrates on creating a motherboard that can be adopted in general for all-kind polymer microfluidic systems performing bio-chemical analysis that do not use hazardous chemicals (strong organic solvents).

### **1.3. Outline**

The PhD thesis consists of 7 Chapters. The first 5 chapters discuss packaging and interconnections issues in a more general form and the last chapter is entirely dedicated to the motherboard. In particular Chapter 2 gives an overview about the problems related to packaging, it describes the different levels of packaging related to the microfluidic systems, the factors influencing its design and reliability, briefly the material to be used in relation to some influencing parameters, and finally the tests that can be done. Chapter 3 explains and analyzes the theory behind the experimental work done in this thesis to give some tools for a better understanding of the next sections. The first part describes some basic principles of the fluid dynamics that have been used for dimensioning the fluidic interconnections. Following, waveguide theory is explained and is used for designing the waveguides in the fluidic motherboard. Finally, the theory correlated with the optical plugs will be described, in particular with regards to theoretical analysis of optical lenses. Chapter 4 discusses the types of the interconnections and the problems related with them.

Chapter 5 talks about some models developed for fluidic interconnections and the optical plugs. The models ease the dimensioning. Experimental results show their quality. Chapter 6 introduces the microfluidic motherboard and its design, how it has been fabricated and experimental results are discussed. Finally Chapter 7 concludes the work.

## 2. Packaging of Microfluidicsystems

Packaging, as mentioned before, has the function of bearer of the system information; it contributes largely to its overall cost so a good packaging design is essential for the success of a device. A good packaging allows more integration of the several functions of a system, reducing the utilization of large and expensive set-ups, moreover, having a stable, easy, fast, and inexpensive interface.

The packaging has to protect the devices from the environment but also to protect the environment from the device operation enabling interaction with the same environment in order to measure or influence the desired physical or chemical parameters. The protection of the device develops into additional problems when dealing with integrated sensors.

Sealing techniques and mechanical protection are used to ensure structural integrity and dimensional stability, thermal and optical isolation, chemical and biological isolation and protection. The protection of the device includes electrical insulation and passivation of leads and device structures from penetration of moisture and ions.

It is also necessary to protect the environment from the device materials and device operation, so that no undesirable reaction with or contamination of the environment occurs. This is especially important for devices used in biomedical, pharmaceutical and

food processing applications. Biocompatibility and contamination must be considered as factors in the design. For example chemical and biological transducers directly interact with solids, gases, and liquids of all types. In this sense, they require “ports” or inlets in their packaging to permit this interaction.

Packaging provides also the functions of signal redistribution, linking, mechanical support, power distribution, and thermal management, which will be seen deeply in the later sections.

The signal redistribution provides more space to accommodate the interconnection of a traditional wiring board for the electrical contact, of external source of light to optical sensors, or detection points that are too closely spaced. The contacts are redistributed over a larger, more manageable surface by the packaging.

Rigidity, stress release, and protection from the environment (e.g. against electromagnetic interference) are ensured from the mechanical support. Power distribution and thermal management ensure specific working temperature to the device or allow heat removing.

In addition, a means for handling and testing should be provided by the package. Also the choice of the material is important in packaging because the material used for packaging a microfluidic system is often strictly related with its functioning and should have particular physical (like permeability, mechanical strength, elasticity,...), chemical, electrical and/or optical properties. [19]

### **2.1. Levels of packaging**

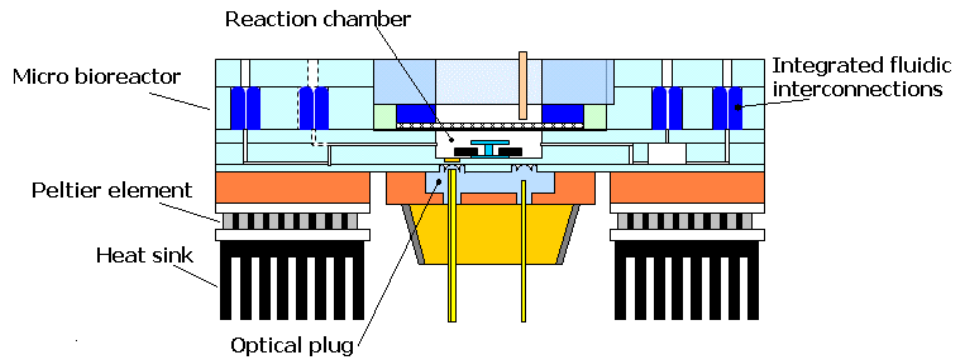
Packaging of microfluidic systems involves additive and subtractive processes, bonding, housing in a protective body and interconnections between different units inside the system or with other devices and the outworld.

Packaging could be divided into three major groups: substrate packaging (first level), multichip packaging (second level) and unconventional packaging (third level).

The first level is related to the packaging of a single chip fabricated with different microtechnologies depending on the materials used and on the fact if it is a prototype or some device to produce massively. The second level is related to the demand of packaging more chips together, while the “unconventional packaging” comprises non

standard packages dictated by the specific application and, in these cases, sometimes no conventional microfabrication methods should be applied. This is related to the interfacing between the system and the outerworld.

The various levels of packaging and their interconnections are illustrated in the following figures.

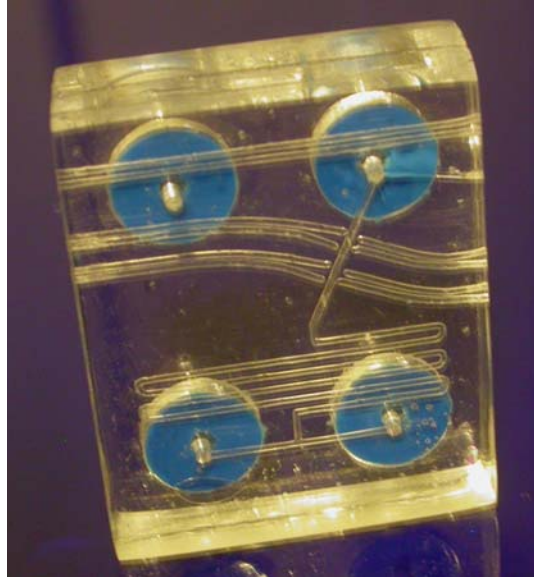


**Figure 2-1: Schematic view of a Microbioreactor cassette [20].**

In the figure, the microbioreactor and the integrated fluidic interconnections belong to the first level of packaging, the heating and cooling system, the optical plugs and the demountable reaction chamber belong to the third level of packaging.

### 2.1.1. Substrate Level Packaging

This level of packaging regards the monolithic horizontal integration, in which all the components are fabricated on different substrates in a single process. This kind of packaging takes full advantage of batch fabrication techniques, reducing the number of manual assembly steps and also results in small system size.



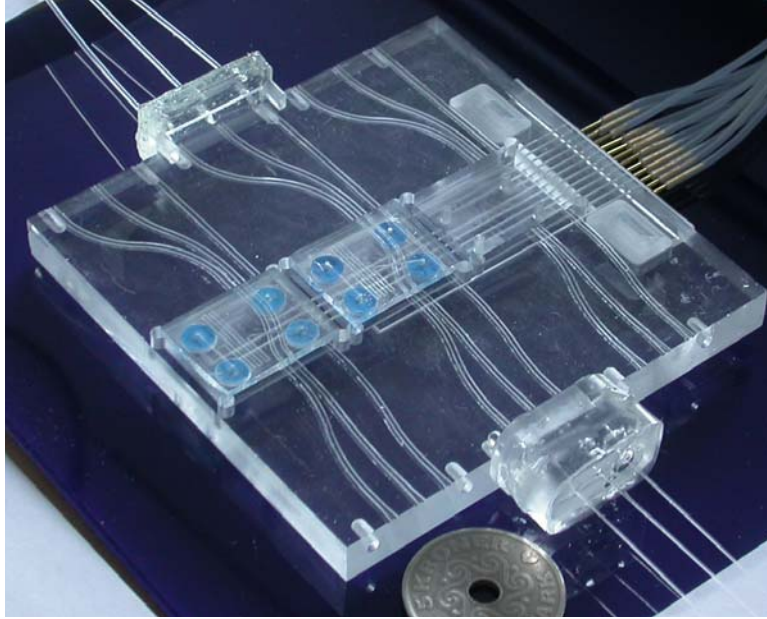
**Figure 2-2: Polymer chip with integrated fluidic interconnections and optical waveguides [21]**

Substrate level of packaging also includes the bonding of the machined layers for sealing purposes. The bonding techniques depend on the used substrate. When dealing with polymer microfluidic systems the techniques usually used for bonding are mainly thermal bonding [22,23], laser bonding [24], chemical bonding [25] using liquid polymers [26,27], glue, adhesives or UV curable material bonding [28,29,30] and wire bonding [31].

Finally, hybrid bonding techniques can be used for fabricating a silicon/polymer microfluidic system, such as those involving ultraviolet patternable polymers, used for inexpensive batch solutions [32].

### **2.1.2. Multichip Packages**

Microchips may be mounted laterally as made in multichip modules (MCMs) or they may be stacked using micromachining. In the latter case, it is possible to pack individual dice, blocks of dice, and substrate where more than one chip is placed, on top of each other and interconnections can be run vertically from plane to plane. This level of packaging also includes the bonding of different machined layers for stacking more units together.



**Figure 2-3: Picture of an horizontal modular concept or motherboard**

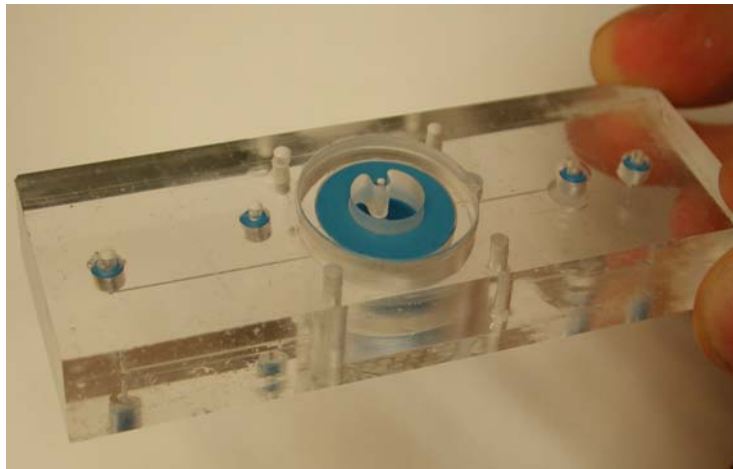
Usually, the MCM approach involves bonding or plugging of unpackaged chips to a substrate which provides the different kinds of connections. In relation with the materials used, channels can be machined within the substrate, electronic traces are patterned on the substrate surface using PC-board manufacturing techniques, even optical traces can be patterned with manufacturing techniques (that will be explained deeper in the next sections) and the fabricated fluidic components are surface mounted. Individual microfabricated components can be stacked [33] or otherwise grouped together to form modular systems with the advantages of flexibility, serviceability, and the ability to test parts individually before assembly.

### **2.1.3. Unconventional packages**

However, micro components like pumps, flow meters, mixers, sensors and reactors typically require device-specific, non-standard fabrication processes and a hybrid package is usually required for some aspect of the system to interface them with the outerworld.

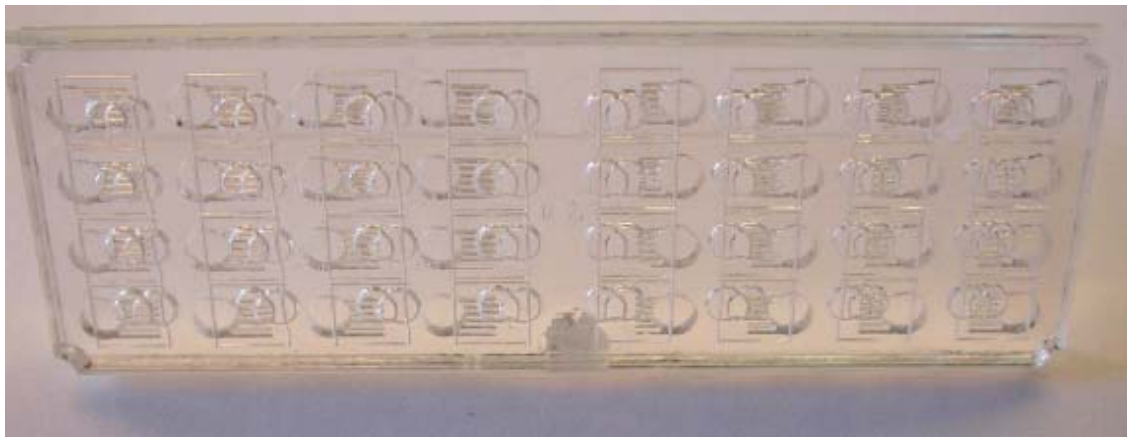
The specific application, often, dictates the package.

The several natures of micromachining application and the unconventionality of the package necessitate a design approach starting from the package. Moreover, unconventional packages must be applied for special application. For instance, the microbioreactor in the following figure developed at MIT needs a sealed reactor that should be opened at a certain point to clean it and change the sensors. In this case a demountable cap for the reaction chamber has been developed.



**Figure 2-4: Microbioreactor for culturing of cells [20]**

Another example can be depicted by the next picture where a dispensed PDMS grid has been used for sealing reaction chambers on top of a glass slide used for DNA array analysis.



**Figure 2-5: Multiplexed microarray Microsystems for Campylobacter spp. Detection [34]**

## **2.2. Factors influencing the packaging design and reliability**

There are several factors that influence the design of a part or the entire system. Those to be considered in packaging are listed below:

1. Material requirements: strength, fracture behaviour, Young's modulus, corrosion, weight, wear, flexibility, stiffness, biocompatibility, bioresistance, permeability;
2. Thermal requirements: thermal conductivity, thermal match with other materials ;
3. Flatness requirements (often in connection with the optical properties): average roughness (surface finishing), sides polished;
4. Interconnection requirements: separation of electrical, optical and fluidic interconnects, sealing properties;
5. Optical requirements: transparency in certain wavelength regions, index of refraction, reflectivity;
6. Electrical and magnetic requirements: conductor or insulator, dielectric constant, magnetic properties;
7. Process compatibility: chemical compatibility, ease of metallization, machinability;
8. Space requirements: shape, size, volume, dead volume;
9. Economic requirements: reliability, utility, cost, safety, styling, maintenance;

Some of these factors are directly related to the dimensions, the material, the processing, and the assembling of the elements of the system. Other factors affect the configuration of the total system.

These factors influence also the size of the package, which is dictated by the need to interface it to a bigger structure or limited by traditional machining methods, or by the need for manual handling of the structure.

Even the manufacturing technique for the micromachining of the system can be considered one of these factors and it is strictly related to the specification and cost of the system. For instance, if many serial processes are involved, the packaging will end up to be expensive, while techniques allowing the packaging in batch will reduce its cost.



There are also factors, influencing the reliability of the system, related to packaging. Some of those are in correlations with the materials and the processes used for packaging which are:

- 1) Residual stresses: especially critical in presence of mismatches between mechanical properties of the materials;
- 2) Mechanical protection and stress relief structures: Rigidity, size, replacements, structures that absorb stresses must be considered;
- 3) Electrical protection and passivation: electrostatic and electromagnetic shielding must be ensured and moisture penetration must be avoided;
- 4) Alignment during bonding: using optical set-ups or alignment pins;
- 5) Thermal performance: good control is needed where chemical reactions need relatively high temperature to perform properly and in general for microbioreactors where cells needs specific temperature to grow, to be confined in a place and to control their metabolism;
- 6) Surface treatments: Chemical resistance when liquid or harsh chemicals are used, sticking for immobilization or anti-sticking for culturing when dealing with cells or DNA;
- 7) Protection during bonding and packaging: to avoid external contamination or cracking.

### **2.3. Materials**

The materials used have a great role in packaging of a microfluidic system [9]. In relation to the functions of the different units inside a system and the environment where the system will work, some materials can show more advantageous characteristics than other materials. The main properties to consider regarding the packaging are physical, mechanical, electrical, optical and the costs.

Silicon is often used and it shows a lot of good characteristics whenever there is a need to integrate electrochemical sensors, photodiodes and, in general, where electrical traces or patterns are present. Optical traces like silicate waveguides are possible but the fabrication process is time consuming and expensive. Silicon is a well suited material for integrating electrical connections but integrating fluidic interconnection is more difficult. It is a brittle material but it is resistant to high pressure and temperature. Finally, silicon circuitry is sensitive to temperature, moisture, magnetic fields, electromagnetic interference, and light.

Ceramic and glass packages have a significant cost and they are difficult to machine.

Glass is a brittle material and it is not a good conductor but it is readily amenable for metallization and it is resistant to harsh chemicals, moreover it has good optical properties.

Due to its relatively high thermal dissipation, ceramic packaging could address several problems. Ceramic packaging presents also good properties regarding the utilization in chemical harsh environments. The mechanical concerns regarding ceramics are due to the inherent brittleness of these materials.

Polymers can present good optical properties, usually are inexpensive materials and easy and flexible to machine, they have also good mechanical properties. They are advantageous to use even regarding weight, performance and mechanical ruggedness perspectives. On the other hand, it is difficult to deposit metal onto them and so it is problematic to have electrical traces into a polymer system especially where high voltage must be applied to the terminals. Moreover the permeability is quite high and this can create problems for certain applications but it is an advantage for others like applications where for instance gas membranes are involved [20].

Polymers, in general, have a low conductivity. Thermal dissipation requirements in polymer packaging for moderately high thermal operating environments therefore need to be satisfied by the use of some cooling mechanism.

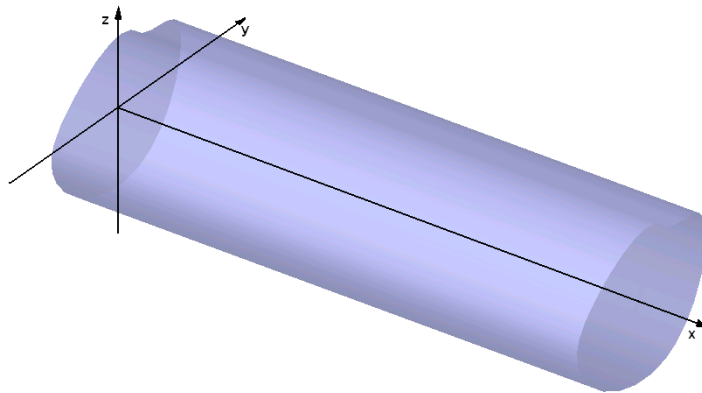
Thermosetting polymers (Teflon, Polyester, epoxies,...) are an alternative to thermoplastic polymers (Plexiglas, Lexan, Polystyrene, Topas). The definition of a thermosetting material is that it undergoes an irreversible transition upon exposure to heat, or, in some cases, UV radiation, to form a network that is interconnected in a three dimensional fashion. In contrast, thermoplastic materials behave more like metals with relatively distinct melting points that do not change as the polymer is exposed to a number of thermal cycles. Thermoplastics consist of long molecular chains that can entangle with one another but do not form chemical connections into a three dimensional network. The advantage of using a thermosetting material rather than a thermoplastic material is the higher strength, typically lower and more isotropic coefficient of thermal expansion, and the ability to maintain some mechanical integrity even when the glass transition temperature is exceeded. In high temperature applications, thermosetting materials can also be easier to process since the long chain molecules of high temperature thermoplastics generally have very low solubility in desirable process solvents and tend to be very brittle. Typically these materials are rated for use up to the 175-250 °C range, and as bare substrate with single sided circuitry, they perform quite well. Another advantage is their resistance to harsh chemicals. The problem with use of these materials is the cost, they do not have good optical properties and they are more difficult to machine.

Some description must be spent also for the elastomers. Elastomers (PDMS, EPDM, TPV,...) are polymers that present particular characteristics. They are flexible and have a low Young modulus. They can be used as gaskets for sealing fluidics and they are also often used for fabricating microfluidic systems due to the ease of casting them. They are resistant to high temperature and they can present good optical properties (PDMS). On the other hand it is difficult to repair them and they are relatively difficult to bond (they need for instance surface treatment).

## 3. Theory

### 3.1. *Fluid Dynamics*

When dealing with the dimensioning of the fluidic interconnections, it is important to know the pressure inside a system. For ensuring a tight connection without leakage it is necessary that the external pressure applied (in case of reversible interconnection) or the adhesive pressure (in case of permanent interconnection) at the interface is bigger than the internal pressure of the system. To know the pressure inside the system, fluid dynamics rules must be taken in account.



**Figure 3-1: Schematic three-dimensional view of a generic channel**

### 3.1.1. Navier-Stokes equations

The gradient of pressure and the motion of a fluid are, generally, regulated by the equations of motion conservation or Navier-Stokes equations (second Newton's law for fluids) in the space [35].

$$\begin{aligned} \rho \left( \frac{\partial u}{\partial t} + u \frac{\partial u}{\partial x} + v \frac{\partial u}{\partial y} + w \frac{\partial u}{\partial z} \right) &= \rho g_x - \frac{\partial p}{\partial x} + \mu \left( \frac{\partial^2 u}{\partial x^2} + \frac{\partial^2 u}{\partial y^2} + \frac{\partial^2 u}{\partial z^2} \right) \\ \rho \left( \frac{\partial v}{\partial t} + u \frac{\partial v}{\partial x} + v \frac{\partial v}{\partial y} + w \frac{\partial v}{\partial z} \right) &= \rho g_y - \frac{\partial p}{\partial y} + \mu \left( \frac{\partial^2 v}{\partial x^2} + \frac{\partial^2 v}{\partial y^2} + \frac{\partial^2 v}{\partial z^2} \right) \\ \rho \left( \frac{\partial w}{\partial t} + u \frac{\partial w}{\partial x} + v \frac{\partial w}{\partial y} + w \frac{\partial w}{\partial z} \right) &= \rho g_z - \frac{\partial p}{\partial z} + \mu \left( \frac{\partial^2 w}{\partial x^2} + \frac{\partial^2 w}{\partial y^2} + \frac{\partial^2 w}{\partial z^2} \right) \end{aligned} \quad , \quad (3-1)$$

where  $x, y$  and  $z$  are the orthogonal axis that define the space,  $u, v$  and  $w$  are, respectively, the components of the local velocity of the fluid along the  $x, y$  and  $z$  axis. The variable  $\rho$  is the density of the fluid,  $\mu$  is the dynamic viscosity of the fluid and  $g_x, g_y$  and  $g_z$ , are, respectively the value of the gravity acceleration along the  $x, y$  and  $z$  axis.

In a microfluidic system the gravity can be neglected, dividing by the density and rewriting these equations in a vectorial form, it is possible to have a more compact equation:

$$\frac{\partial \bar{v}}{\partial t} + (\bar{v} \cdot \nabla) \bar{v} = -\frac{1}{\rho} \nabla p + \nu \nabla^2 \bar{v} \quad (3-2)$$

Where  $\nu = \frac{\mu}{\rho}$  is the kinematic viscosity,  $\bar{v} = (u, v, w)$  is the velocity vector,

$\nabla p = \left( \frac{\partial p}{\partial x}, \frac{\partial p}{\partial y}, \frac{\partial p}{\partial z} \right)$  is the gradient of pressure,  $\nabla = \left( \frac{\partial}{\partial x}, \frac{\partial}{\partial y}, \frac{\partial}{\partial z} \right)$  is the nabla operator.

### 3.1.2. Continuity equation

Another important equation that governs the continuous deformation of a fluid is the equation of mass conservation or continuity equation. For an incompressible fluid it is

$$\frac{\partial u}{\partial x} + \frac{\partial v}{\partial y} + \frac{\partial w}{\partial z} = 0 \quad , \quad (3-3)$$

and in vectorial form

$$\nabla \cdot \vec{v} = 0 \quad (3-4)$$

### 3.1.3. Analytical solutions

Combining the Navier-Stokes equations and the equation of continuity we have four equations and four unknowns. But, in general, finding an exact analytical solution for these equations is difficult. However, there are some important cases where it is possible to define all the boundary conditions and it is possible to simplify the problem. In our case, a steady-state problem where a viscous and incompressible liquid is pressure-driven into a channel (Hagen-Poiseuille flow) with a generic cross-section will be considered. The total length of the channel ( $L$ ) will be under a constant pressure difference ( $\Delta p = p(L) - p(0)$ ).

The constant difference of pressure along  $x$  implies a linear behavior of the pressure along  $x$ :

$$p(x) = \frac{\Delta p}{L}(L - x) + p(L) \Rightarrow \frac{\partial p}{\partial x} = \frac{\Delta p}{L} \quad (3-5)$$

The channel is parallel to the  $x$  axis and is assumed to be translation invariant in that direction.

Then the equation of continuity becomes

$$\frac{\partial u}{\partial x} = 0, \quad (3-6)$$

which means that the velocity will not vary in the  $x$  direction.

The Navier-Stokes equations is

$$\begin{aligned} \frac{\Delta p}{\mu L} &= \left( \frac{\partial^2 u}{\partial y^2} + \frac{\partial^2 u}{\partial z^2} \right) \\ 0 &= -\frac{\partial p}{\partial y} \quad . \\ 0 &= -\frac{\partial p}{\partial z} \end{aligned} \quad (3-7)$$

Finally, considering a no-slip boundary condition at the solid wall of the channel we have

$$u_w=0 \text{ (velocity along } x \text{ on the wall)} \quad (3-8)$$

The shape of the cross-section of the channel will give other information about boundary conditions that together with (3-8) and the first of (3-7) will allow to calculate the profile of the velocity  $u(y,z)$  inside the channel. At this point it is also possible to calculate the flow rate  $Q$  as the integral of the velocity over the area  $A$  of the cross-section of the channel

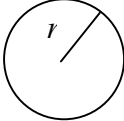
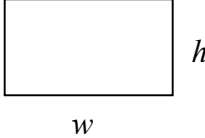

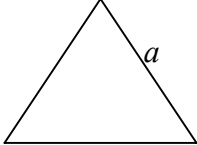
$$Q = \int_A u(y,z) dydz \quad . \quad (3-9)$$

Through the equation 3-9 and the profile of the velocity, it is possible to know the gradient of pressure as function of the flow rate as

$$\Delta p = RQ \text{ (Hagen-Poiseuille equation)} \quad (3-10)$$

where  $R$  represents the fluidic resistance of the channel that depends on the shape of the cross-section of the channel. So that for the most common cross-section in microfluidicsystems is explained in the following table [1].

**Table 1: Fluidic resistance of fluidic channels having different geometry**

Circular cross-section, $r$ is the radius  $R = \frac{8\eta L}{\pi r^4}$	
Rectangular cross-section, $w$ is the larger edge and $h$ is the smaller edge  $R = \frac{12\eta L}{wh^3}$	
Square cross-section, $a$ is the side  $R = \frac{28.454\eta L}{a^4}$	
Regular triangle cross-section, $a$ is the edge  $R = \frac{184.751\eta L}{a^4}$	

Equation (3-10) becomes important when dealing with fluidic interconnections because it allows determining the pressure at the inlet of the network of a microfluidicsystems. This pressure is critical at the interface between system and external connection and must be taken in account when dimensioning the fluidic interconnections.

### 3.2. Optical waveguiding

An optical waveguide can be defined as a dielectric structure that transports an electromagnetic wave with a wavelength in the UV, visible, or infrared range. The confinement of light in a certain region happens if the light travels in a medium of high

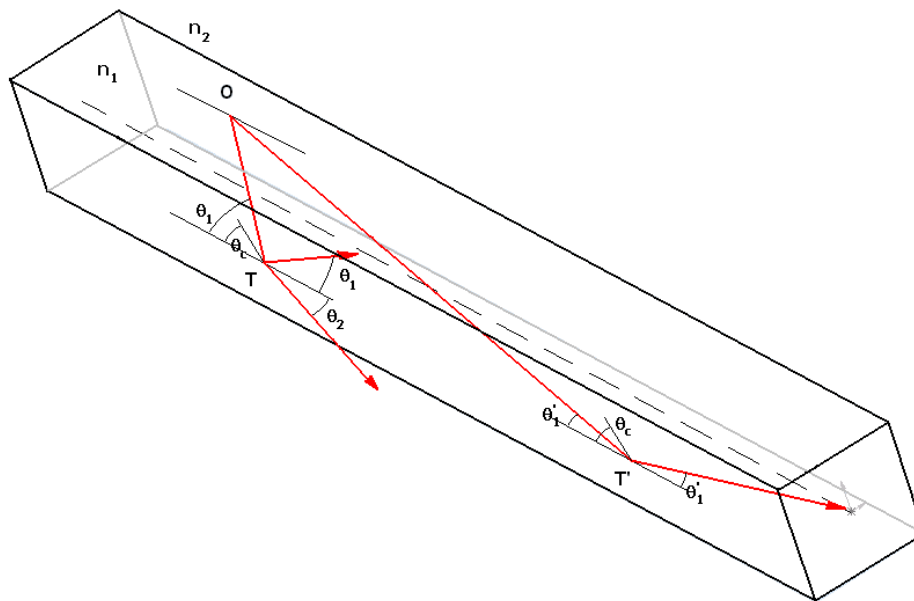


refractive index (core), which is surrounded by a material of low refractive index (cladding) that acts like a trap for the light. In this way the light will be driven by total internal reflection.

The light propagation, governed by Maxwell's equation, happens in discrete modes depending on the waveguide dimension. A single-mode waveguide has a dimension in the same order of the wavelength of the light traveling inside it [36].

In this section, multimode waveguides will be considered, where simple ray tracing can be used for describing the light propagation.

The assumptions that will be considered are that the profile of the waveguide does not vary. This means, the waveguide will be translationally invariant and results in a step-index waveguide where the light will propagate along straight lines.



**Figure 3-2: Schematic three-dimensional view of waveguide and propagation of light at different angles**

A straight waveguide with a refractive index  $n_1$ , surrounded by a cladding of refractive index  $n_2$  is considered. A ray that originates at point O at the interface of the waveguide making an angle  $\theta_1$  with the waveguide axis will touch the opposite interface at a point T and it will be refracted forming an angle  $\theta_2$  with the waveguide axis. The relation between the angles of refraction and incidence is governed by the Snell's law

$$n_1 \cos \theta_1 = n_2 \cos \theta_2 \quad (3-11)$$

At certain values of  $\theta_1$ ,  $\theta_2$  will be zero. This occurs when  $\theta_1 = \theta_c$ , where  $\theta_c$  is the critical angle

$$\theta_c = \cos^{-1} \left\{ \frac{n_2}{n_1} \right\} = \sin^{-1} \left\{ 1 - \frac{n_2^2}{n_1^2} \right\}^{1/2} \quad (3-12)$$

The incident ray will be totally internally reflected if  $0 \leq \theta_1 < \theta_c$  and is partly reflected and partly refracted if  $\theta_c < \theta_1 < \pi/2$ .

It is obvious that for having an efficient waveguide the light must travel at angles smaller than the critical angle and this is mainly a limitation to the modes that can be coupled into a waveguide.

It is important to note that a ray incident from air into the waveguide becomes a guided ray if it makes an angle  $\theta_1$  with the waveguide axis smaller than  $\theta_c$  upon refraction into the core. Applying Snell's law at the air-core boundary, the angle  $\theta_a$  in air corresponding to  $\theta_c$  in the core is given by

$$\theta_a = \sin^{-1} NA \quad (\text{allowed incidence angle}), \quad (3-13)$$

where  $NA = (n_1^2 - n_2^2)^{1/2}$  is the numerical aperture of the waveguide.

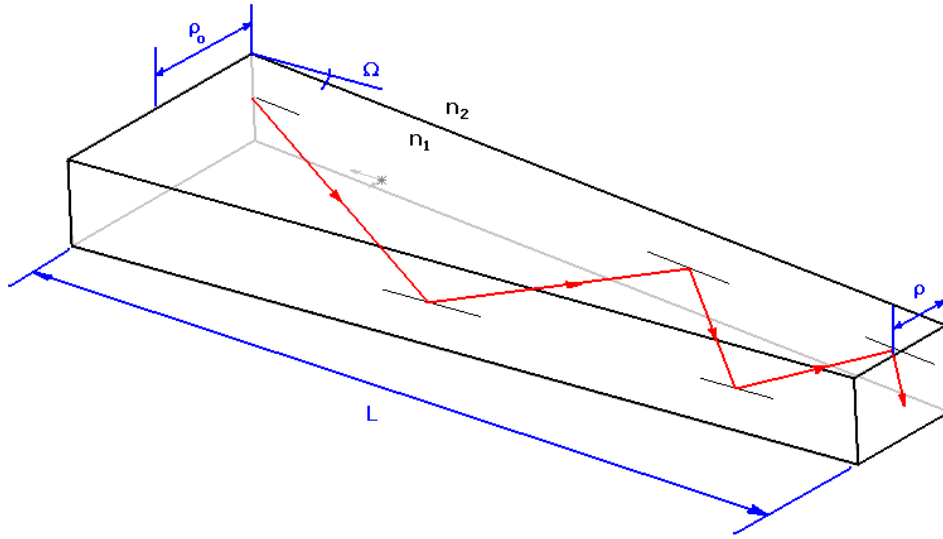
### 3.2.1. Tapers and light concentration

Often, the light beam that must be coupled into a waveguide originates from a source which is larger than the waveguide itself. It becomes useful to use tapers to collect more light from the source. The tapers must be designed in a way to be very efficient in terms of light-concentrating properties. In order to do that ray tracing can be used.

Considering a linear taper, each time that the light will be reflected, the angle of incidence from one interface to the other will become bigger and if the length of the taper is not long enough in relation of the difference between the cross-section at the inlet and

outlet of the taper, the angle will become bigger than the critical angle and the tapers will be leaky.

An on-axis collimated beam enters a step-profile, linear taper at  $z=0$  at an angle  $\theta_0$ , where the core half width is  $\rho_0$  at the beginning and  $\rho$  at the end of the taper at  $z=L$ . The core index of the taper is set to be  $n_1$  and the taper cladding index is  $n_2$ . Each on-axis ray reflects from the linear interface so that the angles of incidence and reflection relative to the tangent to the interface are equal.



**Figure 3-3: Ray-tracing three-dimensional representation of light propagating into a taper**

Considering that the taper angle is  $\Omega$ , the minimum taper length which ensures that all the power incident on the taper is transmitted to the end will be

$$L_{\min} = \frac{\rho_0 - \rho}{\tan \Omega}; \quad \frac{\rho \sin(\theta_c + \Omega)}{\rho_0 \sin \theta_0} = 1 + \frac{\tan \Omega}{\tan \theta_0} . \quad (3-14)$$

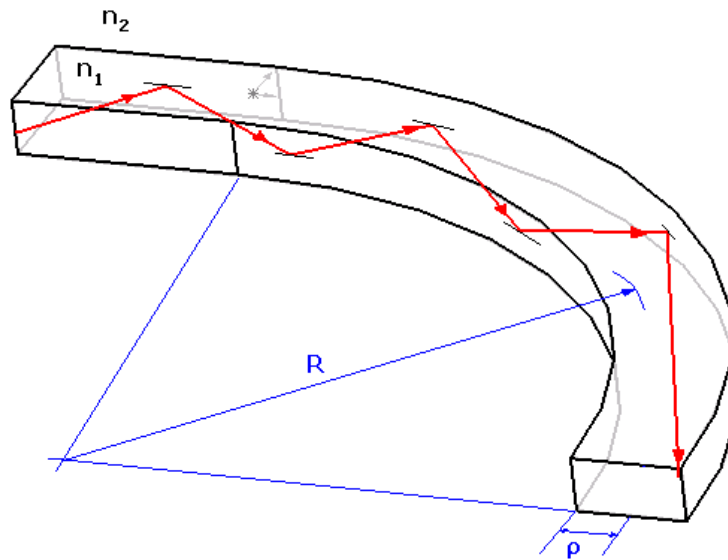
The solution for  $\Omega$  is obtained numerically, but if all the angles involved are small, there is an approximate solution given by

$$L_{\min} \cong (\rho_0 - \rho)^2 / (\theta_c \rho - \theta_0 \rho_0) . \quad (3-15)$$

This result applies to both direct on-axis illumination by a collimated beam, i.e.  $\theta_o=0$ , and the inclusion of a lens which transforms the paraxial beam into a cone of meridional rays at angle  $\theta_o>0$ .

### 3.2.2. Bends

Bended waveguides are important as they are useful for distributing the signal on a larger area and at the same time for avoiding the problem of stray light.



**Figure 3-4: Ray-tracing three-dimensional representation of light propagating into a bended waveguide**

It is easy to understand that in this case the light at the bend will touch the surface of the waveguide at an higher angle than during the straight part.

We deduce that if  $\theta_1>\theta_c$  the ray refracts at the interface, and if  $\theta_1<\theta_c$  it tunnels. The same is valid for the inner and outer interface.

From experimental measurements it is possible to individuate the fraction of power loss as a function of  $z/\rho$  and  $R/\rho$ . From these graphs, realized using waveguides with  $\theta_c = 0.1$ , it is possible to see that for values of  $R/\rho > 10^3$  the bending losses are negligible [36].

### 3.2.3. Power attenuation

Another factor that must be considered when dealing with waveguides is the absorption of the materials that constitute the core and cladding of the waveguide. The attenuation of the light power depends on the wavelength of the light and the refractive index into the core. For an uniformly absorbing core the power attenuation corresponds to

$$P(z) = P(0)\exp\{-\alpha_{co}z/\cos\theta_1\}, \quad (3-16)$$

where  $P(z)$  is the power at a specific coordinate  $z$  of the waveguide axis,  $P(0)$  is the power at the beginning of the waveguide,  $\alpha_{co} = 2kn_1$  is the absorption coefficient for the core and  $k = 2\pi/\lambda$  is the wavenumber.

Absorption of power is due also to an absorbing cladding. In this case the absorption happens to each reflection point of the ray path. At the interface, the lost energy associated with the local plane waves (evanescent field) decrease exponentially with the reciprocal of the wavelength of the light and is proportional to the refractive index of the cladding.

In this case the power attenuation can be expressed as

$$P(z) = P(0)\exp\{-\gamma_{cl}z\}, \quad (3-17)$$

where  $\gamma_{cl} = \frac{\alpha_{cl}}{V} \left(\frac{\theta_1}{\theta_c}\right)^2 \frac{1}{\{1 - (\theta_1/\theta_c)^2 \sin^2 \theta_\phi\}^{1/2}}$  is the power attenuation coefficient,  $\theta_\phi$  is

the angle that the projection of the ray on the end face of the waveguide makes with the azimuthal direction at the point where the ray is coupled,  $\alpha_{cl} = 2kn_2$  is the absorption coefficient for the cladding,  $V = \frac{2\pi\rho}{\lambda}(n_1^2 - n_2^2)^{1/2}$  is the waveguide parameter and  $\rho$  is half-width of the waveguide.

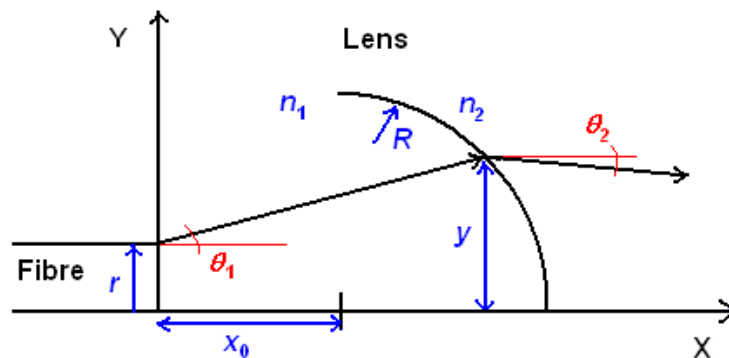
Other sources of attenuation are scattering of light due to the inhomogeneity of the material and roughness at the interface. Usually it is proportional to the inverse fourth-power of the wavelength (Rayleigh's inverse fourth power law) [37].

### 3.3. Lenses

Ray optics theory can be used to estimate the behavior of the light from a light source through media of different refractive indices and lenses. Considering the radius ( $R$ ) of the lens, the radius ( $r$ ) and numerical aperture (NA) of the of the light beam, the relative position between the light source and the lens ( $x_0$ ), the refractive index ( $n_1$ ) of the material used between the light source and the lens, and the refractive index of the medium in which the light propagates after the lens ( $n_2$ ), (see also Fig.2) the theoretical trajectory of the light can be estimated by

$$\vartheta_2 = \frac{n_1}{n_2} \vartheta_1 - \frac{n_2 - n_1}{n_2 R} y \quad (3-18)$$

where  $\theta_1$  is the angle created by the light source with the x axis and  $y$  is the height at which the ray meets the lens. The height  $y$  can be calculated considering the intersection between the line representing a specific ray and the circle representing the lens, while the angle  $\theta_1$  can be calculated knowing the numerical aperture of the light source and the refractive index of the plug.

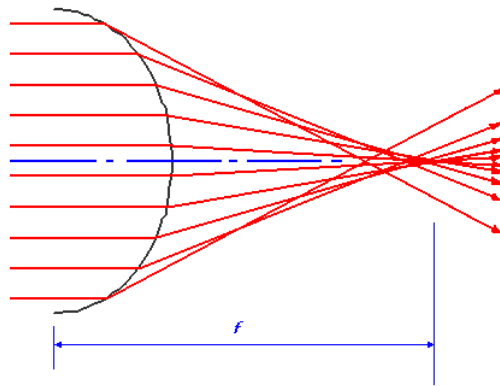


**Figure 3-5: Two dimensional representation of light propagating from a source with a specific NA through a lens**

Though, we must consider that ray optics is an approximate theory which is based on having paraxial rays, that means the light travels at small inclinations (such that  $\sin\theta \approx \theta$ ) around an optical axis about which the optical components (in our case the lens) are centered.

According to the paraxial approximation for a plane convex lens the focus length will be

$$f = \frac{R}{n_{lens} - 1} \quad (3-19)$$



**Figure 3-6: Caustic curve**

The deviation from paraxial approximation will result in the formation of a caustic curve that will focus within an area more than a point giving aberration.

### 3.3.1. Diffraction

The light propagation through a lens is dominated from diffraction and it is related to Heisenberg's principle of uncertainty. Accurate diffraction patterns can be obtained by numerical wave front calculations ending to the fact that the focused light beam has an intensity distribution that follows a Gaussian shape, Beam optics theory can be used to estimate the focal spot and the depth of focus of our plugs.

Although in ideal case no other aberrations are introduced, the focus will have a finite extension. Diffraction at the lens aperture ( $D$ ) causes a blur of the focus. In this case the width of the focal spot, in absence of aberrations, is

$$\delta x \approx 2.44 \frac{\lambda f}{D} \quad (3-20)$$

where  $\lambda$  is the wavelength of the light

and  $D$  is the diameter of the beam (considering a parallel beam)

### 3.3.2. Surface roughness

For a good functionality of a refractive optical element is important that the roughness will be below  $\lambda/10$ . Perturbation smaller than this does not result in significant scattering of the light [38].

### 3.3.3. Aberration due to a spherical lens

The ideal profile for focusing the light in a single point is a paraboloidal lens [27], on the other hand, a spherical lens is easier to fabricate. However a spherical lens doesn't focus in a single point bringing to aberration.

In fact, when the light ray travels at a considerable distance from the axis it will be introduced some errors in the calculation of the focus by spherical aberration. The lateral spherical aberration can be calculated as

$$y_{LSA} = \frac{0.272y^2}{f} \quad (3-21)$$

which gives the distance between the real focus from the theoretical one and where  $y$  again is the distance from the center axis at which the light passes the lens.

This source of aberration can be minimized fabricating the lens two or three times the diameter of the light beam [39], in this way the part of the lens near the axis can be approximated to a parabola.

In practice, the angular distribution of the light source will be often the dominating factor for the spot size. The bidimensional model that will be explained in the next chapter, that comprises the angular distribution of the light, is a useful tool to estimate the real focus.



Other sources of aberration are caused by defects of the lens, like impurities and deviation from the ideal profile.

### 3.3.4. Limits of coupling from a lens to a waveguiding structure

Finally, the last consideration concerns the maximum NA of the lens allowed.

Considering a source which emits a collimated beam of radius  $r_d$ , focused onto the endface of the waveguiding structure, having a core of refractive index  $n_2$  by a lens of radius equal to the beam radius and focal length as shown in fig. 3.7

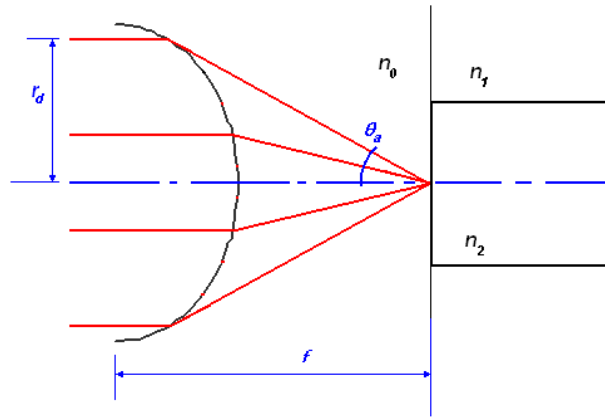


Figure 3-7: On-axis lens focused onto the fiber end-face

All of the light from the source excites only bound rays where the focal length exceeds a certain minimum.

$$f \geq r_d \frac{\left\{ (n_0/n_2)^2 - \sin^2 \theta_c \right\}^{1/2}}{\sin \theta_c} \cong \frac{n_0 r_d}{n_2 \theta_c}, \quad (3-22)$$

where  $n_0$  is the refractive index of the medium located between the lens and the waveguiding structure. The approximation applies to weakly guiding fibers with  $\theta_c \ll 1$ . The presence of the lens increases the power entering bound rays, and therefore the source efficiency by a factor  $(r_d/\rho)^2$  compared with direct illumination by the same source[37].

## 4. Interconnections

As mentioned before, the interconnections have the function of bringing the information of the systems among different units or between systems and the outer world together.

We can identify three kinds of interconnections regarding microfluidic systems, which are fluidic, electrical and optical interconnections.

Each different kind of interconnection can be grouped in a specific family and each family interacts with the system at different levels of packaging as described in Chapter 2.

The fluidic interconnections can be divided in two families, integrated into the system and those external to the system. Moreover, they can be used for providing modular functionality.

The electrical interconnections can be those used to connect different layers inside a system or different parts inside the same system and they are defined as feedthrough connections. Apart from that exist techniques like wire bonding (WB), tape automated bonding (TAB) and flip chip bonding to connect the system modularly usually to a PCB board. Finally, there are a lot of connectors on the market to connect the system to the substrate.

Optical interconnections make usually use of optical fibers, waveguides to guide light in or between different part of the system, while butt-end coupling, gratings, prisms and lenses help to connect the system to the outer world.

Several methods have been experimentally used to interconnect systems and that will be analyzed in the following sections.

#### **4.1. Fluidic interconnections**

One of the main quests in packaging is a good design and dimensioning of the fluidic interconnections. In function of them the systems will have specific limits of pressure or flow rate that regulates chemical reactions or mixing inside the system or detections in a lot of applications.

Important requirements for the interconnections schemes to have a good control of the system are low pressure drop, low dead volume, ease of fabrication, reliable and repeatable performance and biocompatibility. Moreover, in order to prevent loss of fluids or undesired function of the system all fluidic interconnections must be sealed hermetically. These parameters are critical, since they play an important role for the functionality of the system. For instance, generation of spurious signals or excessive base-line signals are generated if the dead volume is not small enough.

Since the systems typically would comprise a variety of applications, components, materials and technologies, considerable attention should be paid to the integration-concept of such systems.

Fluidic interconnections can be divided into permanent and reversible interconnections.

Permanent interconnections involve those methods where gluing or welding is used for permanently sealing at the interface between a system and the external package.

Several types of adhesive can be used to bond thin tubes into holes fabricated in the substrate where the fluidic network is machined [40,41, 42, 43,44].



**Figure 4-1: Examples of permanent glued fluidic interconnections**

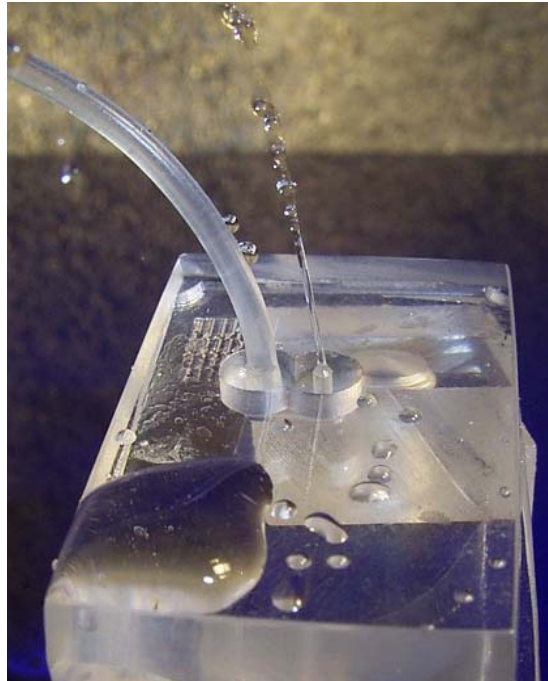
This method has also been used to glue wells where reservoirs are needed at the inlet and outlet of the system [45]

Gluing a tube is a very simple process. Though, it brings in the risk of clogging due to infiltration of the glue by capillary forces at the gap between tube and channel inside the network. This problem can be solved by using highly viscous glues reducing the capillary forces but the use of glue implies manual work that implicates not controllable and reliable processes. Moreover, the glue around a tube limits the density of the number of interconnections that can be integrated. Finally it is a time-consuming process.

Reversible interconnections imply a reusable packaging which has different advantages versus the permanent packaging. In case of microsystem malfunction, it can be replaced using the same structure for packaging a new system and vice versa, if the package is damaged, the system can be recycled. Another advantage is that a reversible packaging could be used for testing different microsystems in a fast way saving the time to fabricate permanent packages for each one of the tested microsystem.

Reversible interconnections use soft elements at the interface between system and external packaging. Sealing is ensured pressing the system to the external package by external forces generated by screws or clamps.

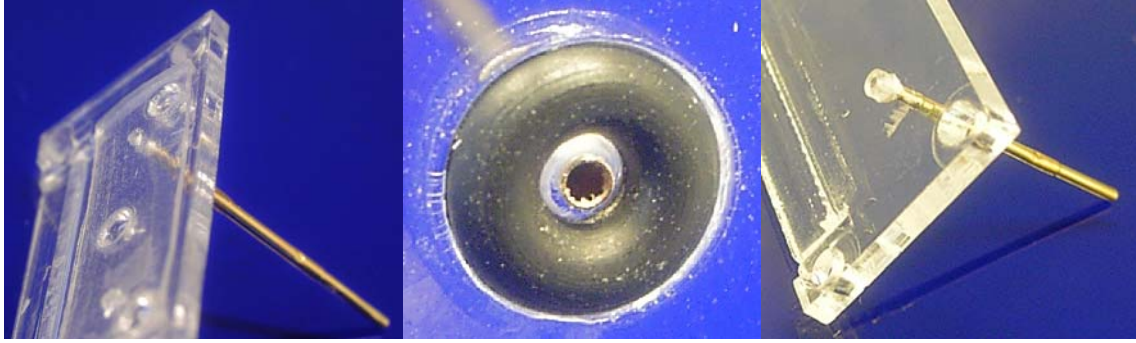
These interconnections can be further divided in two sub-groups: integrated [46,47,48] and external [49, 50, 51, 52, 53, 54, 55] to the system. The first group implies more steps for designing and fabricating the microsystems, while the external interconnections implies more steps for designing and fabricating the package. The integrated interconnections often bring more practical solutions, but the choice of one group or another depends on the application, material, and technology used for the microfluidic system. Integrated interconnections are convenient for polymer devices, where adding fabrication steps for integrating such interconnections is usually less expensive and more flexible than, for instance, silicon microfluidic systems.



**Figure 4-2: Integrated fluidic interconnection in a polymer system**

In the latter case, external interconnection would reduce the cost of the overall package due to a simplified process for the system where the costs contribute mainly.

In both cases sealing soft elements are gaskets [51, 52], o-rings [53, 54, 55], and soft tubes [15].



**Figure 4-3: PDMS gaskets (left) , o-rings (center) and soft silicone tubes (right) placed into a polymer housing that will be pressed towards a microfluidicsystem to ensure sealing**

A gasket that covers all the entire surface of the system that includes inlet and outlet needs high forces to ensure a high pressure at the interface and so a strong packaging configuration. On the other hand, this method is readily amenable for high density interconnections, low dead volume and it ensures a homogenous pressure at the interface, preventing bending stresses that in some cases can cause the chip breaking.

O-rings are an economic solution and easy to integrate. To keep them aligned, grooves can be fabricated around connection holes of the package and external tubes. Due to limited deformation capabilities of the o-rings, it is mandatory that all grooves have exactly the same depth. In case of more than one connection this becomes important because a varying distance between microstructure and holder would not be compensated. Further, asymmetric distribution of o-rings leads to different pressures applied to the single o-ring. All this is critical in terms of chip breaking and leakage of the interconnection.

In comparison to the o-rings, soft tubes are more deformable which results in a better sealing quality. This leads also to more tolerance of the connection angle between microsystem and holder.

Another group of interconnections comprises the multi chip modules (MCM) interconnections [14, 15] where the interface between chips on the macro-scale is achieved by a separate module. In this case a motherboard can be used to connect modularly several chips. Alternatively a bendable strip including fluidic channels can be used to connect more chips together.

The most relevant solutions regarding fluidic interconnections are summarized in Appendix A.

## **4.2. Electrical Interconnections**

Electrically isolated low impedance connections between hermetically sealed regions or between devices or the outer world are important for microsystems [56].

The requirements include good insulation capability, low feedthrough resistance, hermetical seal, small size, vias to go through layers of great thickness.

We can distinguish different levels of interconnecting microfluidic systems electrically.

The first level regards feedthrough techniques developed to provide electrical connections from hermetically sealed cavity to out-side. This techniques are mostly used for silicon or ceramic microfluidic systems and not for polymer microfluidic systems due to the difficult depositing metal on polymers.

The most common electrical feedthrough techniques are those related to doping, migration and depositing of metal on a silicon, ceramic, or plastic substrate.

Some of those can be applied only on silicon, but, since this work will focus on polymer microfabrication we will neglect the description. Those that can be applied in general are

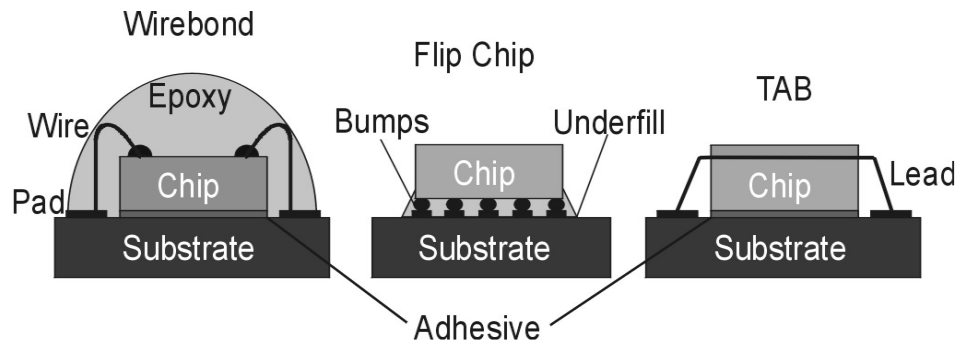
- Metal deposition including on polymer but more suitable for ceramic, silicon and glass;
- Feedthrough channels, where narrow channels are machined and then fed with conducting materials and finally sealed by glue, or deposited or bonded insulators that can maintain the hermetic seal. This technique is not automated and requires handling which elevates the costs.
- Connection through holes (vias)

Mechanical holes may be used to provide electrical connections between the two sides of the wafer or device. These holes must be small and placed at precisely defined locations to be compatible with the micro-components or systems.

It has to be noticed that deposition of metal on polymers is a complex process and it gives a lot of limitations for the potential that can be applied, especially in wet applications.

The second level of packaging considers the modular connections between systems or between a system and a substrate in order to distribute the electrical pattern from a small area to a larger more manageable one.

The main three interconnection technologies belonging to this level are wirebond (WB), tape automated bond (TAB) and flip chip (FC) technologies, that are summarized in Figure 4-4 [57].



**Figure 4-4: Sketch of three interconnection technologies: wirebonding (WB), flip chip bonding (FC), tape automated bonding (TAB) [5]**

WB uses wires (4-500 $\mu\text{m}$  in diameter) to create connections, in TAB (10 $\mu\text{m}$ -5mm) are used tape leads (10 $\mu\text{m}$ -5mm wide) and in FC (50 $\mu\text{m}$ ) bump drops of metal (50 $\mu\text{m}$  in diameter) are used.

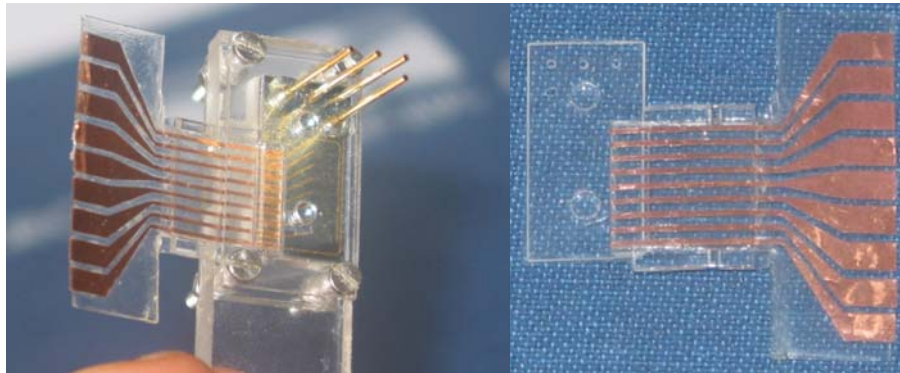
WB is the cheaper technology and most commonly used. TAB needs a smaller pad and pitch, has lower lab costs and has a better electrical performance. The disadvantages are dictated by the fact that it is time consuming, by the cost for designing and fabricating the tape and by the more expensive equipment. FC ensures small size, better electrical performance, improved thermal capabilities and low cost. The disadvantages include the difficulty of testing of bare dies and the limited availability of bumped chips and the repairing is difficult or impossible. These technologies are often used for silicon and not for polymers due to the reasons explained in section 2.3.

Usually these bonding techniques are done on substrate like PCB, polyamide, or thermosetting polymers. A lot of issues related to these materials are limited transition temperature, internal stresses and thermal expansion mismatch. A solution can be the use of a reinforced material that has a three dimensional structure. Such honeycomb



structures are available in Teflon and Teflon-like materials, but usually these material don't have mechanical stability. For polymer the easiest solution for electrical interconnection is to access from outside into the system with more rigid electrical components or tapers that can be embedded into the system or pressed to it using reversible techniques.

In the following picture, copper leads were glued onto a PET layer, cased and embedded in PDMS and bonded to the PDMS gasket to provide fluidic and electrical connections integrated together. The PDMS under the PET layer will act like a spring to the copper leads allowing a good contact with the system. For the electrical interconnections a copper tape was glued onto a thin layer of PET or PMMA covered by a photoresist exposed under UV for 30 seconds using a printed overhead transparency as lithographic mask with the specific pattern of the interconnections. The photoresist was developed in Sodium Hydroxide. Finally, the copper was etched with a 10% of Sodium peroxodisulfate to create the specific shape of the interconnections. The electrical connections are cased in PDMS and bonded to the PDMS layer used in the fluidic interconnections. The system will be pressed on this structure to ensure sealing and electrical connections.



**Figure 4-5: Electrical interconnections embedded in PDMS and integrated together with fluidic gasket [49]**

Once the electrical connections are distributed and connected with the process described above on a silicon board or PCB, commonly used sockets and connectors can be applied to connect the system to a PC, power supply or signal detector.

### **4.3. Optical interconnections**

Optical detection is widely used in bio-chemical analysis [6] because it is a simple, non-invasive method readily for high scalability, applicable for a wide choice of analyte.

Several types of miniaturized systems have been realized for bio-chemical analysis using optical detection methods like absorbance measurements [58,59,60], refractive index measurements [61] and fluorescence detection [62,63]

Integrating optics is very challenging since optical components like fibers, waveguides lasers, LEDs, modulators, switches, couplers, sensors and photodetectors can be difficult to precisely align and mount, requiring considerable amount of manual work, often done under optical microscopes. All this increases the manufacturing and packaging costs that contribute largely to the overall cost of the system. It is then important to find packaging technologies allowing reducing the costs and ensuring, at the same time, a robust design. Considering that the packaging costs are mainly due to the time required to assembly and package the system, the components to be aligned must be reduced. Therefore, coupling methods with large alignment tolerances and alignment features allowing passive self-alignment assembly instead of active driving of the device should be adopted. In this way, it is possible to reduce the mounting and alignment operations avoiding the need of external equipments for precision alignment, providing stable fixing of the different components. Moreover, methods for increasing the coupling efficiency and the alignment tolerances could further ease the packaging and this can be done, for instance integrating lenses. When fiber connections arrays are involved, the packaging technologies become more important because of the high number of involved components.

Another point to be analyzed in integration of optics is that, at the microscale, it is very difficult to couple a sufficient amount of light avoiding stray light to maintain a high signal-to-noise ratio and high sensitivity.

In fact, the reduction of sample volumes is proportional to a reduction of the number of molecules, ions, particles, cells and so on, to detect, which results in more difficult analysis [64]. So, it is easy to understand that the integration of a good detection method in terms of sensitivity and S/N is very important.

Several approaches for optical interconnections have been proposed. Most of them are based on combo-systems, where detecting microdevices and free-space optics meet to

perform analysis [65, 66, 67]. Free space optics has different limitations since expensive, huge mechanical and optical systems such as translation stages movable mirrors, or confocal microscopes and high mechanical stability are required. Using fiber-optic solutions or waveguides in combination with alignment schemes it is possible to overcome these restrictions, directly integrating the detection system on the chip. This solution enables the fabrication of small and clearly spaced optical elements, their precise alignment with respect to the microfluidics and the realization of original detection system configurations.

In both cases S/N and sensitivity gives information of the quality of the optical analysis and those can be increased reducing the losses originating at the optical interconnections and stray light.

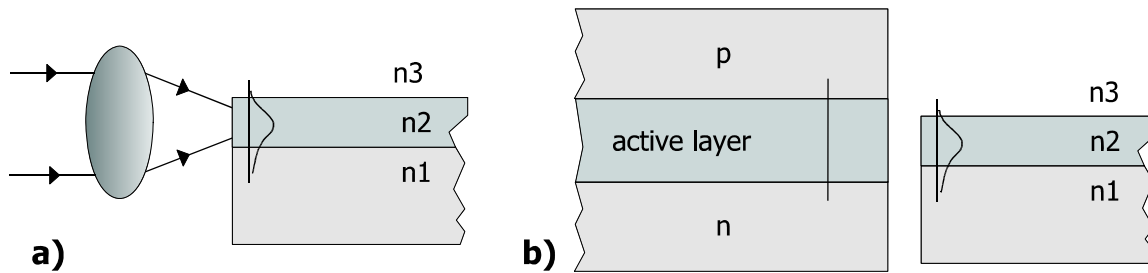
The losses to minimize in order to increase the performance, quantifiable in energy losses of the excitation light, are alignment mismatches, coupling losses across the liquid channel, insertion and reflective losses and propagation losses. Coupling loss is due to the energy lost when the light travels unguided and it is related more to the light lost inside the detection point of the fluidic channel. While propagation losses are related to that lost inside an optical fiber or waveguide caused by absorption and scattering of light. Insertion and reflection losses are related to the interface between the system and the light source or detectors. But while the first increases if the modes and so the NA between the two connecting parts don't match the second increases with the increases of surfaces the light needs to pass [18].

As explained in the previous section, different levels of interconnections or packaging can be considered. The first level includes the detection point and so the interface between the fluidic channel and the medium driving the light, the second level comprises the interfaces between optical components inside the system, the third level is related with the interface between the system and the outworld. The optical fibers can be brought directly close to the fluidic channel [68,69,70,71,72] in this case the layout of the system is extremely simplified, the reflecting surfaces, the optical components and the connecting parts and so the reflecting losses are minimized but often the fibers are difficult to be aligned. It requires manual work to mount the fibers and they introduce limitation in case of multiple point detection due to the dimension limit of the optical

fiber. Otherwise optical waveguides can be integrated into the system [73, 74, 75, 76, 77, 78] to interface, on one side, the detection point inside the fluidic channel of the device and, on the other side, the optical fibers or directly the light source and the detectors. The waveguides allow a precise alignment within the detection point and can be spaced close to each other adding freedom to the detector but they introduce one more reflecting surface when they have to be connected to the outer world.

In general it is difficult to couple the light from free-space (optics) or other waveguiding structures like optical fibers or semiconductor lasers, into modes which can be guided into a system.

The most common techniques to do that are the transverse coupling and surface coupling mentioned [79].



**Figure 4-6: Lens coupling a) and End butt coupling b)**

End-Butt coupling (Fig.4.6b) [80, 81] is the simplest technique for transverse coupling and consists of bringing two waveguiding structures into close contact, or a light source (like a light-emitting diode or laser diode) in a way to allow the light to propagate from one structure to the other. For doing this, it is important that the two structures have waveguide modes compatibility. This technique is often used for coupling waveguiding layers of semiconductor lasers or fibers to waveguides. If the waveguiding structures are adjusted a coupling efficiency of 68% can be achieved [82]. However the adjusting and alignment processes can be difficult and time consuming.

As can be depicted in the figure 4-6a transverse coupling includes also focusing of the light from free-space into a specific structure or sensor using a lens [83,84,85,86,87,88,89,90].

Using the direct focusing technique, in order to have an efficient coupling, the lens should focus the light with an angle which is smaller than the admittance angle  $\theta_a$  of the waveguiding structure that in terms of numerical aperture NA becomes

$$NA = \sin \theta_a = n_1 \sin \bar{\theta}_c = n_1 \left[ 1 - (n_2/n_1)^2 \right]^{1/2} = (n_1^2 - n_2^2)^{1/2}, \quad (4-1)$$

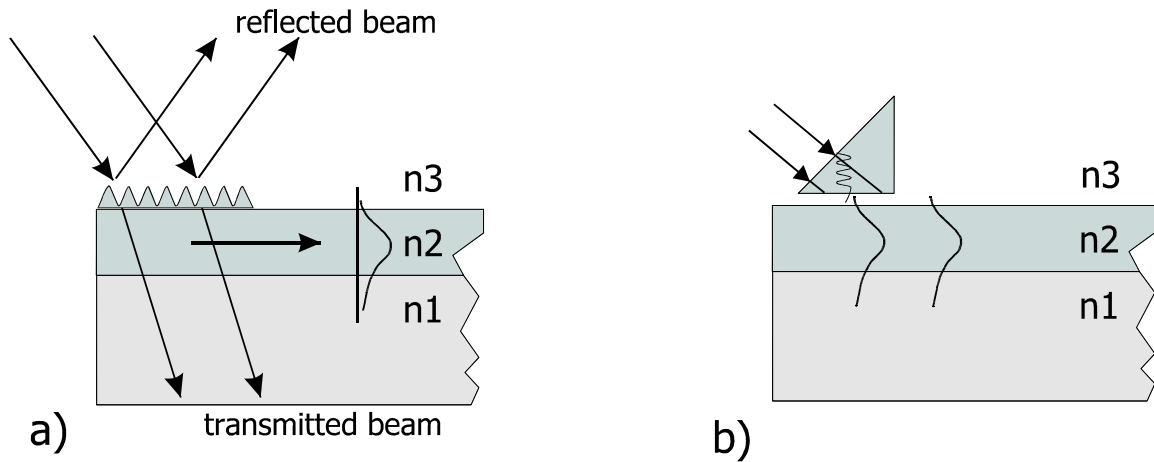
where  $\theta_c = \cos^{-1}(n_2/n_1)$  is the critical angle within the guided rays are confined to.

Considering the right focal length, the ratio between the size of the focal spot and the thickness of the waveguide structure or sensor determines the coupling efficiency. In case of coherent light and good point sources a coupling efficiency of 100% can be reached, using this technique [82].

In general, is good to maintain the NA of the lens as small as possible in order to avoid the excitation of the higher modes only and to decrease the reflection of the light at the interface [18]. Moreover, when the light should pass through a channel for different kind of measurements the collimation of the light only would be better than the focusing since it is possible to increase the sensitivity of the measurement. This technique alleviates also the critical alignment problems, but alignment precision is still required for single mode coupling where the dimensions of the focal spot and waveguiding structures reach the lowest limit. However, sometimes is not easy to use such a technique in term of assembly of the different components.

While transverse coupling uses the edges of waveguiding structures to couple the light, surface coupling excite the waveguiding structures from their planar surfaces. Integrating gratings or prism at the end of those is possible to reach angles of incidence which are large enough to allow coupling of light directly from the surface of the waveguiding structure. In case of grating couplers [91,92], the incident light is diffracted at the periodic structure of the grating and split into a number of modes. Using this technique it is possible to couple the light into specific modes, but it is not possible to couple all the modes from the source. For this reason the efficiency of this technique is lower comparing it with the previous methods in case of multimode excitation but it is very efficient and useful for single mode excitation. An advantage of this technique is that it

avoids stray light to propagate into the system. However, a careful adjustment of the input coupling angle is necessary, moreover, integrating the grating coupler into a waveguiding structure is difficult.



**Figure 4-7: Grating coupling a) and Prism coupling b)**

In the prism coupler, (Fig. 4-7b) the incident light is guided inside the structure by internal reflection at the interface between the prism material and the gap between prism and waveguiding structure [93]. If an optical wave is incident into the prism at a certain angle, the interference between the incident and reflected wave results in a standing wave inside the prism thus forming a transverse field distribution traveling in the  $z$  direction that extends outside the prism and decays exponentially in the space separating the prism and the waveguiding structure. If the distance between prism and waveguide is sufficiently small, the wave is coupled to a mode of the waveguiding structure. In the same way it is possible to extract light from the waveguiding structure to the free-space. The prism coupling method needs a precise coupling angle alignment as well as good contact with the waveguiding structure. Moreover, the prism component is difficult to integrate. Using prism or grating coupler, if the angle of the incident light varies it is possible to excite specific modes in the waveguide [82].

Several groups have proposed different solutions for coupling light into microfluidic systems. The main solutions proposed are grouped in the table in the Appendix B .

In this thesis an optical connector plug that integrates optical fibers and lenses to ease and improve the efficiency in the transverse coupling has been designed, fabricated and tested as it will be described in Chapter 5 and 6.

## 5. Modeling

Often, the packaging of microfluidic systems is over-dimensioned resulting, in the best case in loosing the definition of microsystems since the package requires a lot of space but, in the worse case, this also leads to cracking of the chip. In other cases the packaging is under-dimensioned leading to malfunctioning of the system. Modeling is a valid tool that allows knowing in advance the behavior of certain parameters to analyze. The models facilitate the dimensioning of the interconnections allowing also to reduce until the limit of resistance the dimension of the package. Experiments will show the validity of the models.

### **5.1. *Fluidic interconnections***

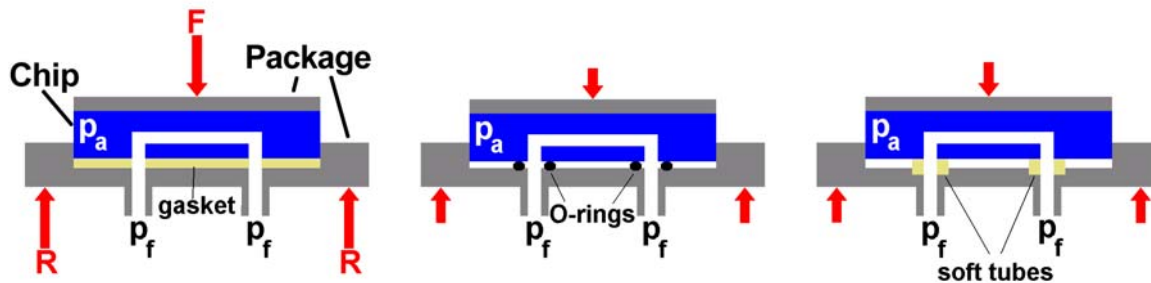
The fluidic interconnections, as mentioned before, can be divided in permanent and reversible interconnections. The first family comprises those interconnections based on welding or gluing. Often, these processes are made manually and it is difficult to reach reliable results.



The reversible interconnections are based on reliable manufacturing processes and they are readily amenable for modeling. In this section, two models will be shown, one will regard reversible external connections, and the second will consider integrated interconnections.

### 5.1.1. External interconnections modeling

When a system is connected externally in a reversible manner, gaskets, o-rings or soft tubes can be used for ensuring sealing at the interface between the system and the external tubes. The system can be connected from the side or from the top depending on its structure. The following picture shows a schematic model about how a system can be connected and the forces and pressures in play.



**Figure 5-1: Schematic model of interconnected microfluidic systems ( $p_a$  is the pressure at the interface due to the external applied forces  $F$  and  $R$  that press the system toward the package ensuring sealing,  $p_f$  is the internal pressure of the fluid)**

The model is based on the assumption that the applied external pressure ( $p_{ext}$ ) must be bigger than the pressure at the inlet of the system ( $p_{int}$ ) to prevent leakages. The pressure at the inlet is due to the resistance of the system itself and can be calculated as described in Chapter 3.

Comparing the internal pressure with the applied external pressure, it is possible to find a relation between the external force to apply for ensuring sealing that can be easily controllable by using a force sensor and the flow rate running into the system controllable, in this case by using a syringe pump. In fact, knowing the flow rate ( $Q$ ), it is possible to calculate the internal pressure at the inlet of the system, and knowing the applied external force it is possible to calculate the external applied pressure by dividing

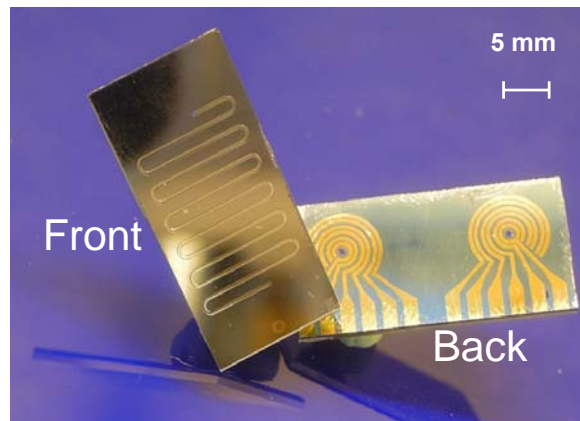
the force ( $F$ ) by the contact area ( $A_c$ ) between the system and the packaging that integrate the sealing method and external tubes by

$$P_{ext} = \frac{F}{A_c} > P_{int} = RQ, \quad (5-1)$$

$A_c = wh$  (bed of PDMS),  $A_c = \pi(r_o^2 - r_i^2)$  (silicone tubes and O-rings) where  $r_o$  and  $r_i$  are, respectively, external and internal radii of the silicone tubes or O-rings.

If the flow rate and the network of the system in terms of length and cross-sectional area are well know, it is possible to calculate which range of forces the package must stand, so it is easy to dimension it robustly, regarding its physical and mechanical characteristics for not having a leakage.

Leakage tests were performed on the external interconnections in order to experimentally confirm the models using a test chip. The chip simulated an integrated lab-on-a-chip system that fit in the packaging. It detects leakages in packages having fluidic and electrical interconnections. It has twelve circular coils manufactured in gold around two holes connected to the channels. It was produced in Si/Glass using clean room techniques as thermal oxidation for isolating the semiconducting silicon base, etching using masks and photoresists for production of the channels and through holes inside the silicon and deposition for depositing the gold electrodes on the bottom. Finally the lid made of glass has been bonded to the silicon wafer using high voltage anodic bonding.



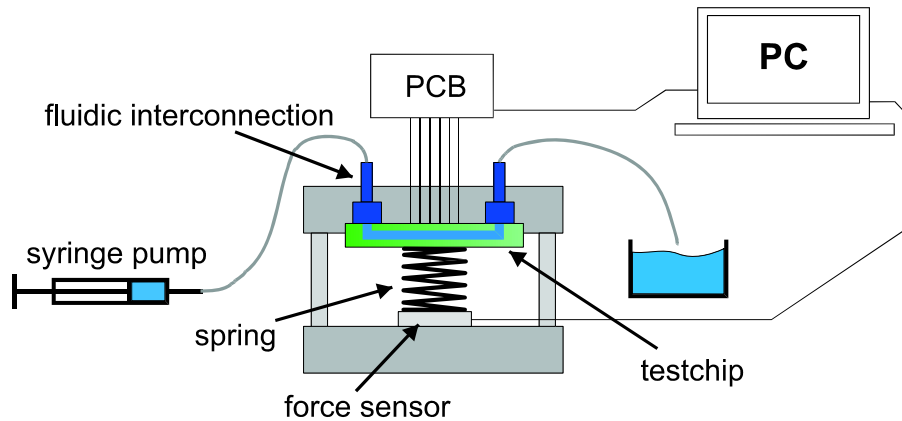
**Figure 5-2: Chip used for testing the fluidic interconnections**

As result of this process, different chips were produced with the dimension 20x10x0.9 mm and channels with width of 0.5 mm, 0.25 mm and 0.15 mm respectively. The length is 12 mm or 105 mm and the height is approximately 100  $\mu\text{m}$ . The following table shows the specific dimensions of each chip, their relative hydraulic resistance and how they are named.

**Table 2: Chip dimensions and resistances**

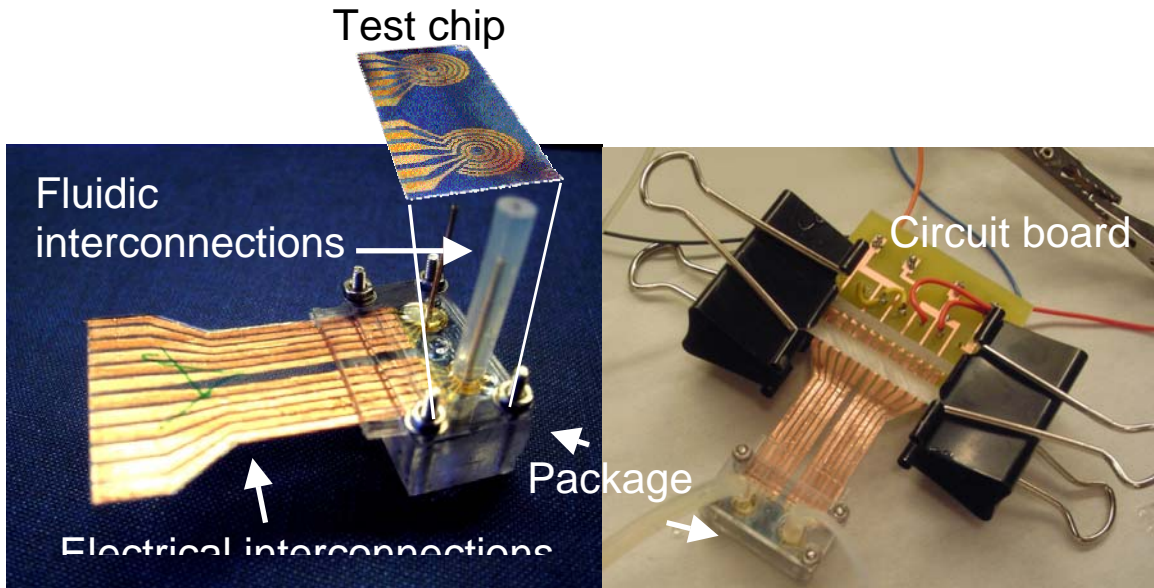
<u>Chip 1-6:</u> Length 12 [mm] Width 0.5 [mm] Height 100 [ $\mu\text{m}$ ] Resistance 2,89E+11 [N*s/m <sup>5</sup> ]	<u>Chip 7-9:</u> Length 105 [mm] Width 0.5 [mm] Height 100 [ $\mu\text{m}$ ] Resistance 2,53E+12 [N*s/m <sup>5</sup> ]	<u>Chip 0 and 16:</u> Length 12 [mm] Width 0.15 [mm] Height 100 [ $\mu\text{m}$ ] Resistance 9,62E+11 [N*s/m <sup>5</sup> ]
<u>Chip 10-12:</u> Length 105 [mm] Width 0.25 [mm] Height 100 [ $\mu\text{m}$ ] Resistance 5,05E+12 [N*s/m <sup>5</sup> ]	<u>Chip 13-15:</u> Length 1,20E-02 [mm] Width 0.25 [mm] Height 100 [ $\mu\text{m}$ ] Resistance 5,77E+11 [N*s/m <sup>5</sup> ]	

The chip was then attached to a holder that was provided with either o-rings, a PDMS-gasket, or silicone tubes. To apply a comparable stress to the different connection types, a force sensor in combination with a spring and 4 screws was used, as shown in the following picture.



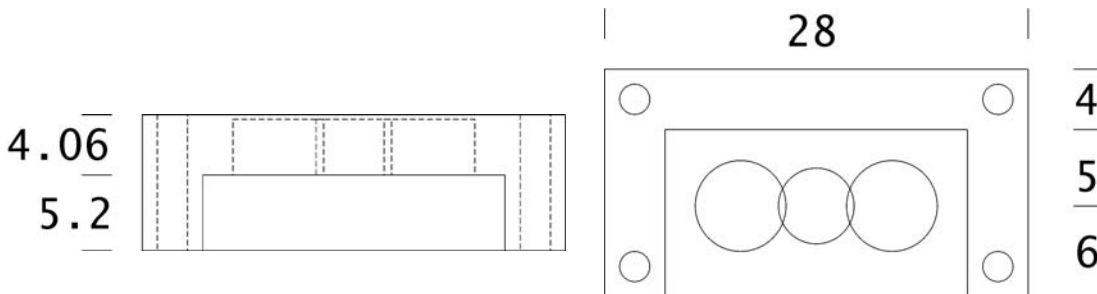
**Figure 5-3: schematic of the set-up used for testing the fluidic interconnections**

The test-chips were inserted into the holder, aligned to the interconnections, pressed and kept in position with the springs. Fastening the 4 screws resulted in a compression of the spring and therefore higher stress applied to the chip, which could be determined with the force sensor. Syringe pumps were used to pump liquid through the chips at various flow rates. In combination with the different channel dimensions of the test chip, pressures between 0 and 10 bar could be achieved. As liquid an aqueous soap solution was used, which, in case of leakage, bypassed the coils and immediately resulted in an increased conductance. The distance of  $100\mu\text{m}$  between the single coils ensured high sensitivity already to small leakages. For the electrical interconnections a copper tape glued onto a thin layer of PET or PMMA has been machined by photolithographic techniques as described in Chapter 2. The electrical interconnections were connected to a PCB board which was connected to a personal computer for recording the signal.



**Figure 5-4: Frame of the reversible package and zoom-in of the testchip.**

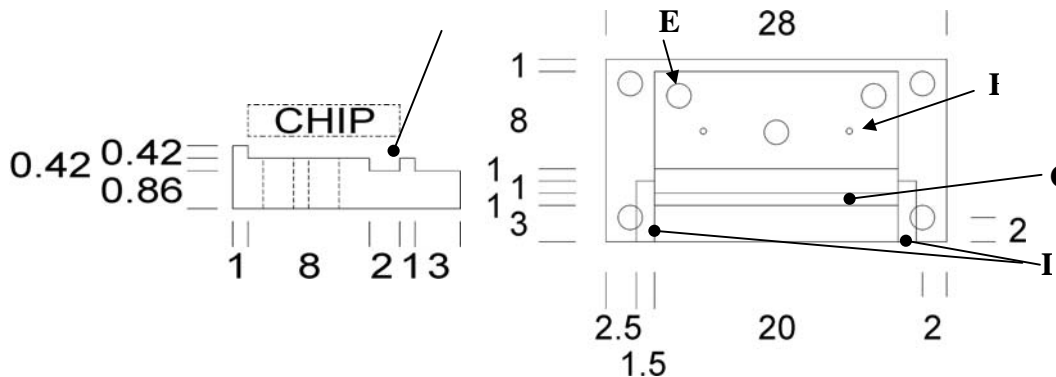
The upper part of the packaging was fabricated by milling in PMMA using the dimensions given in figure 5-5.



**Figure 5-5: The design of container after having added holes for spring guidance viewed from the side and top respectively (the dimensions are in mm).**

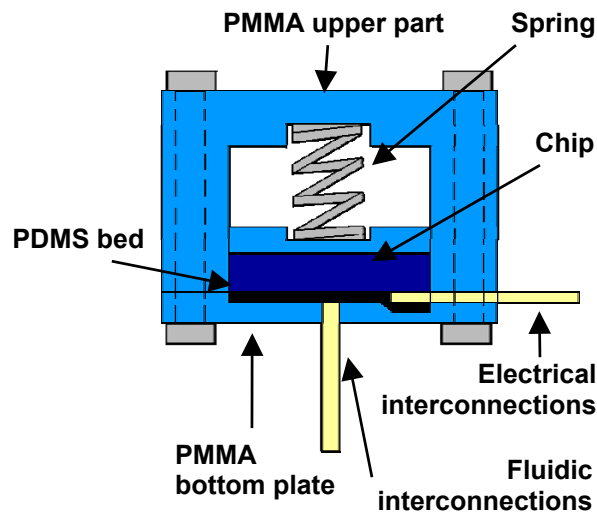
The lower part of the packaging has to be kept at dimensions that do not exceed 28x15 mm. When designing the bottom plates, it is important that the interconnections are produced in a manner, which ensures both even pressure on the fluidic part and also take into account that the alignment to inlets and electrodes is kept stable. In this case the bottom plates were fabricated in PMMA by laser machining. Three bottom plates (2 mm thick) were fabricated by laser machining for housing, respectively a PDMS bed, o-rings and silicone tubes.

The bed of PDMS, is embedded in the plate (Fig. 5-6: A). In order to secure alignment, the electrical interconnection is integrated in the PDMS-layer, which includes alignment pins that fit in corresponding holes in the plate as seen in figure 5-6: E. The two small holes are for the in- and outlet for the fluid having a diameter of 0.8mm (Fig. 5-6: B).



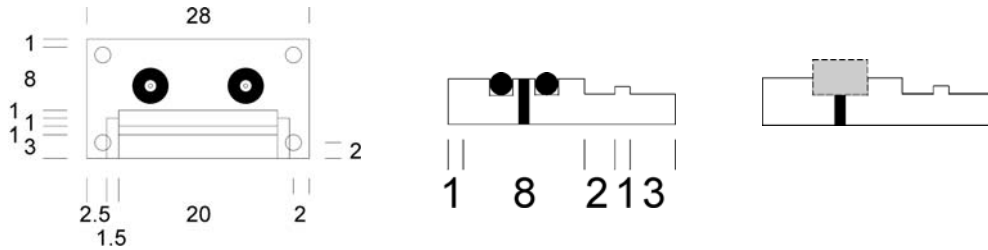
**Figure 5-6: Side and top view of the bottom plate for PDMS (The dimensions are expressed in mm): A is the place where the PDMS bed is housed, B are the inlets and outlets of the package, C is the barrier that press the electrical interconnections to the chip**

A small barrier has been made just outside the chip in order to press the plate of copper against the bottom of the chip (Fig. 5-6: C). The two small cavities on the side of the barrier seen on the top view are necessary to keep the different PDMS-parts together (Fig. 5-6: D), the softness of the base is constant under the chip as the PDMS-layer has the same thickness under the relatively stiff electrical interconnection as under the rest of the chip, resulting in an even pressure distribution (Fig. 5-7). Finally, external ferrules, used as external tube connections are glued in the bottom plate.



**Figure 5-7: Schematic side view of the assembled package using the PDMS bed**

A similar construction is chosen for the packaging using O-rings and silicone tubes. Figure 5-8 shows the two plates for the O-rings and the tubes.

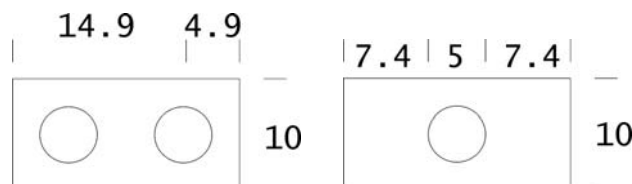


**Figure 5-8: The bottom plates for the O-rings seen from above and side and the bottom plate for the tubes sketched as seen from the side (The dimensions are in mm)**

The barrier of the O-ring model is lowered 0.25 mm in order to make the electrical interconnection softer and thereby concentrate most of the pressure on the rings. When unloaded the O-rings protrude approximately 0.48 mm above the surface, which is 0.06 mm more than the electrical interconnection allowing the rings to deform before the chip reaches the electrical interconnection.

Concerning the tubes, the electrical interconnection as well as the barrier have been lowered even more, as the tubes deflect more than the O-rings due to the soft material. Further more, the barrier has been moved slightly (0.35 mm) away from the chip for concentrating the pressure on the tubes. The tubes protrude unloaded 0.42 mm above the surface and are embedded 0.8 mm into the plates.

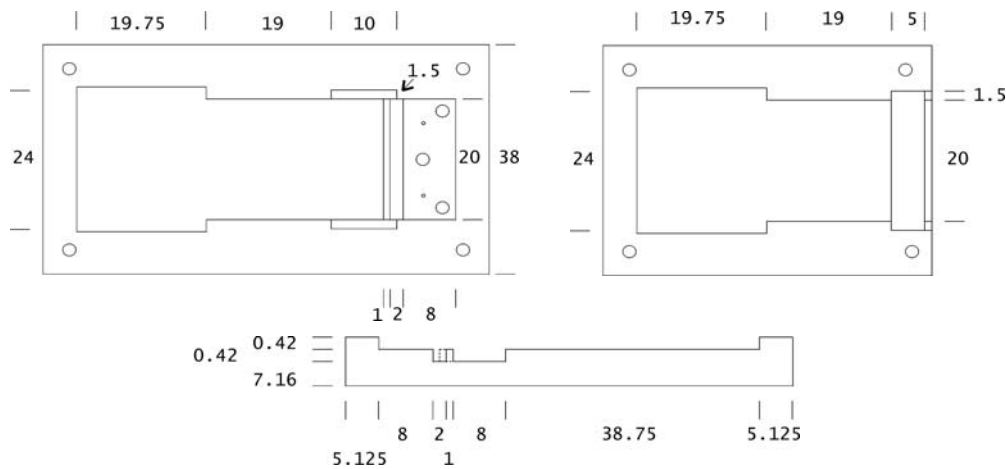
An even pressure on top of the brittle chip has been applied inserting a PMMA plate (2mm thick) between spring and chip fabricated by laser machining. Cavities on the topside of this plate have been machined, having the function of keeping the springs in position and perpendicular to the surface of the chip (Fig. 5-9).



**Figure 5-9: Two types of top plates made for even pressure distribution and control of spring position (the dimensions are in mm).**

The springs were pressed between this plates and the upper part of the package. The above described two configurations were used for having a wider range of external applied forces by varying the number of springs. The width of the plates is 19.8 mm whereas the chip and the inside of the upper part of the package is 20 mm. This has been done to make sure that the plates will not be stuck in the sides ensuring them to apply the required pressure.

The molds for casting the PDMS have the same dimensions as the cavities for PDMS in the corresponding bottom plates in order to fit the PDMS into these. Furthermore they must also be designed in a way, that the electrical interconnections are joined properly to the PDMS making a stable structure. A way to solve this problem is to make a belt of PDMS around the copper/PET-sheet outside the rest of the packaging system as shown in figure 5-7. The molds for the underside and the belt are shown in figure 5-10.



**Figure 5-10: The lower and upper mold for the PDMS construction seen for above and the lower mold seen from the side (The dimensions are in mm).**

The molds were fabricated in PMMA by laser machining.

The molds for the electrical interconnections integrated in the package where the O-rings and tubes were tested are the same of those used for the PDMS-construction, but the part for the PDMS bed is removed.

The PDMS was cast in the molds and put for two hours in a vacuum chamber for bubbles removal and then was baked in the oven at 80°C for the entire night in order to reach a Young modulus for the PDMS of  $E = 2.5$  MPa.

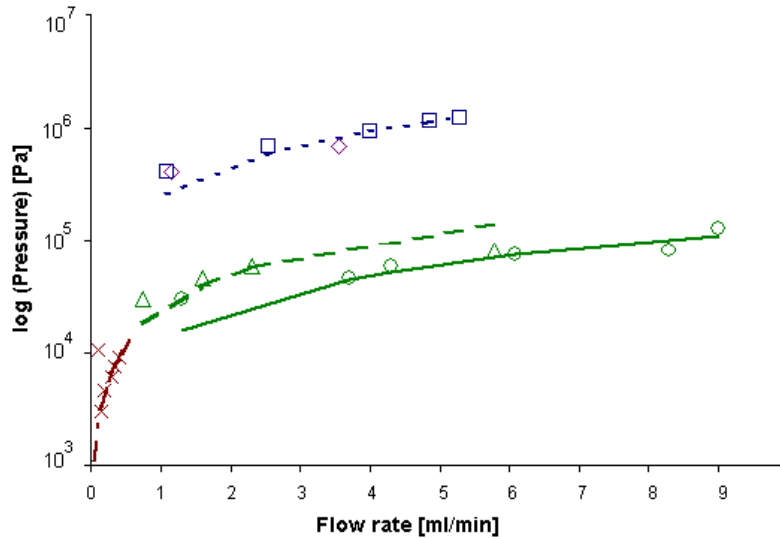


Two types of o-rings and silicone tubes having different dimensions were used for the tests as can be depicted from the following table showing the dimensions of the different sealing components used.

**Table 3: Dimensions and areas of sealing components**

PDMS bed:					
Length	20 mm				
Width	10 mm				
Thickness	0.42 mm				
Area	200 mm <sup>2</sup>				
O-ring:					
Outer radius	1.75 mm				
Inner radius	1.25 mm				
Area	9.42 mm <sup>2</sup>				
Silicone tubes 0.7	Silicone tubes 1	Silicone tubes 1.4			
Outer radius	0.35 mm	Outer radius	0.5 mm	Outer radius	0.7 mm
Inner radius	0.2 mm	Inner radius	0.3 mm	Inner radius	0.3 mm
Thickness	1.22 mm	thickness	1.22 mm	thickness	1.22 mm
Area	0.518 mm <sup>2</sup>	Area	1.01 mm <sup>2</sup>	Area	2.5 mm <sup>2</sup>

Leakage experiments were performed using the setup shown in Figures 5-3 and 5-4 and the package configurations described above to test the three types of reversible interconnections and mounting the sealing components described in table 3. The experiments match the theoretical predictions very well as shown in Fig.5-11. Each line represents the calculated internal pressure, corresponding with an equivalent applied external pressure, for each particular test chip used. The points represents the leakages observed at specific values of flow rates and applied external pressure mounting the different types of sealing components. A safe factor of 2 has been used into the model to consider the fabrication errors that didn't allow to have an ideal package.



**Figure 5-11: Experiments and theoretical prediction of the external interconnections: “—” “Theoretical internal pressure into the chips 1 to 6, “o” observed leakages using o-rings and chips 1 to 6, “- - -” Theoretical internal pressure into the chips 13 to 15, “▲” observed leakages using o-rings and chips 13 to 15, “.....”Theoretical internal pressure into the chips 10 to 12, “◆” observed leakages using silicone tubes ( $\Phi$ 1mm) and chips 10 to 12, “□” observed leakages using silicone tubes ( $\Phi$ 1.4mm) and chips 10 to 12, “— · —” Theoretical internal pressure into the chips 1 to 6, “x” observed leakages using PDMS bed and biochips (the pressure is in log scale).**

It has been seen that the silicone tubes can ensure a sealed contact even at very high pressures built up with a conventional syringe pump. No leakage has been observed on silicon tubes with a pressure of up to 1.23 MPa. The o-rings ensure a seal contact at a relatively high pressure (0.14 MPa) while the bed of PDMS leaks already at a low pressure (10000 Pa), since it has a large contact area between chip and interconnection. Therefore it needs a strong external force, to ensure an external pressure higher than the internal pressure of the chip as depicted in Equation 5-1, that deflect the package causing leakage. The silicone tubes show the big advantage that they ensure a seal contact also at high external forces and so in presence of the deflection of the package. In fact the tubes follow the deflection of the package maintaining an adherent contact to the chip, while the o-rings seem to suffer from inhomogeneous distribution of the stress inside the package and a deflection of the structure, moreover they introduce high dead volumes.

The fact that the PDMS gasket leaks at relatively low pressure, doesn't mean that it is a weak connection method, but that it needs a stronger packaging configuration that doesn't deflect at certain values of external forces. On the other hand, this method is readily

amenable for high density interconnections, low dead volumes and ensures a more even pressure all over the system preventing it from bending stresses that in some cases can cause the chip breaking [94].

### 5.1.2. Integrated interconnection modeling

As mentioned in Chapter 4, integrated fluidic interconnections bring to more practical solutions than external fluidic interconnection and are, usually, convenient to fabricate into polymer microfluidic systems. A new type of integrated fluidic interconnection is presented and modeled, composed of custom-made cylindrical rings that can be integrated in a polymer housing next to the fluidic ports of the fluidic system allowing a plug&play functionality between external tubes and the system (Fig.5-13).

An integrated reversible fluidic interconnection can be schematically represented by the following sketch.



**Figure 5-12: Schematic cross-sectional view of the *plug'n'pump* fluidic interconnection(left) and description of the parameters involved into the model (right)**

The integrated fluidic interconnection was modeled as a function of the interference between o-ring-ferrules ( $\delta_{ferrules}$ ) and o-ring-frame ( $\delta_{frame}$ ) and the internal pressure ( $P_{int}$ ) as seen in the Equation 5-2 deduced by the theory of axial symmetric bodies [95].

The model is based on the assumption that the pressure at the interface between the ferrules and the rings ( $p_{ferrule}$ ), and the frame and the ring ( $p_{frame}$ ) must be bigger than the pressure at the inlet of the system ( $p_{int}$ ) in order to prevent leakages. The pressure at the inlet is limited by the hydrodynamic resistance of the system itself, or by the performance of e.g. the pump used in the system. A pressure at the interface between ring

and frame occurs when the outer radius of the ring is bigger than the radius of its housing, while the pressure at the interface between ring and external tube exists when the internal radius of the ring is smaller than the outer radius of the tube.

The internal pressure can be calculated as a function of the flow rate, or can be detected by a pressure sensor. The external pressure at the interface between frame, ring and ferrule is a function of the dimensions and the material properties of the different components constituting the fluidic interconnections. Comparing the two pressures, it is possible to dimension the interconnection to withstand a given pressure.

When the ring is fitted in the polymer frame, it will be deformed of a quantity

$$\delta_{frame} = r_{frame} \epsilon_{ring} \quad (5-2)$$

Similarly, when the tube is inserted in the ring there will be a deformation

$$\delta_{ferrule} = r_{ferrule} \epsilon_{ring} \quad (5-3)$$

assuming that the polymer frame and the external tube will not deform and assuming that  $\epsilon_{ring}$  is the tangential unit strain of the elastomeric ring given by

$$\epsilon_{ring} = \frac{1}{E} (\sigma_t - \nu \sigma_r) \quad (5-4)$$

where  $E$  and  $\nu$  are, respectively, the Young's modulus and Poisson ratio of the ring,  $\sigma_t$  and  $\sigma_r$  are, respectively, tangential and radial stress due to the compression of the ring. The tangential and radial stress, according to the theory of the axial symmetric body [32], will have behaviour along the radial direction of the ring given by

$$\sigma_r = A + \frac{B}{r^2} \quad (5-5)$$

$$\sigma_r = A - \frac{B}{r^2} \quad (5-6)$$

where  $r$  is the radial coordinate, and  $A$  and  $B$  are constants that can be determined by the boundary conditions at the interface between frame-ring and ring-tube.

At the interface between frame and ring,

$$\begin{aligned} A &= \frac{p_{frame} r_o^2}{r_o^2 - r_i^2} \\ B &= \frac{p_{frame} r_i^2 r_o^2}{r_o^2 - r_i^2} \\ r &= r_{frame-ring} = r_{frame} \end{aligned} \quad (5-7)$$

where  $p_{frame}$  is the pressure at the outer interface when the ring is forced into the housing and  $r_{frame-ring} = r_{frame}$ . The outer radius of the ring is set to the radius of the frame, which is rigid.

In the same manner, at the interface between ring and external tube,

$$\begin{aligned} A &= \frac{p_{ferrule} r_i^2}{r_o^2 - r_i^2} \\ B &= -\frac{p_{ferrule} r_i^2 r_o^2}{r_o^2 - r_i^2} \\ r &= r_{ring-ferrule} = r_{ferrule} \end{aligned} \quad (5-8)$$

where  $p_{ferrule}$  is the pressure induced between the ring and the ferrule when the tube is forced in the ring and  $r_{ring-ferrule} = r_{ferrule}$ . The ferrule does not deform, while the inner radius of the ring will be enlarged.

Substituting (5-8) and (5-7) in (5-6) and (5-5) we obtain the stresses in the ring as a function of the pressure at the interface. Using these in (5-4) and substituting the results in (5-3) and (5-2) it is possible to calculate the pressure at the interface between the

frame, the ring and the tube as a function of the mismatches given by the difference in radius between frame-ring and ring. To ensure sealing, we can write that

$$\min \left\{ \begin{array}{l} P_{frame} = \frac{E\delta_{frame}}{r_{frame}} \left[ \frac{(r_{frame}^2 - r_i^2)}{r_{frame}^2 + r_i^2 - \nu(r_{frame}^2 - r_i^2)} \right] \\ P_{ferrule} = \frac{E\delta_{ferrule}}{r_{ferrule}} \left[ \frac{(r_o^2 - r_{ferrule}^2)}{r_{ferrule}^2 + r_o^2 - \nu(r_o^2 - r_{ferrule}^2)} \right] \end{array} \right\} > P_{int} \quad (5-9)$$

Using this equation is possible to dimension the fluidic interconnections in function of the geometric specifications, the material properties of the elastomer and the mismatches between polymer housing, ring and external tubes and the pressure inside the system.





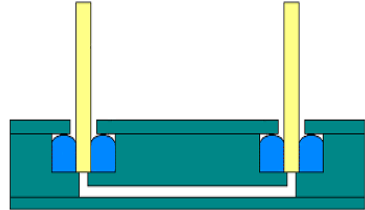
This model does not consider the contribute that the pressure induced between ring and ferrule transfers at the interface ring-frame and vice versa. This approximation becomes more realistic as the thickness of the ring increases. In fact, along the radial direction, the stress decreases (equation 5-5 and 5-6) when going away from the point where the pressure is generated. Anyway, the neglected term brings a positive contribution to the dimensioning of the interconnection, since it builds more pressure at the interface, thus making the interconnection itself more resistant to leakage. The model also does not consider the errors and uncertainties stemming from fabrication defects and flaws. In addition, the height of the ring is not correlated to the model which assumes a homogenous contact all around the interface. In reality, there are always some defects in the structure creating inhomogeneities.

Once the external tubes are inserted into the frame, a mismatch is created between them and the rings creating a pressure at the interface ensuring sealing

The assumption is that the pressure developed at the interface between rings, tubes and frame given by the mismatch in dimension between those three elements, must be bigger than the internal pressure at the inlet of the system to ensure sealing.

A test chip has been fabricated in PMMA, integrating fluidic interconnections for testing purposes in order to confirm the model. The cylindrical rings were made by casting, in polycarbonate (PC) molds fabricated by micromilling technology, the Sylastic ® RVM elastomer (Dow Corning) which has been left at room temperature for 24 hours to

polymerize in order to get a Young modulus of  $E=2.5$  MPa. The test chip has been fabricated by micromilling following the process described in figure 5-11. It is composed of 3 PMMA layers and it contains a simple fluidic network with channels  $100 \mu\text{m}$  wide and  $100 \mu\text{m}$  deep.

Step	Description
	Machining of the housing for the rings, in the second PMMA layer 5cm x 3 cm wide and 5mm thick. The housing has a cylindrical shape having a diameter of 5mm and it is 3.5 mm deep.
	Machining on the bottom side of the PMMA layer of the through holes (0.8 mm in diameter) and the fluidic network
	Insertion of the rings in the polymer housing
	Thermal bonding of the first lid (1.5 mm thick) for keeping in place the rings and of the third lid (1.5 mm thick) for sealing the fluidic network
	Insertion of external metal tubes (0.45 mm of outer radius and 0.4 mm of inner radius)

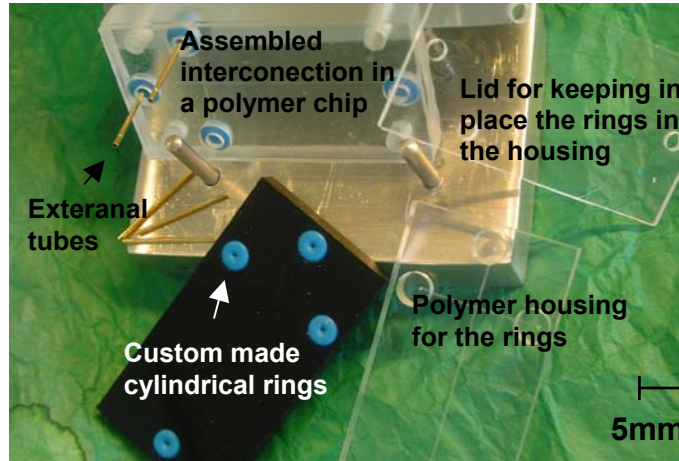
**Figure 5-13: Schematic representation of the different steps for fabricating and assembling a polymer chip with integrated fluidic interconnections**

The first layer is a lid for the second layer where the fluidic network, the housing for the custom made cylindrical rings and the through holes, are machined. The third layer is a lid for keeping in place the rings.

All layers are bonded together thermally by applying pressure ( $\sim 0.5$  MPa) and annealing them in an oven for 1 hour at a temperature of  $111^\circ\text{C}$ . The bond energy reached by using such a bonding method can be estimated to  $40 \text{ J/m}^2$  [96, 97]. Metal pins allow alignment of the different polymer layers with a precision of  $50 \mu\text{m}$ .

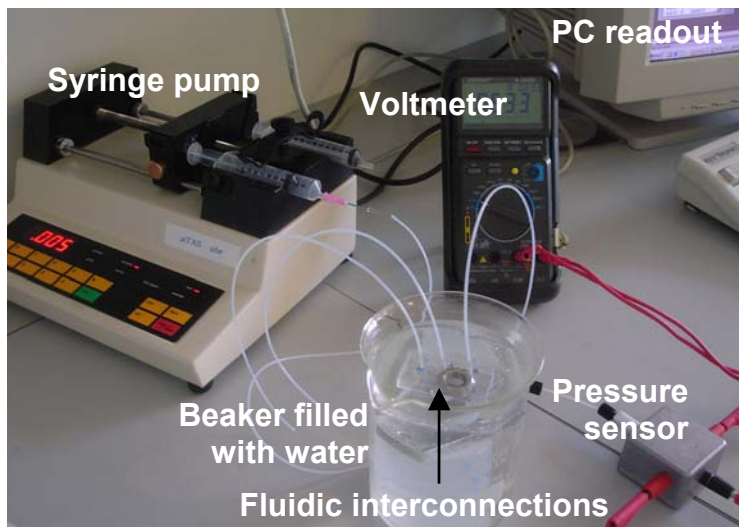
Different cylindrical rings have been fabricated having different inner radii in order to have different mismatches when the external tubes were inserted to vary the pressure at

the interface and making possible the experimental study on the model. In particular, a length of the rings of 3.5 mm and an outer radius of 5.5 mm has been kept constant in the fabrication, while the inner radius has been varied. Rings with inner radii of 0.05, 0.15, 0.25 and 0.35 mm have been fabricated in order to have a mismatch at the interface rings-tubes of, respectively, 0.4, 0.3, 0.2 and 0.1 mm.



**Figure 5-14: Integrated fluidic interconnections house in a polymer test chip**

Static tests have been performed in the integrated interconnection assembled in the test chips for the different sized rings, using a pressure sensor, clogging the outlet of those chips and pumping air by using a syringe pump, for detecting the pressure drop if leakage occurs. The fluidic interconnections have also been immersed into a beaker filled by water in order to detect the location of the leakage looking at bubble formation. In the following picture the set-up for the leakage testing is shown.

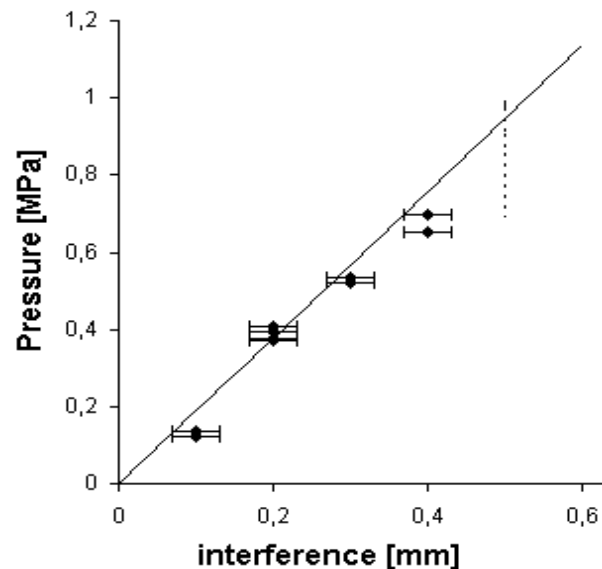


**Figure 5-15: set-up used for performing statci tests on fluidic interconnections**



The experiments, as can be seen in Figure 5-16, fit the theoretical prediction very well [87]. The line in the figure is the calculated pressure at the interface between rings and external tubes in function of their mismatches. Leakages occur if the internal pressure, increased by pumping air in the clogged system, is higher than the calculated pressure at the interface. The points in the figure are the detected pressure drops by using rings having different inner radii. It can be seen that when the mismatch between rings and tubes increases the pressure drop is detected at higher values of the static pressure and the point follow very well the trend of the line.

Moreover, the experiments show that the integrated interconnections could reach the operational limits of the pressure testing set-up of 0.7-0.75 MPa without any leakage using rings without holes in the middle having a mismatch of 0.45 mm with the tubes.



**Figure 5-16: Experiments and theoretical prediction of the integrated interconnection : “ — — — ” “Theoretical pressure at the interface ferrules-o-rings; “- - - -” “Theoretical pressure at the interface frame-o-rings, “♦” observed leakages.**

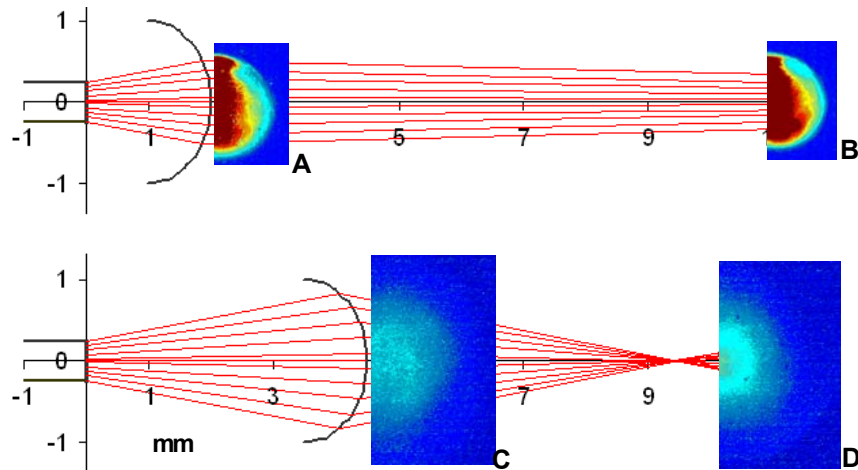
The dashed line in Figure 5-16 represents the theoretical pressure at the interface frame-rings, considering the constant mismatch that there are between rings and frame of the fabricated test chips. That mismatch has been designed to give a pressure at that interface that is bigger than the pressure developed at the interface between rings and tubes. In this way, the analysis could be concentrated just on the internal interface between rings and tubes, being more critical. The leakages were all observed by bubble formation at the interface between rings and tubes, according to the above mentioned assumption.

## 5.2. Optical connector plugs

As it has been explained in chapter 4 a good method for coupling light into waveguides or detection points from optical fibers is to use lenses. An optical connector plug is presented and modeled in this section. The optical connector plug integrates several fibers on one side aligned to an identical number of PDMS spherical lenses on the other side and everything is embedded in PDMS.

Ray optics theory is used to develop a two-dimensional model of the optical connector plug that considers the radius ( $R$ ) of the lens, the radius ( $r$ ) and the numerical aperture ( $NA$ ) of the fiber, the relative position between the fiber and the lens ( $x_0$ ), the refractive index ( $n_1$ ) of the material used for the plug, and the refractive index of the medium in which the light propagates after the plug ( $n_2$ ), (see Fig. 3-5).

Using Equation 3.18 of Chapter 3 it is possible to estimate the theoretical trajectory of a ray of light through the plug, creating an angle  $\theta_1$  with the x axis and meeting the lens at a point of height  $y$ , as well as its propagation after the plug. The height  $y$  can be calculated considering the intersection between the line representing a specific ray and the circle representing the lens, while the angle  $\theta_1$  can be calculated knowing the numerical aperture of the fiber and the refractive index of the plug.



**Figure 5-17: Comparison between the ray tracing model and images of the distribution of light through the two plugs (A, B, C, D). The images of the distribution of the light were recorded by a CCD connected to a microscope which has been focused at different distances from the plugs. The plugs were mounted perpendicular to the objective of the microscope. The different colors of the recorded images represent different intensities of light. The ray tracing model and the distances, at which the recorded images are attached to the model, are in scale.**

Two optical connector plugs have been fabricated having the optical fibers at two different distances from the lenses. The two plugs were used for making experiments to study the behaviour of the light through them. They were fabricated for having a distance between fiber and lens, of 3.5 mm and 1 mm, in order to get focusing or collimation of light, respectively, in accordance with the model. The process to fabricate those and the different dimensions and parameters related with them are described deeply in chapter 6. To compare the model with the propagation of light through the plugs, they were mounted on a stage and placed perpendicular to the objective of an optical microscope (ZEISS Axiovert 200 inverted fluorescence microscope) connected to a CCD camera (AVT Marlin F-046C, SVGA 780 x 582). The opposite ends of the fibers were connected to a laser diode ( $\lambda = 637\text{nm}$ ,  $P=7\text{mW}$ , Thorlabs) and the distribution of light through the plugs was recorded [98].

For the first type of connector two images were recorded at different distance from the plug, the first image was recorded focusing the microscope on the lens of the plug (Fig5-17:A) and the second at a distance of 8mm from that position (Fig. 5-17:B). The images showed that the area of the distribution of light is maintained constant and so the lateral distribution of light, even at certain distance from the plug, demonstrating collimation of light. For the second connector, again, images of the distribution of the light were recorded focusing the microscope on the lens of the plug (Fig. 5-17:C), but the second image was recorded, this time, when the smallest spot of the light was reached (Fig.5-17:D), the distance from the lens of the plug at which the image was recorded which represent the focal length of the lens was estimated to be 5.5mm while theoretically, in accordance with the model should correspond to 5mm. The second experiment showed a more intense light and distribution within a smaller spot in the second recorded image than the distribution of light recorded in the first image , demonstrating focusing of light. In general, the images of the lateral distribution of light follows the ray traces of the model quite well (Fig. 5-16), showing that it is possible to collimate or focus the light at specific locations as a function of the distance between the fiber and the lens.

The difference in distance between the focal spot showed by the model and the one found experimentally was probably due to diffraction phenomena caused by defects in the lens.

## 6. Microfluidic motherboard

As mentioned in Chapter 4, integrating and interfacing optical elements is a difficult task [99]. On the one hand, the interface from micro and macro world must be mechanical stable, inexpensive, small and easy to use.

On the other hand, the signal-to-noise ratio must be kept high, which means that the insertion, propagation, coupling losses and stray light must be minimized.

These issues become more critical if optics and fluidics must be interfaced and assembled together at the same time.

To solve these problems a motherboard including fluidic and optical interconnections has been designed, fabricated and tested [12].

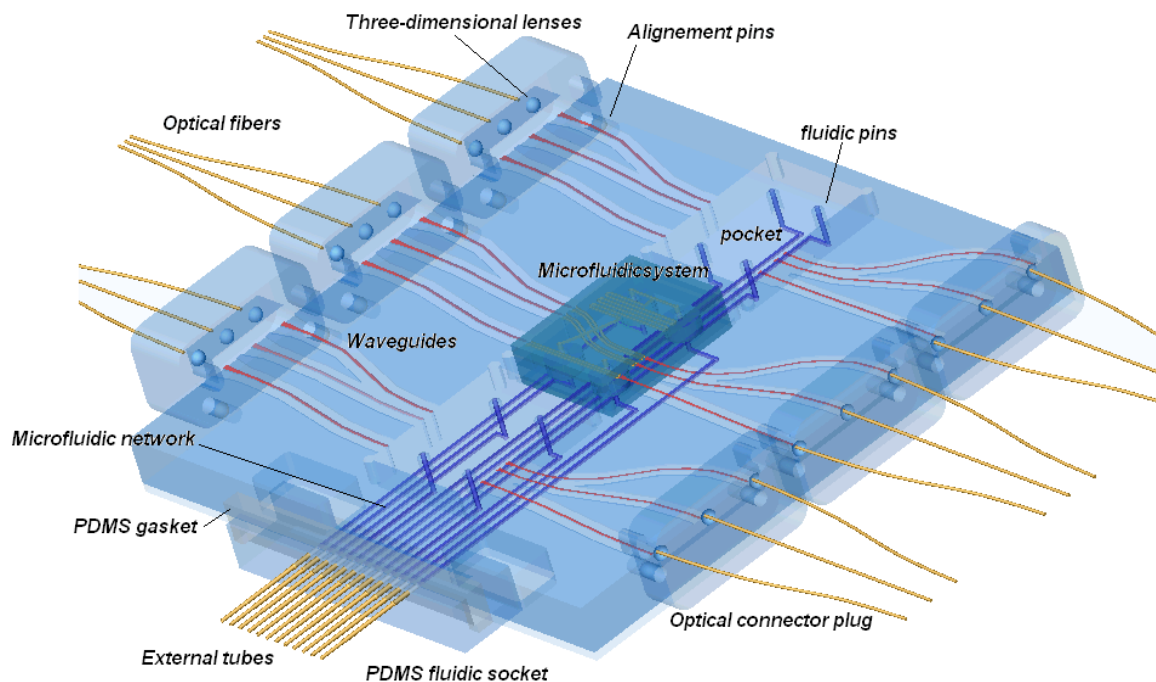
The motherboard can provide connection of several microfluidic systems for multiplexed and simultaneous analysis as well as can function as modular network for microfluidic chips allowing to perform complex microfluidic processes, where each microchip has a particular function. In this work, the motherboard has been designed to accommodate three microfluidic systems, each containing four fluidic ports.

The motherboard can be divided in:

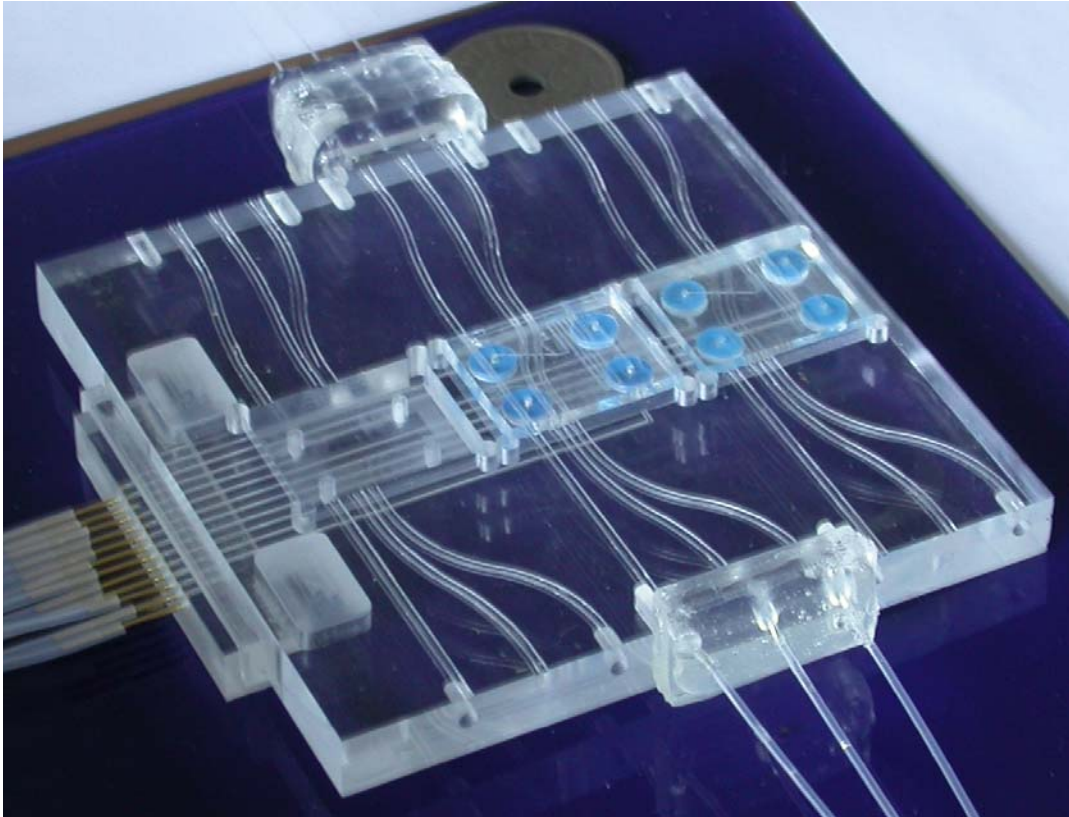
- a main body, having:

- a fluidic network in the bottom side and through holes to the top-side;
- 3 pockets for the chips having four pins each, concentric to the through holes, that will be aligned to the fluidic ports of the chips on the top side (Fig.6-20);
- 18 waveguides, 6 for each chip on the top-side to drive the light in and out of the chip (Fig. 6-24);
- holes to the side allowing to fix the optical plugs (Fig. 6-15);
- a PMMA lid for sealing the networks;
- an external PDMS fluidic socket to connect external tubes with the microfluidic network of the motherboard;
- integrated fluidic interconnections to connect the microfluidic network from the motherboard to the chip;
- external optical connector plugs, to connect external fibers to the waveguides of the motherboard;
- fluidic systems;

A three dimensional view of the motherboard is shown in the following picture.



**Figure 6-1: Three-dimensional view of the motherboard designed using a CAD software.**



**Figure 6-2: Three-dimensional view of the motherboard which has a size of 10X10 cm<sup>2</sup> and is 1 cm thick.**

### **6.1. Fabrication**

The motherboard (Fig 6-2) has been fabricated in PMMA by using a CNC-milling machine (Fig. 6-3)[100].

The design of the motherboard (Fig. 6-1) has been done by using the CAD-software Solidworks. The design has been exported in dxf format to the CAM software Dolphin 3D CAM which allows to set the parameters to manufacture the motherboard. The informations from this software are sent to the CNC-machine in the form of NC language. Since of its flexibility regarding ease of changing parameters and design, the milling machining is an optimum tool for prototyping purposes. Moreover it allows to fabricate three-dimensional macro-features and micro-features, which is important especially when dealing with interfacing the macro to the micro world. In particular, an air turbine motor has been mounted on the machine that can run at a velocity up to 30.000 rpm allowing the use of micro-tools down to 25 $\mu$ m in diameter. The roughness that can be reached, optimizing all the parameters is around 200 nm.

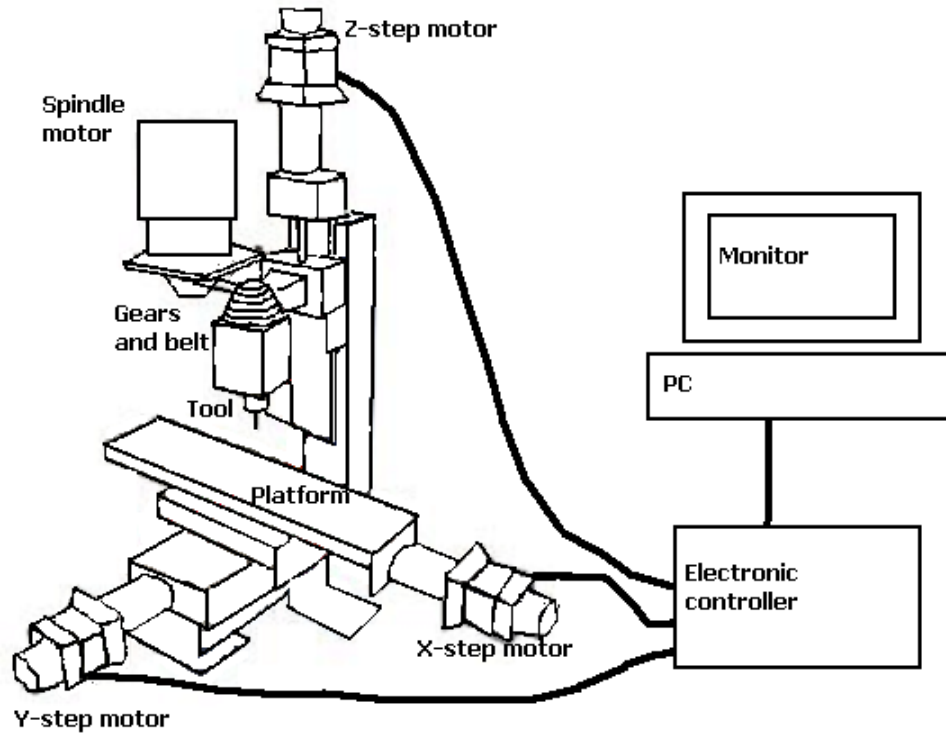

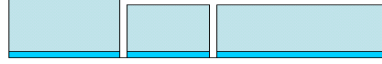

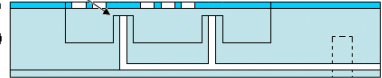


Figure 6-3: Sketch of the milling machine used

## 6.2. Main body

Since the main body must be machined on all the sides, in order to machine the features in the proper position, it is important to set the coordinates of the features properly, so that it is possible to know how to align the plate in respect to the machine each time the side of the plate must be changed. The alignment is done optically using a microscope mounted on the machine.

The main body of the motherboard has been made of a PMMA plate 10x10 cm<sup>2</sup> wide and 8 mm thick. In the following sketch the different processing steps are shown.

Steps	Description
1) 	Spinning-on of 100 $\mu\text{m}$ thick layer of PMMA+SAN
2) 	Machining of the fluidic network and through-holes from the backside
3) 	Thermal bonding of a PMMA lid for sealing the network and machining of the pocket for fixing the PDMS fluidic socket
4) 	Machining of the housing of the chip including the pins and the waveguides

**Figure 6-4: Schematic representation of the different steps for fabricating the main body**

The bottom side of the plate has been machined for creating a fluidic network consisting of 12 channels each 400  $\mu\text{m}$  wide and 400  $\mu\text{m}$  deep. On the same side, 12 through holes to the top side of the plate, having a diameter of 800  $\mu\text{m}$ , have been machined in correspondence of the end of each fluidic channel. The holes are aligned on the top with the fluidic ports of the chip.

Subsequently, a PMMA lid 10x10  $\text{cm}^2$  and 1.5 mm thick has been bonded thermally to the bottom side of the machined plate, to seal the fluidic network. The bonding has been performed by pressing the two plates together in a press, applying a pressure of roughly 50 KPa and placing the apparatus in the oven at 111  $^{\circ}\text{C}$  for 1 hour.

After that, the plate is fixed, aligned to the machine and the top-side is machined in order to fabricate the pockets (housing) for the chips and the waveguides.

The pockets are fabricated by using a tool of 3mm in diameter and they are 2.5x2.75  $\text{cm}^2$  wide and 5.1 mm deep. The pins in the pockets have a height of 3.2 mm and a diameter



of 2mm. The height of the pins is important because it regulates the alignment of the waveguide from the chip to the motherboard along the axis perpendicular to the motherboard.

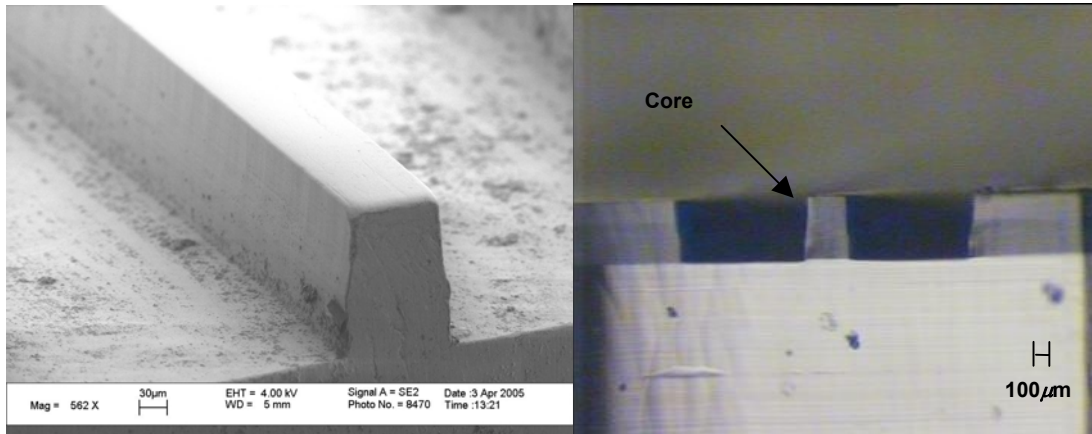
### **6.3. Waveguides**

The waveguides have the function to distribute the light from a small area in the chip to a bigger more manageable one, allowing at the same time to avoid stray light. They also allow having a perfect alignment inside the channel where the light is coupled for performing absorbance or fluorescence measurements.

#### **6.3.1. Fabrication**

As explained in Chapter 3, in order to have waveguiding properties, it is important to have a difference in refractive index between core and cladding. In particular the refractive index of the core must be higher than that of the cladding. The first issue to solve is to give a double index property to the top-side of the motherboard. In order to do so, a 100 $\mu\text{m}$  thick layer of PMMA with a higher refractive index has been spin-coated on the top of the PMMA substrate. To modify the refractive index of PMMA, it has been ‘doped’ with styrene-acrylonitrile copolymer (SAN). In this way the refractive index can be varied between 1.49 (100% PMMA) and 1.56 (100% SAN). This refractive index has been measured for a wavelength of 632 nm [101]. For the motherboard a percentage of 80% PMMA and 20% SAN has been used.

This method allows to give waveguiding properties to the top-side of the motherboard. Again, the CNC-machine has been used to shape the waveguides on the top-side of the motherboard, by milling two parallel grooves 250 $\mu\text{m}$  deep with a distance of 200  $\mu\text{m}$  between them using a 0.8mm milling tool. There have been 18 waveguides machined, 6 for each chip of which 3 guide the light in and 3 guide the light out (Fig. 6.25).



**Figure 6-5: SEM picture of the waveguide (left), section of the waveguide (right)**

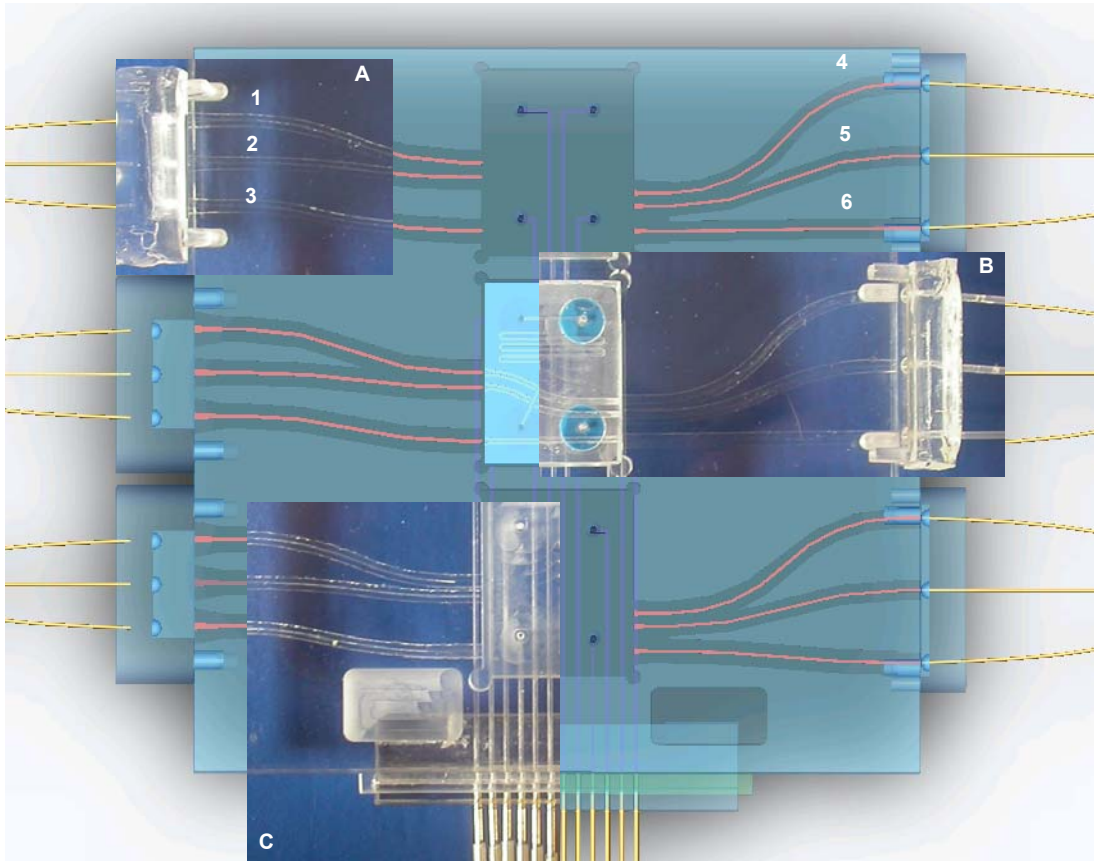
The waveguides have an average length of  $\sim 4.5$  cm and they are bend.

The bending has the function of distributing the optical signal on a larger more manageable area and it allows to avoid stray light during the analysis.

As explained in Chapter 3, to minimize the loss in the bending is important that  $R/\rho > 10^3$  where  $R$  is the radius of curvature of the waveguide and  $\rho$  is half width of the waveguide having a critical angle  $\theta_c = 0.1$ .

In our case  $\rho = 0.1$  mm and the waveguides should have a minimum radius of 100mm but since the critical angle is, this time,  $\theta_c = 0.84$ , there is more tolerance and the waveguides were designed having radii ranging from 20mm (Fig.6-6: 4) to 620mm (Fig. 6-6: 6).

Moreover, tapers have been fabricated at the inlet of the waveguides (Fig. 6-15 and 6-25) to facilitate the coupling of light even with a slight misalignment of the light source. In order to couple all the light from the taper into the waveguides a minimum length of those must be respected (see Chapter 3).



**Figure 6-6: Picture of the topside of the motherboard and comparison between designed motherboard and the prototype (A,B,C). 1,2 and 3 are the waveguides where the light from the optical connector plug goes into the chip. 4,5 and 6 are the waveguides which drive the light from the chip into the optical connector plugs.**

In our case, considering that the light enters the taper at an angle  $\theta_0=0$ , the width of the waveguide is  $200\mu\text{m}$  then  $\rho=100\mu\text{m}$ , the width of the taper at the beginning is  $0.5\text{mm}$  then  $\rho_0=250\mu\text{m}$ , the critical angle considered at the interface waveguide air is  $\theta_c=0.84$  then  $L_{\text{min}}$  (see Eq. 3-15) will be equal to  $0.267\text{mm}$  which is the minimum length to use to couple all the light from the taper. For not exiting the highest modes, a length of  $3\text{mm}$  for the tapers has been chosen. The tapers at the inlet of the waveguides that drive the light to the photodetectors has been designed to have a  $\rho_0=150\mu\text{m}$  but the length of the taper  $L$  has been chosen to be  $3\text{mm}$  as well remaining in a more safe conditions.

### 6.3.2. Characterization and experiments

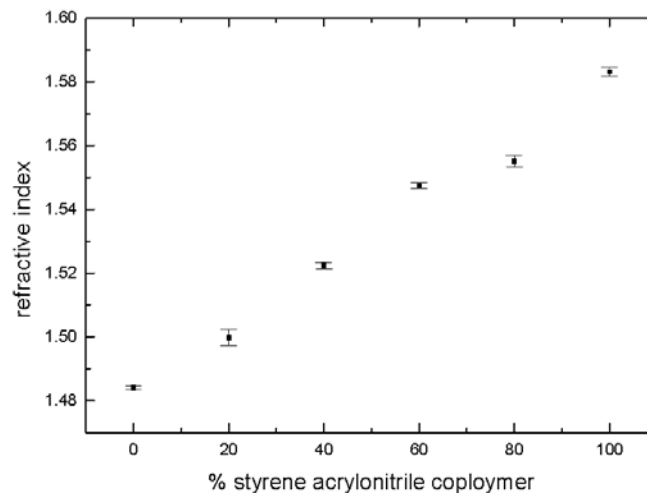
The doping process consisted of dissolving a specific percentage of PMMA and SAN in anisole (methyl-phenyl-ether). Six different mixing ratios of PMMA and SAN, dissolved in 60ml of anisole, were investigated as shown in Table 4.

**Table 4: different ratios of PMMA and SAN investigated**

PMMA	SAN
0%(0 g)	100%(30 g)
20%(6 g)	80%(24 g)
40%(12 g)	60%(18 g)
60%(18 g)	40%(12 g)
80%(24 g)	20%(6 g)
100%(30 g)	0%(0 g)

Anisole has been chosen as solvent due to its high boiling point and consequent long evaporation time. This allows to have good film qualities once the doped PMMA is spun-on. The doped PMMA in different percentage has been spun onto a PMMA substrate using different velocities and the thickness of the doped PMMA has been investigated to determine the spinning-curves.

A prism coupler has been used to measure the refractive indices of the different ratios of doped PMMA (see Fig. 6-7). In order to do that a very thin layer ( $\sim 4\mu\text{m}$ ) of the different doped PMMA spun-on silicon wafer have been used.



**Figure 6-7: Measured refractive indices in relation with the ratio PMMA+SAN used**

The optical properties of the milled waveguides have been investigated by determining the propagation loss. In order to do that a deuterium-halogen light source and a spectrometer were connected to optical fibers that were aligned to the waveguides using xyz-stages. The transmission spectrum of waveguides with different length was determined between 380 and 850 nm.

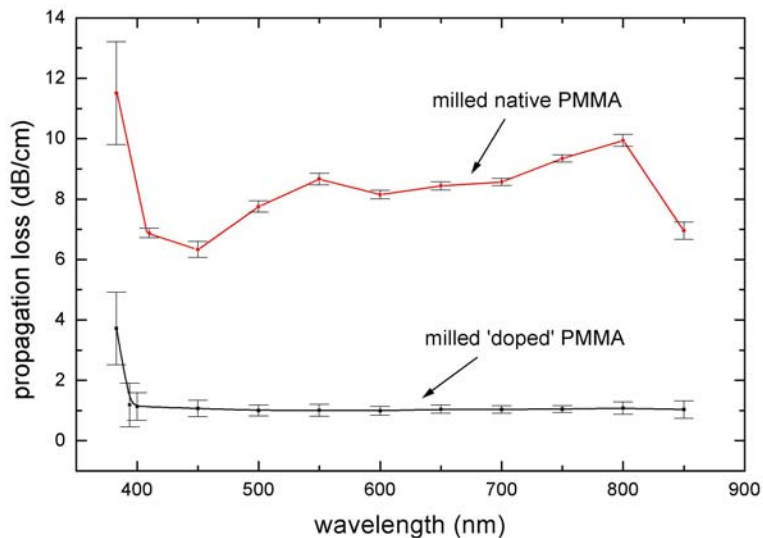
A reference spectrum of the light source has been used to normalize the measured spectra and the total insertion loss of the waveguide has been calculated as

$$a = -10 \log \frac{P_{\text{waveguide}}}{P_{\text{reference}}} \quad , \quad (6-1)$$

where  $P_{\text{waveguide}}$  and  $P_{\text{reference}}$  are the measured radiated power of, respectively, the waveguide and the reference.

A linear fit of the insertion loss versus waveguide length was calculated to obtain the propagation loss (dB/cm) as a function of wavelength.

Keeping the optical losses low is important for having high transmittance and therefore a high signal-to-noise ratio. In the following picture the propagation losses in function of the wavelength measured in waveguides milled in doped PMMA are shown and compared with those measured using waveguides milled in native PMMA.



**Figure 6-8: Propagation losses of the optical waveguides that were milled into doped PMMA and comparison with the propagation losses measured in waveguides milled into native PMMA**

It can be seen that the losses remain around 1 dB/cm for almost the entire visible range. At wavelength smaller than 400 nm, the propagation loss increases rapidly. The losses increase in the near-UV range because of the absorbance of the material. While, for the higher wavelengths regions the losses are due, mainly, to scattering of light due to surface roughness. The surface roughness can be minimized optimizing the milling parameters such as feed rate, rotational speed of the tool, cooling rate and sharpness of the tool. The roughness is also related to the intrinsic material properties and its transition temperature. Thermal and/or chemical treatment [102] can be used to further reduce the roughness. In general the result obtained is very good if compared with other waveguides for lab-on-a-chip fabricated using other materials and processes [101].

#### 6.4. Optical plug

The optical connector plug allows easy insertion of different fibers along an array or matrix form into a system or a motherboard (see fig. 6.15), to couple light in correspondence of sensors or detection points, or into waveguides. It circumvents the critical issue of alignment due to the lens effect that focus the light in a specific point giving the possibility of having an admissible error, coupling the same intensity of light even if the fiber is not perfectly centered to a waveguide or detection point of the system as can be depicted from figure 6-9.

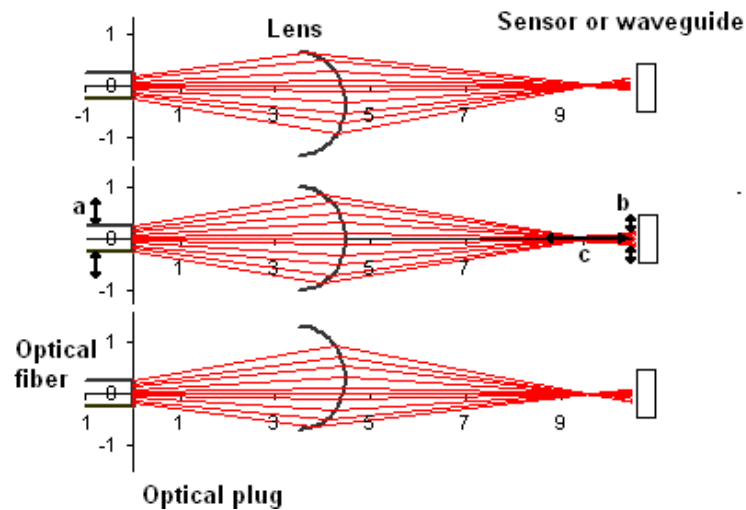


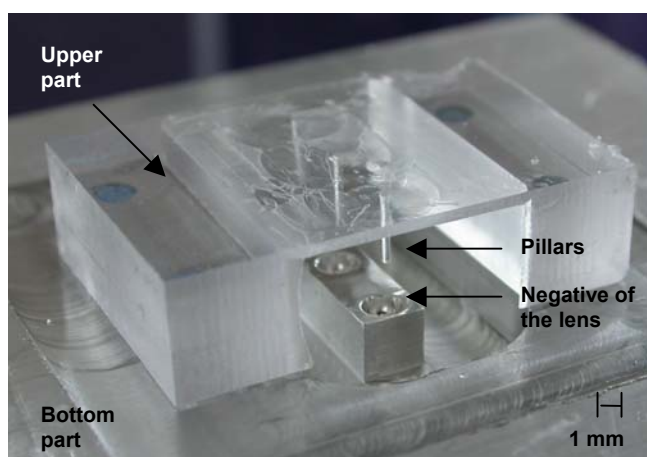
Figure 6-9: Ray tracing showing the tolerance admissible (a,b,c) using the optical connector plug

Finally it allows performing multiplexed and simultaneous analysis either for absorbance or fluorescence measurements [20].

### 6.4.1. Fabrication

The optical connector plug has been fabricated by casting PDMS in a mold composed by a bottom part made of aluminum and an upper one made of polycarbonate.

Both parts of the mold have been machined by conventional milling using a rotational velocity of 5000 rpm. The aluminum mold contains the negative shape of the body of the plug, the studs for attaching the plug and the shape of the lenses.



**Figure 6-10: Molds used for casting PDMS in order to fabricate the optical plugs**

The negative molds of the lenses have a diameter of 2mm and the plug has an overall height of 10mm. To reduce the roughness of the mold and in particular for the part reproducing the lenses, the surface at this area has been mechanically polished applying an abrasive paste using a rotating cotton swab. The upper part, fabricated in polycarbonate, contained 5mm long protruding columns that would later allow for the housings of optical fibers with the same diameter. Assembling the mold, these columns are aligned centrally to the lens molds keeping a well-defined distance between column end and mold surface. We investigated two different proximities, 3.5mm and 1mm, eventually leading to the same distances between the optical fibers and the spherical lenses, thus realizing, respectively, focusing and collimation of the light.

Once the transparent upper part of the mold is aligned to the bottom part using a microscope and fixing with tape, the PDMS is cast into the cavity. Subsequently, the

mold is put into a vacuum chamber for 2 hours to remove gas bubbles and then is then cured at 80 °C for 2 hours. Afterwards, the upper mold is removed and the optical fibers are inserted into the holes left by the columns, thereby auto-aligning of the fibers to the center of the lenses.

The flexibility of the PDMS, and the possibility of strong bending forces from unsupported fibers could result in a deformation of the plug and consequent misalignment and tilting of the fibers. To prevent this, additional PDMS is cast to completely fill the fiber housing and embed the fibers.

Finally, the plug is removed from the mold and epoxy is cast on the upper side to improve the mechanical stability of the plug. The sequence for producing an optical connector plug is depicted in Figure 6-11.

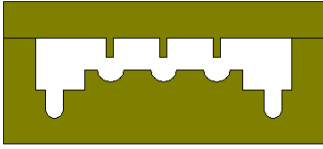
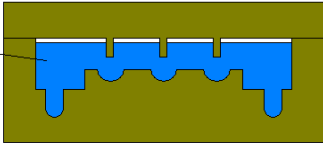
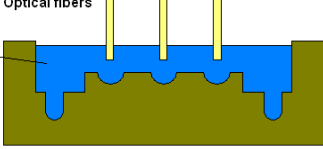
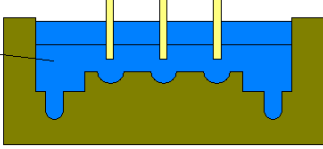
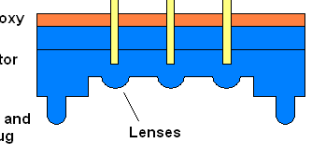
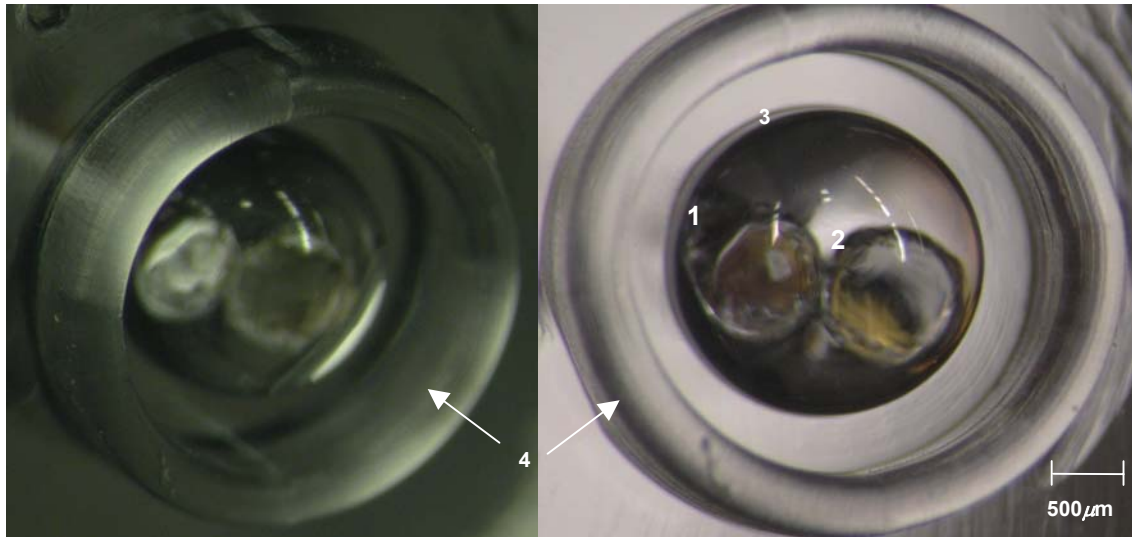
Steps	Description
 <p>Upper mold Bottom mold</p>	Assembling and alignment of the transparent upper mold under optical microscope
 <p>Upper mold PDMS Bottom mold</p>	Casting of PDMS and baking
 <p>Optical fibers PDMS Bottom mold</p>	Removal of upper mold and insertion of the optical fibers
 <p>Optical fibers PDMS Bottom mold</p>	Further casting and baking of PDMS for embedding the fibers
 <p>Optical fibers Epoxy Optical connector plug Pillars to fix and align the plug Lenses</p>	Casting of epoxy for improving the mechanical rigidity

Figure 6-11: Working sequence of the plug fabrication process



The aluminum mold contains also 4 pins allowing to fix the plug into the motherboard (Figures 6-11 and 6-17).

The process for fabricating the optical connector plugs is very versatile and plugs having different configurations can be fabricated for different purposes. It is possible to fabricate plugs having fibers in an array or matrix arrangement. They can be used for coupling light into a waveguides or directly into a detection point. It can be used for absorbance or fluorescence measurements. In the last case two fibers must be mounted on one lens as it is shown in Fig. 6-12



**Figure 6-12: Close-up of the optical plug used for the microbio reactor developed at MIT to perform fluorescence measurements sending light from an optical fiber (1), collimating the light on a fluorescence sensor by the lens (3) and detecting the light back from the sensor through another optical fiber (2). The optical plug could be fixed and aligned to microbio reactor by the ring fabricated around the lens (4) which also protect the lens: isometric view (left) and top view (right) [13].**

#### 6.4.2. Characterization and experiments

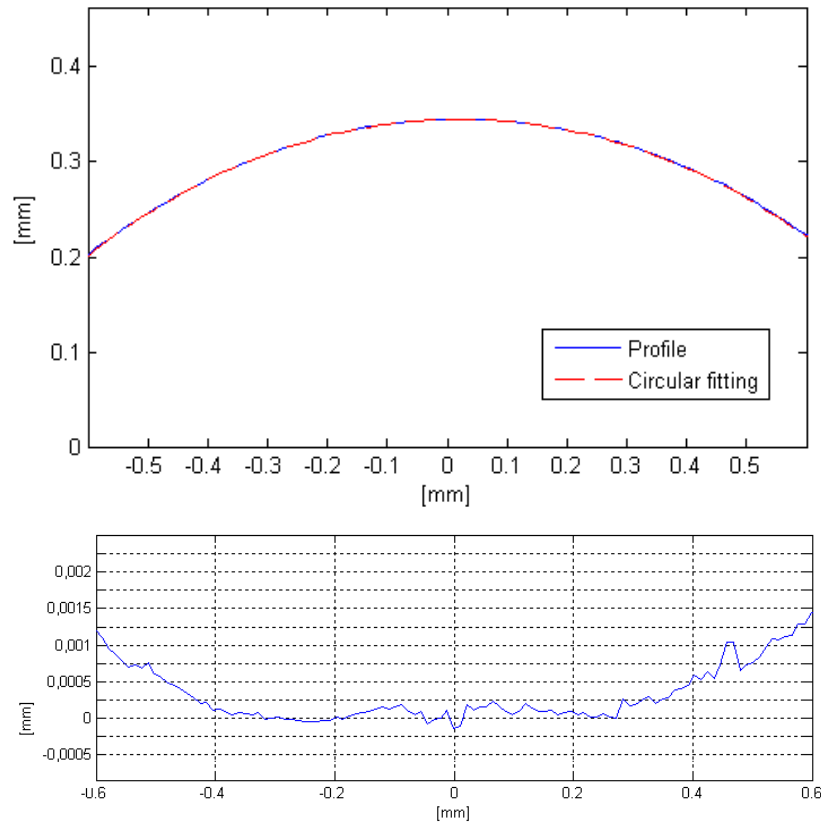
A profilometer DEKTAK has been used to evaluate the roughness, the quality of the lens surface and sphericity. In order to scan the center of the lens a series of 2D-scanning has been performed at different coordinates and choosing the profile more close to the center.

The data of the profile has been post-processed to exclude influences from the stylus tip (which had a radius of  $5\mu\text{m}$  at the tip and cone angle of  $60^\circ$ ).

In order to test the efficiency of the connector plug, it and a cleaved fiber were mounted on a stage and placed perpendicular to the objective of an optical microscope (ZEISS Axiovert 200 inverted fluorescence microscope) connected to a CCD camera (AVT Marlin F-046C, SVGA 780 x 582). The plug and the cleaved fiber were focused onto the microscope to define a “zero” position and then displaced from that position using a translation stage. The opposite ends of the fibers were connected to a laser diode ( $\lambda = 637\text{nm}$ ,  $P=7\text{mW}$ , Thorlabs) and the distribution of light through the fiber alone and through the fiber-plug combination was recorded. The images were exported to Matlab and analyzed to extract the distribution of light as a function of the lateral position (Fig6-15) [103]. For this experiment two types of plugs were investigated in which the fibers were embedded at distance of 1mm and 3,5 mm from the lens, respectively.

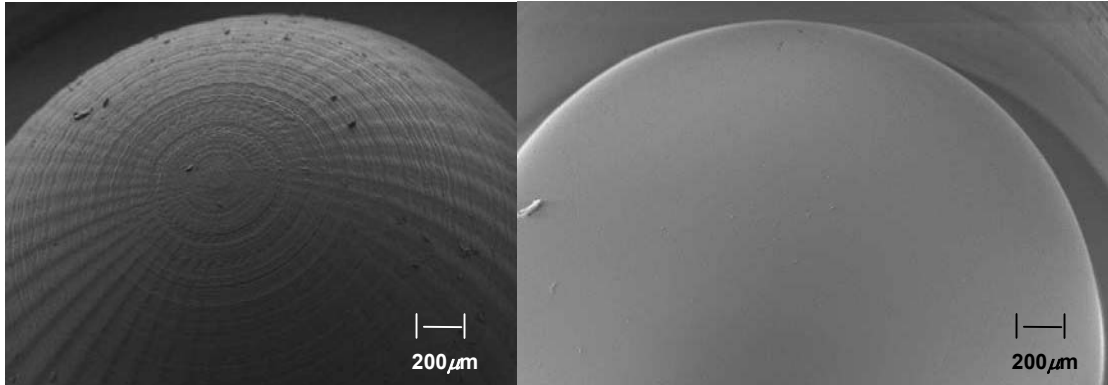
As mentioned before, an advantage of using the optical connector plug is that the focusing of the light leads to more tolerance during the alignment step. For demonstrating this, insertion losses measurements has been taken from coupling the light from one fiber to another mounted on three-dimensional stages and introducing controlled misalignments in x-y and z direction. The same experiments has been repeated mounting the optical plug on one part of the stages and this time insertion losses measurements were taken from coupling light from the plug to the fiber. The fibers were connected from one side to an NICHIA green-LED while to the other side to a photodiode connected to a powermeter. The experiments were repeated for inlet fibers of  $200\mu\text{m}$  and  $500\mu\text{m}$  while leaving always an outlet fiber of  $500\mu\text{m}$ .

As it can be seen from Fig. 6-13 the measured profile fits very well with a circular profile.



**Figure 6-13: Profile of the top-part of a 2mm lens compared with a circular fitting (top); Deviation from a circle, calculated as difference between the profile and the circular fitting (bottom).**

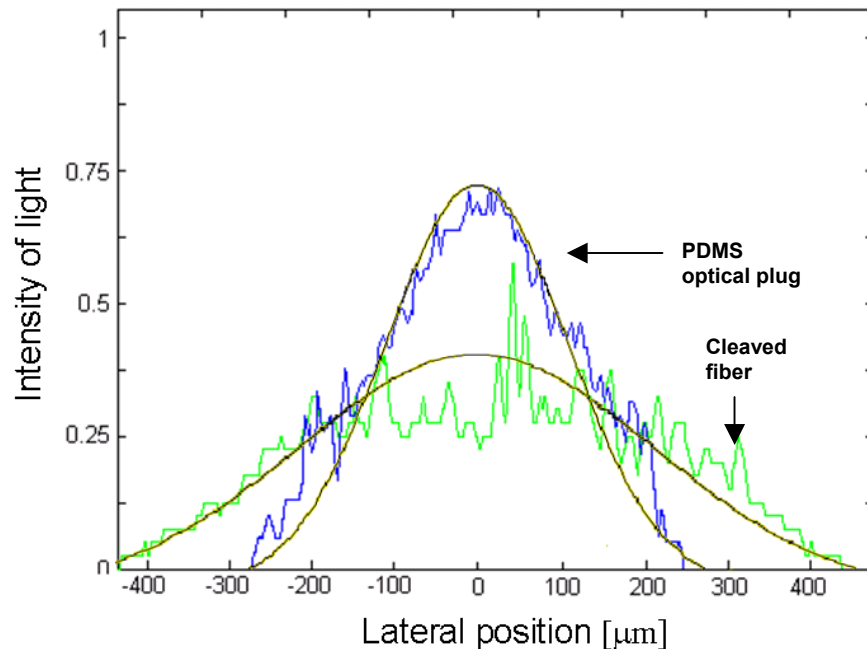
The deviation from a sphere has been calculated by differentiating the profile with the spherical fitting. The deviation is below 250 nm from the center part of the lens to a distance of 0.4 mm from the center after which it increases. This is probably due to the shape of the particular cotton swab used for polishing that did not fit perfectly to the spherical mold. Having on average more physical contact with the side, it removed more material in those areas. The result did, however, not affect the efficiency of the lens because light mainly passed through the center part of the lens where the deviation from a spherical fit, was low. Additionally an average roughness of  $0.1\mu\text{m}$  after polishing of the mold has been measured (Fig. 6-14).



**Figure 6-14: SEM images of the lenses obtained from a mold which has not been polished (left) and from one which has been polished (right)**

In literature, however, the value usually suggested for the roughness of an optical refractive element for avoiding totally aberration is of 1/10 that of the wavelength of the light passing through it. In our case a red laser diode has been used for the experiments performed, having a wavelength which is roughly 6 times the value of the roughness and this justify the aberration obtained but in general a good result has been obtained.

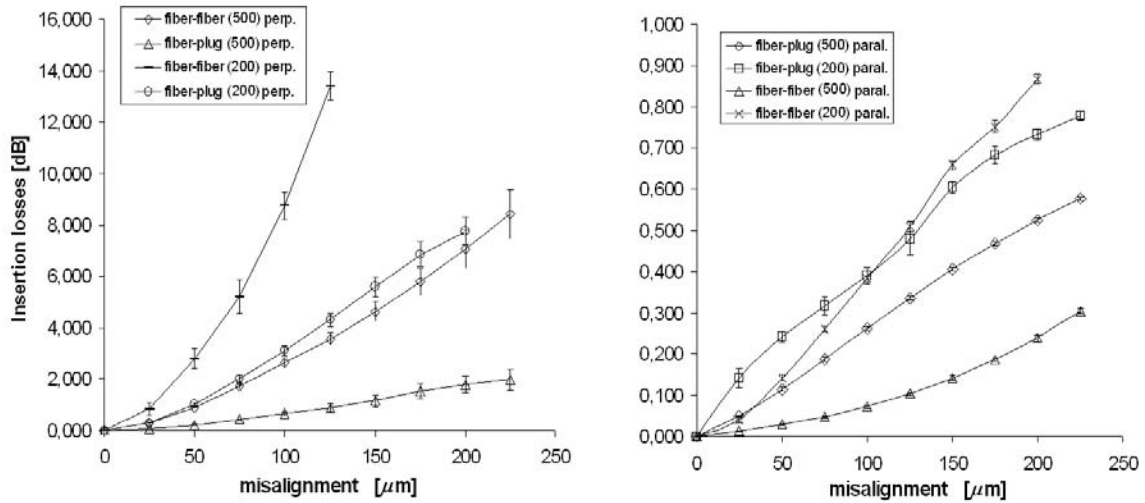
The measurements show a maximum light intensity for the plugs, which is  $\sim 50\%$  higher than for the cleaved fiber itself and more focused with respect to lateral distribution (Fig.6-15).



**Figure 6-15: Intensity of the light versus lateral distribution of a cleaved fiber (green line) and the optical connector plug (blue line).**

The light distribution at the focal point presents some aberration comparing with the theoretical model due, probably, to the value of the roughness which is a little high and the fact that placing a fiber with a NA equal to 0.22 at a distance of 3.5 mm from the lens makes the paraxial approximation not totally valid since the incoming light invest a large area of the lens even the part distant from the axis.

Finally the insertion losses measurements as function of induced mis-alignments show an improved coupling of the plug with respect to a cleaved fiber.

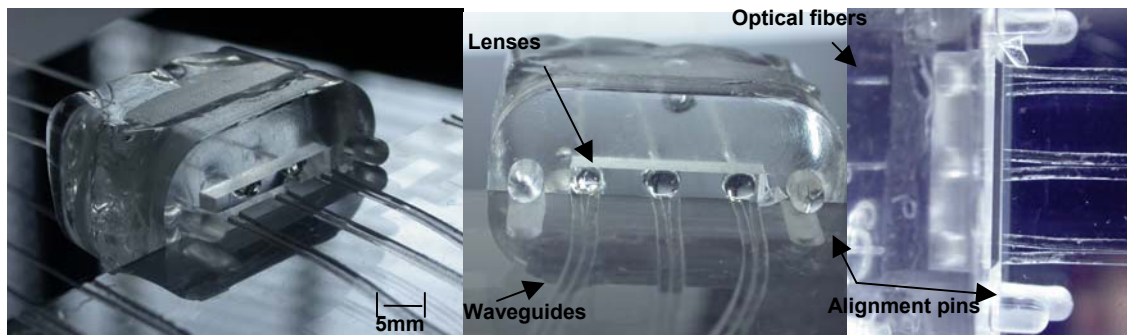


**Figure 6-16: Insertion losses versus induced misalignment moving the two parts perpendicularly to each other (left), and parallel to each other (right).**

From figure 6-16, it is possible to see that the insertion losses rise fast and exponentially with the increasing of misalignment for the fiber-to-fiber connection, while they rise slow and linearly for the plug-to-fiber connection. Already at a misalignment of  $25\mu\text{m}$  there is a difference of 100% of coupled light power between the two.

It is also possible to see that coupling the light from a plug integrating a fiber of  $200\mu\text{m}$  leads to an higher efficiency (in terms of increase of insertion losses in function of misalignments) in comparison to the optical plug integrating a fiber of  $500\mu\text{m}$ .

This is probably due to the fact that the aberration is less for the smaller fiber where the light goes through the center part of the lens therefore the paraxial approximation is more respected. The difference in efficiency between fiber to fiber coupling and plug to fiber coupling is less evident in the experiments where the two parts are pulled away from each other as shown in Figure 6-16(right). This is, probably due on one hand to the low NA of the fibers which gives low losses when the two fibers are pulled away, on the other hand to the aberration effects of the plug. Anyway, when the fibers are pulled away from each other the insertion losses increase with a velocity which is in scale an order less than the losses induced when the connection is displaced perpendicularly showing to be less critical.



**Figure 6-17: Different view of the optical plug connected to the waveguides of the motherboard, where the light is coupled in.**

## 6.5. Chip

The chip is the unit containing:

- a fluidic network having the function of reactor or mixer and bearer of the fluid to the detection point;
- Waveguides going from the edges of the system into proximity of the fluidic channel allowing optical analysis of the liquid;
- Integrated fluidic interconnections.

The chip is composed of 4 PMMA layers as shown in the following picture.

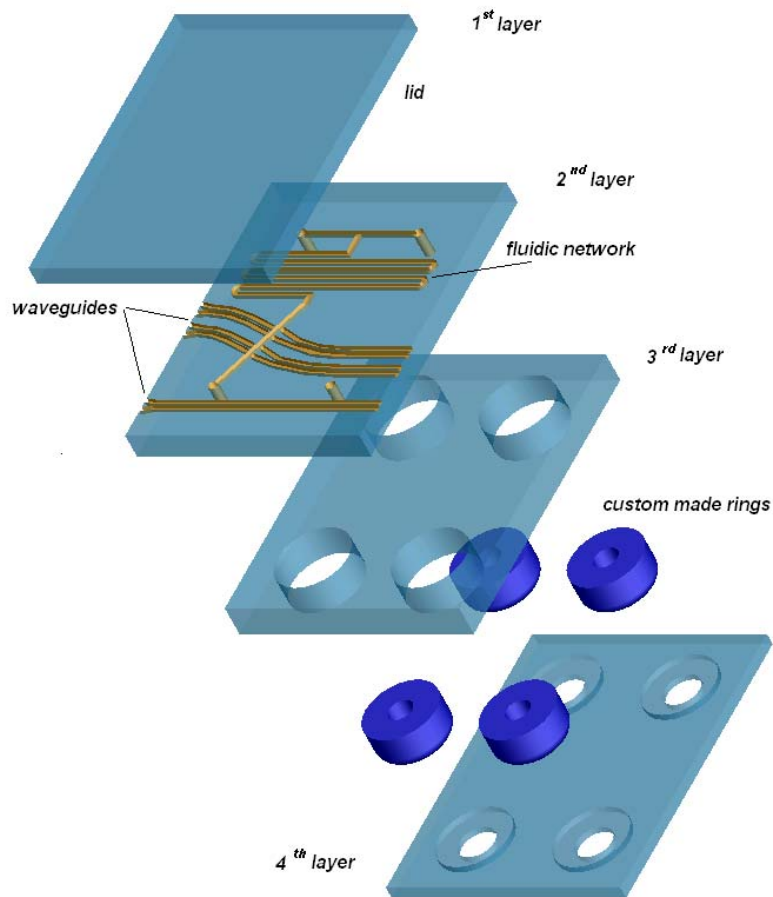
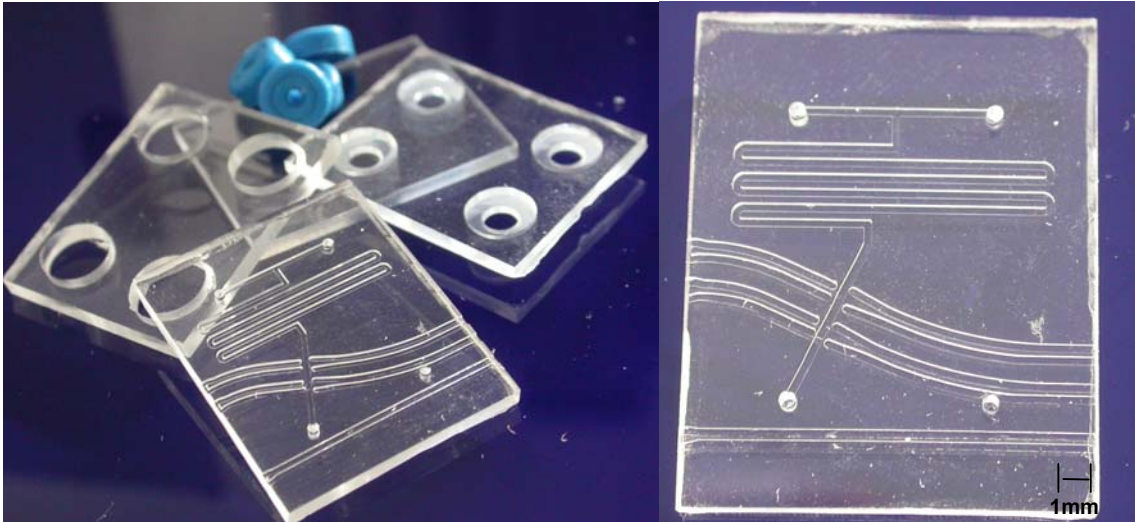


Figure 6-18: Exploded view of the chip designed in Solidworks

The first 1<sup>st</sup> layer is a lid for the 2<sup>nd</sup> layer where the fluidic network, waveguides and through holes, are machined on one side at the same time.



**Figure 6-19: Close-up of the different parts constituting the chip (left); top view of the 2<sup>nd</sup> layer of the chip**

For the waveguides, the same technology of the motherboard has been used with the same consideration regarding minimum radius of bending and length of tapers, but this time, 2mm long tapers have been fabricated while bended waveguides have been designed for having radii ranging from 10 to 50 mm.

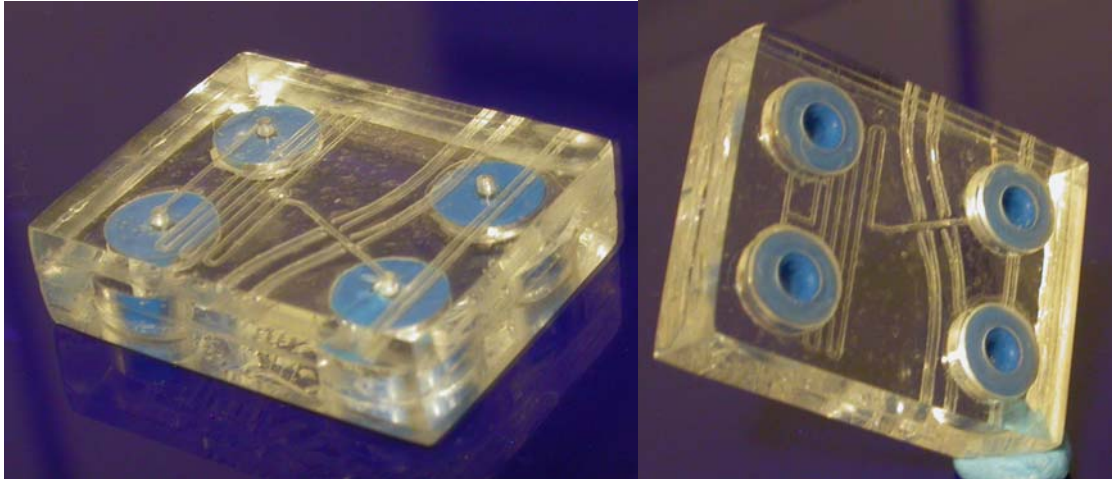
The waveguides have a width  $100\ \mu\text{m}$  and a depth of  $250\ \mu\text{m}$ . The fluidic channels have a rectangular cross-sectional area  $500\ \mu\text{m}$  wide and  $250\ \mu\text{m}$  deep.

The 3<sup>rd</sup> and 4<sup>th</sup> layers are made for housing custom made o-rings that will be part of the integrated interconnections.

All layers are bonded together thermally by pressing them in the oven for 1 hour at a temperature of 111 C.

Once everything is bonded the edges are mechanically polished to improve the coupling of light into the waveguides.





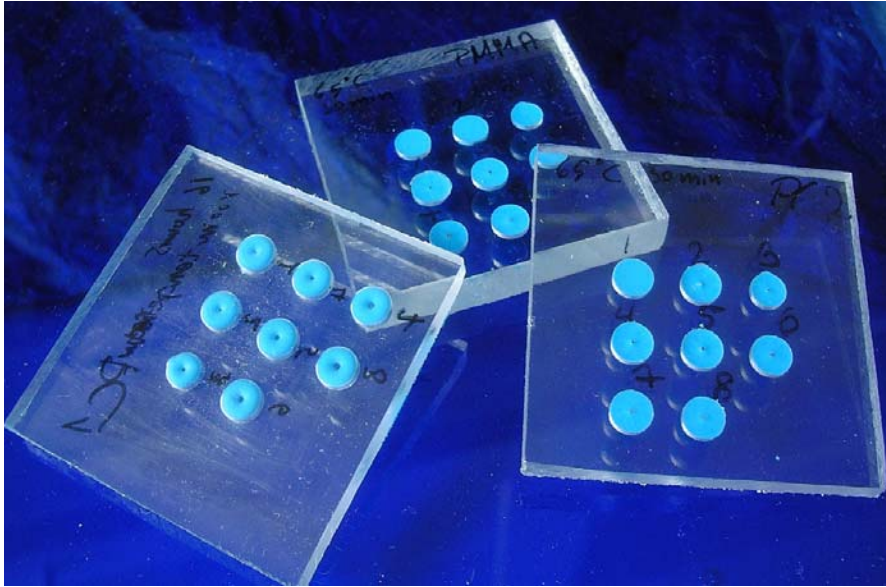
**Figure 6-20: Close-up of the bonded chip**

## **6.6. Fluidic interconnections**

As mentioned, two different types of fluidic interconnection have been used. An integrated plug'n'pump fluidic interconnection allowing an easy plug functionality of the system to the motherboard and a demountable PDMS fluidic socket allowing high density interconnection between the motherboard and external tubes.

### **6.6.1. Plug'n'pump fluidic interconnection**

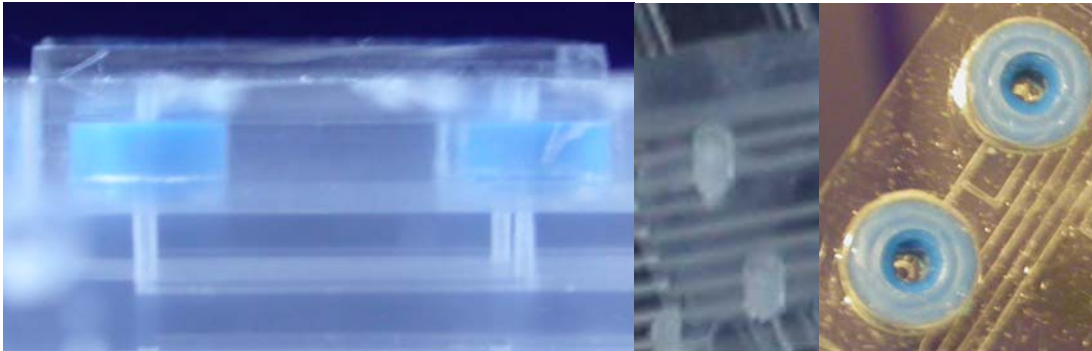
This type of interconnection has been explained theoretically in chapter 3. In this specific case the custom-made o-rings are integrated in the chips by using the process explained in the previous section. The custom-made cylindrical rings have been fabricated from Sylastic<sup>®</sup> RVM elastomer (Dow Corning). The elastomer has been cast into PMMA molds reproducing the negative shape of the rings having an outer diameter of 6.5 mm and an inner diameter of 1.8 mm and a depth of 2.65 mm.



**Figure 6-21: Molds used for the custom made elastomeric rings**

The rings were left one night at room temperature obtaining an Young modulus of  $E=4.5\text{MPa}$ .

Once they were ready, they were fit into the 3<sup>rd</sup> and 4<sup>th</sup> PMMA layers, as explained in the previous section and bonded together to the chip.



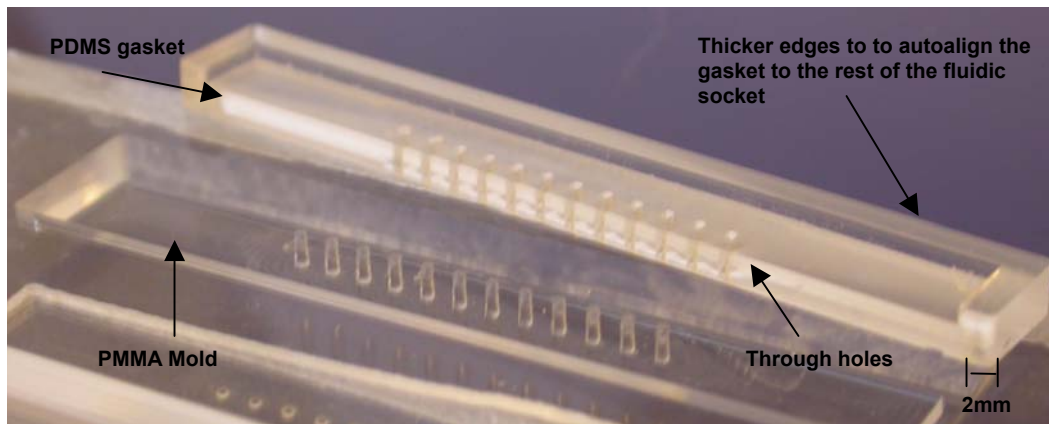
**Figure 6-22: Close up of the integrated interconnections while the chip is plugged into the motherboard (left), pins on the motherboard (center) for fixing and aligning the chip, custom rings integrated into the system (right)**

Once the chip is inserted into the motherboard (Fig. 6-22: left), a mismatch of 0.2 mm is created between the rings and the pins. Here, the chip is pressed creating a pressure at the interface which is 4 bar, according to the model.

In figure 6-22 (left) it is possible to see a very good alignment between the channels in the motherboard and those into the chip.

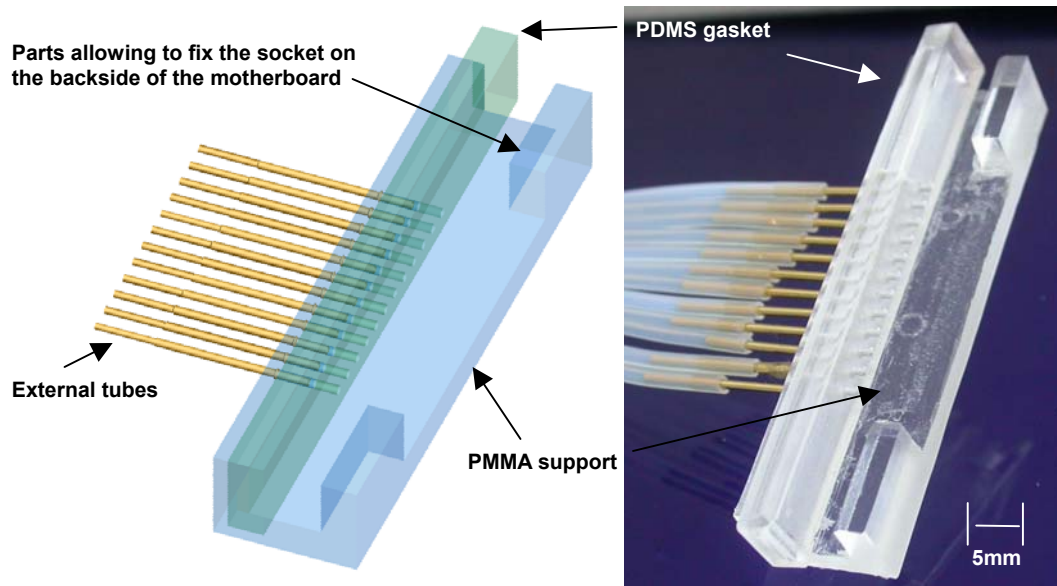
### 6.6.2. PDMS fluidic socket

The PDMS fluidic socket is made of a rigid PMMA support where 12 external metal tubes are connected by pressing them into holes. The sealing between the tubes and the PMMA support is ensured by the mismatch between the metal tube which has an external diameter of 0.85 mm and the holes in the PMMA support which has a diameter of 0.8 mm. The tubes are spaced 2mm between each other which is the same distance of the channels in the fluidic network of the motherboard.



**Figure 6-23: PMMA mold for casting the PDMS gasket and the PDMS gasket**

To ensure sealing between the motherboard and the external tubes a PDMS gasket has been utilized (Fig. 6-23). It has been fabricated from casting it into a PMMA mold, which has been previously machined by using a CNC-machine, then it has been baked all the night in the oven at a temperature of 80 °C, to have a Young modulus  $E=2,5\text{MPa}$  for the PDMS. The gasket includes 12 holes of 0.8 mm in diameter spaced at the same distance of the tubes and channels in the motherboard. It also contains thicker edges that will surround the PMMA support auto-aligning the gasket holes with the support in PMMA (Fig. 6-24).



**Figure 6-24: PDMS fluidic socket: designed in Solid works (left); prototype (right);**

The gasket is pressed between the external PMMA support and the motherboard and aligned optically since the transparency of the materials. The distance between the PMMA support and the motherboard is 1.7 mm, while the thickness of the gasket is  $l=2\text{mm}$ . This means that when the socket is in position the gasket is deflected of  $\Delta l=0.3\text{mm}$ .

Considering that  $E=2,5\text{MPa}$  and the unit strain is

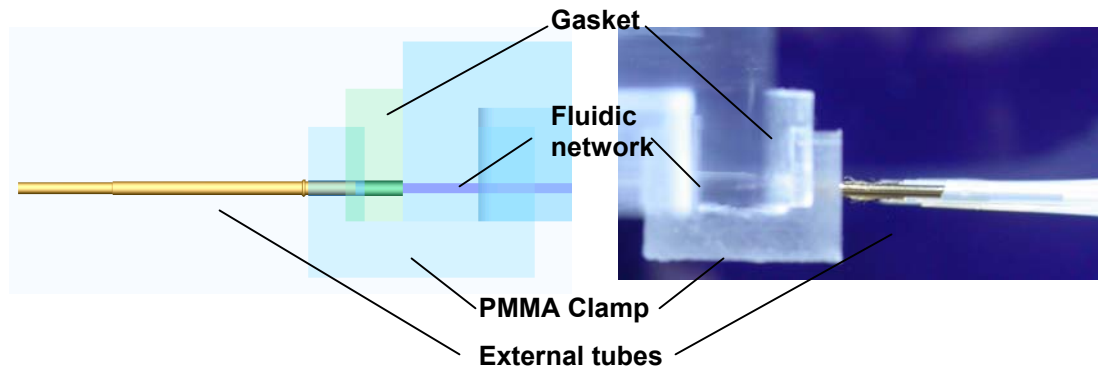
$$\varepsilon = \frac{\Delta l}{l} = 0.15 \quad (6-2)$$

There will be a pressure at the interface given by

$$\sigma = E\varepsilon = 0.375\text{MPa} = 3.75\text{bar} \quad (6-3)$$

which is, theoretically (see Chapter 3), the internal pressure of the fluid that this interconnection can stand without any leakage.

The sides of the PMMA support contain U-shaped parts (Fig.6-24) acting like a clamp (Fig. 6-25) allowing to fix it into two pockets fabricated on the backside of the motherboard.



**Figure 6-25: Close up-of the side-view of the socket connected to the motherboard: design in Solidworks (left), prototype (right)**

### 6.6.3. Experiments

Static tests of the fluidic interconnections of the motherboard have been performed by clogging the tubes connected with the outlet of the motherboard and pumping air into it. A pressure sensor, connected with the inlets, has been used for detecting pressure drop if leakage occurs. The motherboard has been immersed into a box filled by water in order to detect the point of leakage looking at bubble formation. The set-up used for the experimental tests is shown in figure 5-7.

The static tests have shown leakages at 3.2-3.5 bar in correspondence of the PDMS socket which is in accordance with the model.

### 6.7. Coupling experiments on the motherboard

Insertion loss measurements have been done by coupling a light signal ( $\lambda=637$  nm) from the light source and detecting the power in output connecting fiber-to-fiber, fiber-chip-fiber, fiber-motherboard-chip-motherboard-fiber.

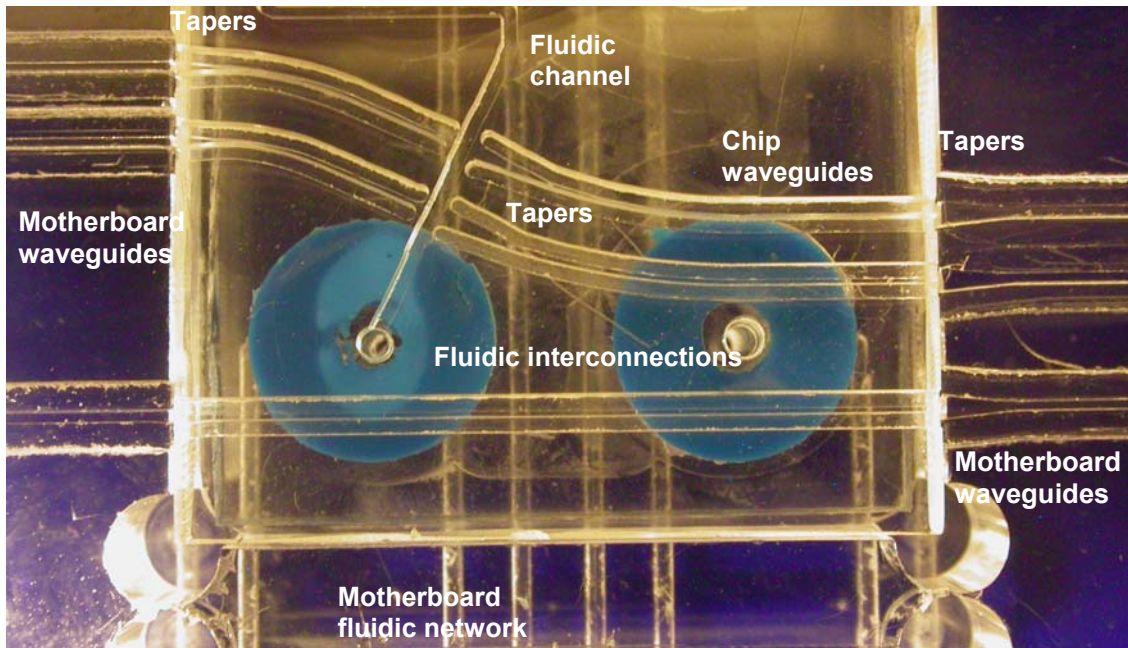
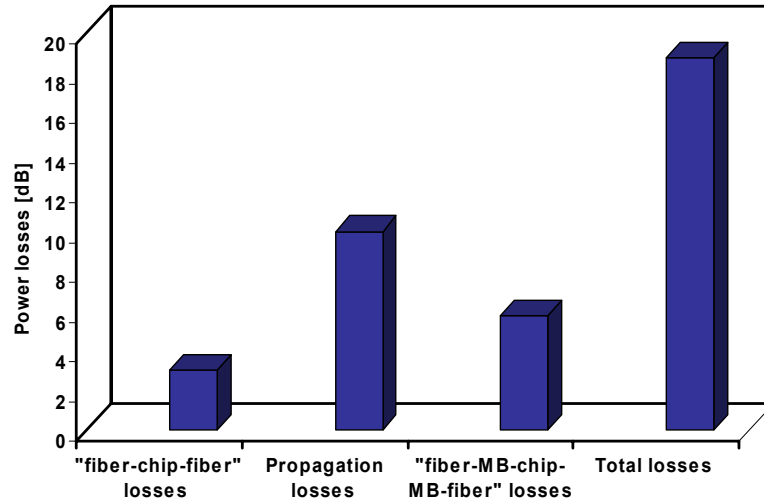


Figure 6-26: Picture of the aligned waveguides to the motherboard

The experiments have shown a recorded power, connecting fiber-to-fiber of  $300 \mu\text{W}$ . For the connection fiber-chip-fiber the power went down to  $150 \mu\text{W}$ . While for the connection motherboard-chip-motherboard the power went to the value  $4 \mu\text{W}$ . The next step would have been to perform absorbance or fluorescence measurements using dyes to characterize better the potential of the motherboard but lack of time didn't allow to do so. In the following pictures the measured losses are showed in Decibel taking as reference the connection fiber to fiber.



**Figure 6-27: Optical power losses measurements through fiber-chip-fiber connection, propagation losses in the waveguides, fiber-MB-chip-MB-fiber, and total losses which is the sum of the propagation losses + the losses measured in the fiber-MB-chip-MB-fiber connection.**

### 6.8. Discussion

The microfluidic motherboard showed ease of fabrication and high flexibility and for the first time, fluidic and optical interconnections have been integrated in a manifold for performing bio-chemical analysis. The motherboard can allow the integration of different types of microfluidic systems having different functions, to perform optical analysis like absorbance or fluorescence measurements. It allows also multiplexed or modular functionality. The motherboard is based on three new ideas which are the three main components constituting it. These are the *plug'n'play* fluidic interconnection, the new process to fabricate polymer waveguides and the optical connector plug. These ideas have been developed and characterized singularly. The integrated fluidic interconnections showed easy of fabrication and high flexibility. They could ensure sealing at high pressure and, at the same time, having a *plug'n'play* functionality. The waveguides were very easy and inexpensive to fabricate. The process used to fabricate them gives flexibility regarding the use of different types of polymers. The measured propagation losses were very low, compared to other common used waveguides in lab-on-a-chips. Moreover, it must be considered that the main losses were due to roughness of the surface that can be reduced by a thermo chemical treatment that has not been done. Finally, the optical connector plugs have shown high flexibility of use, indeed, they have been

utilized not only to couple light into the waveguides of the motherboard but also in microbioreactors, to perform fluorescence measurements, coupling light directly into the fluorescent sensors. The process used for fabricating them was inexpensive and readily amenable for batch production. The experiments done demonstrated the good efficiency of the plug regarding, capability of focusing or collimating the light and coupling of the light in a way to minimize the alignment issues. In general the results obtained on each component of the motherboard were optimum. The experiments done on the motherboard, in which all the components were integrated, showed promising results. Though, optimization on the integration of the different components would be required to improve the efficiency, and reduce the losses borning within and between the different components of the motherboard. The causes of these losses are different.

The length of the waveguides in the motherboard introduces roughly 8 dB of propagation losses according to the waveguide experiments. A solution to this problem could be to make them shorter or to reduce with some thermo-chemical treatment the surface roughness, thus reducing the propagation losses. Another problem could be that, during the thermal bonding, the doped layer is pressed down, getting thinner and reducing the coupling efficiency. This problem can be solved using other bonding techniques. Moreover the spun-on doped layer is not everywhere homogenous but it can vary in thickness around the edges of about  $20\mu\text{m}$  this create problems in term of propagation of light. This problem can be solved by machining the edges of the motherboard removing the parts where the spin-on layer is not homogenous.

Finally, another improvement would be to integrate lenses at the end of the waveguide to focus the light into the chip and to use index matching oil in the junction between the waveguides of the motherboard and the chip improving the coupling efficiency.

Unfortunately lack of time didn't allow to perform further experiments and to optimize the motherboard itself.



## 7. Conclusion

Packaging of microfluidic systems is a part of microtechnology including integration, fabrication, materials and interfacing of a microfluidic system.

The work has been carried out by the need of confining a field that until now has been underestimated but that contributes heavily to the performance, reliability and cost of a microfluidic system.

In a first phase, an effort has been made to individuate the definition of the packaging, what characterizes it, the weak points and difficulties, and all the parameters involved that are important to fulfill a successful protection and interface of a system.

Models have been developed regarding the critical parameters in packaging for simplifying the design and dimensioning of fluidic interconnection and optical external couplers and experiments have been performed to validate those.

Since there is a trend to develop polymer microfluidic systems for bio-chemical analysis, stress has been put on exactly those systems.

We developed a new polymer-based microfluidic motherboard that integrates polymer-based waveguides and fluidic networks providing an interface between microfluidic systems and the outerworld. The motherboard, on one hand, facilitates interconnections of several microfluidic systems for multiplexed and simultaneous analysis. On the other hand, it offers a modular network for microfluidic chips, allowing complex microfluidic processes, where each microchip has a particular function. The motherboard shows a robust design allowing easy interconnectability of several microsystems alleviating critical issues as optic alignment and fluidic interfacing.

To be able to combine microfluidic and optical networks, a difference in refractive index is necessary in order to achieve waveguiding properties. The refractive index of dissolved PMMA was increased to  $n=1.499$  by doping the PMMA with styrene-acrylonitrile copolymer (native PMMA  $n=1.485$ ). This liquid doped PMMA was then spun onto the top-side of a  $10 \times 10 \text{ cm}^2$  (8mm thick) PMMA plate resulting in a  $100 \mu\text{m}$  thick layer. Subsequently, the substrate was baked at  $60^\circ\text{C}$  for 20 min. Microfluidic channels were then machined into the bottom side of the substrate using micromilling technology. Through holes allowed connection to the top-layer. To seal the channels 1.5mm thick PMMA plate was bonded thermally to the bottom of the substrate. Waveguides were directly machined into the previously spun doped PMMA layer on the top side by milling parallel grooves spaced down to  $100 \mu\text{m}$ . This novel process developed to fabricate waveguides is very simple and the waveguides show an excellent performance. Additionally, pins were fabricated; those are part of the fluidic interconnections and allow for alignment of a chip with the waveguides of the motherboard. To establish high density microfluidic interconnections between the motherboard and external tubes, reversible PDMS sockets have been fabricated and tested. For interconnecting the polymer waveguides to the light source and to the detection system, optical PDMS plugs including spherical lenses aligned to several optical fibers to the other side have been fabricated. The optical connector plugs allow focusing of the light from an optical fiber to a waveguide and vice versa.

To demonstrate the performance of the device, test structures were designed. They contained fluidic channels, waveguides and, additionally, custom made o-rings allowing alignment to the connection pins of the motherboard. The single chips were attached to

the motherboard by just pressing them onto the alignment pins. A sealed fluidic connection between chip and motherboard is ensured by the deliberate mismatch in diameter between the o-rings of the chip and the pins of the motherboard.

Characteristic parameters of the motherboard are the maximally applicable hydraulic pressure before leakage and the pressure drop over the fluidics section, as well as propagation and coupling losses for the waveguides and optical interconnections. The milled waveguides show almost constant propagation losses around 1 dB/cm between 400 nm and 850 nm. Scattering caused by surface roughness is a major factor when dealing with micromilled waveguides. Regarding the optical connector plugs, the measurements of the propagation of the light show a maximum light intensity for the plugs, which is ~50% higher than for the cleaved fiber itself and more focused with respect to lateral distribution. Induced misalignments showed less measured insertion losses for the optical plugs than a coupled cleaved fiber. Finally, leakage tests have shown an upper limit resistance of 3.5 bar for the fluidic interconnections.

The coupling experiments made on the motherboard have shown that it is possible to record a power of 4  $\mu\text{W}$  starting from a light source of 300  $\mu\text{W}$ . Although 4  $\mu\text{W}$  is still sufficient for performing bio-chemical analysis, the losses should be further reduced to allow reaching a higher efficiency.

## **A. List of Fluidic interconnections**

## Permanent fluidic interconnections

Working principle	Materials	Resistance	Advantages	Drawbacks
External tubes inserted into v-grooves from the lateral side of the microfluidic chip, in correspondence of the inlet and outlet of the system, and glued using common epoxy for ensuring tight and sealed connection. [23]	metal(for the tubes); PMMA(for the integrated v-grooves); Epoxy;	Not measured but related with the adhesion properties of the epoxy	Fast and simple;  Relatively strong connection;  Cheap;	Manual fabrication, not good for mass production. Ease to clog the fluidic channels; Large space requirements. High dead volume
The teflon tube after pretreatment is introduced into the inlet or outlet of the system. While the system is kept at a temperature of 380°C, the capillary is briefly pressed against the top surface of the silicon channel deforming it and leading to the formation of an integrated O-rings with an outer diameter larger than the inlet/outlet. The tube is pulled into the hole in order to create a temporary seal. The capillary is permanently bonded using high temperature epoxy. A reinforcing teflon sleeve is introduced before bonding. [40]	Teflon; Glass; Silicon; High-temperature epoxy;	275°C;  315 Psi (21.43 atm);	Inert to most chemicals; Few fabrication steps; Resistant to high temperature and high pressure; Low dead volume;	Little possibility to clog the fluidic channels; Manual fabrication, not good for mass production. Only for silicon microsystems;
A mylar film, pre-treated with PVCD coating on one surface, is attached to the wafer, where the systems were pre-micromachined, prior dicing, by thermal bonding and cutted in circular shape for matching the size of the wafer. A glass wafer is placed on top of the Mylar film facing the side without PVCD coating to assist the bonding process. A photoresist is spun on and patterned as an etching mask. An oxygen plasma is applied to pattern the Mylar film and to remove the masking photoresist. Capillary tubes are then fitted through the polymer sealant and the tube inserting process can be automated in parallel. Glue is applied to enhance the bonding strenght. [41]	Mylar; PVDS coating; Photoresist; Instant glue;	190 Kpa;	Integrated process; Batch processing; Strong connection;	Only for high temperature resistant systems; Creation of air bubbles during the bonding of the Mylar film; Relatevely high dead volume;
The needle is inserted in the O-ring and then into the inlet/outlet of the system. There is a interference fit between needle and O-ring so that the depth of the needle into he system can be adjusted manually. A droplet of room-temperaure curing epoxy glue was applied around the interconnection holes to enhance the holding force. [42]	Ethylene propylene (O-rings); Metal needles; Epoxy;	290 Kpa	Simple and fast; Cheap;  Strong connection;	Manual process; Possibility of infiltration of the glue inside the system; High dead volume;
External Polyethylene (PE) tubes were used as fluid connectors and were fixed to the chip. A mask-defined silicon surfac roughening was performed around the fluid openings using DRIE to ensure good adhesion of the tube. A guide wire was used to align the PE tube with the fluid openings on the chip during the tube fixing process. The system is shortly heated to generate a local melting of the PE tube onto the chip. To give additional strenght to the assembly, the interface between he chip and PE tubes are covered with epoxy glue. [43]	PE; Epoxy	Used at 3Kpa with a flow rate of 3.5µl/min but the limit was not investigated;	Low dead volume;  Strong connection;  Few fabrication steps;	Semi manual fabrication process;  Only for high temperature resistant systems;
Capillary tube glued into insertion channel wich is etched into a silicon substrate [44]	Epoxy; Silicon;	tested until 500 psi (3.4Mpa); but supposed to reach 2000 psi (13.8 Mpa);	Fast inegrated process;  Strong connection;  It offers a barrier against the glue;	High dead volume;  Difficult alignment;

## MCM fluidic interconnections

Working principle	Materials	Resistance	Advantages	Drawbacks
A fluidic network is fabricated into the substrate and bonded to another substrate including the through holes for covering the channels and performing inlet and outlet of the system; [14]	Polycarbonate or glass/silicon; Epoxy;	Not measured but comparable with other similar concepts;	Strong connection; Versatile system;	Large size compared with an integrated system; Possibility to clog channels using glue;
Microchannels are etched into polyimide and poly-p-xylylene layers and glued to the modules using epoxy; The poly-p-xylylene has to seal the channels shaped by two polyimide layers; [15]	poly-p-xylylene; polyimide; Epoxy;	110 KPA 10 $\mu$ L/min	Smart structure; Flexibility;	Long process; Possibility to clog the channels using epoxy;
Interlocking fingers ensure mechanical connection while o-rings ensures a sealed fluidic connections[12]	Silicon; Polysiloxane film (O-rings);	20 psi	Good for connecting different devices between them;  Self-aligned;  Flexible system assembly;	Fragile; Relatively long process;
An interlocking hole and notched cylinder pairs accomplish mechanical and fluidic interconnect. The cylinder sidewalls are gasketed for ensuring sealed connections. [13]	Silicon;  Wax, PDMS Parylene (for gasketing);	70 Kpa 1.95 ml/min (if they are gasketed)	No need of external screws;  DRIE is versatile and simple;  Easy to align and interconnect;	Easy to make;  Not very good for outworld connection;  Need to gasket them for reaching a good sealing;

## **Reversible fluidic interconnections: integrated interconnections**

Working principle	Materials	Resistance	Advantages	Drawbacks
The fluidic port integrated into the microsystem allow to fix a silicone tube into that for ensuring a tight and sealed connection. The fluidic port can be injection molded together with the system or it could be possible to micromill that after the fabrication of the system. It is possible also to fabricate the ports apart from the system and those could be thermal bonded in a second time to the system. It could be possible to drop some glue around the connection to increase the strenght of the connection. [www.smb.dk]	All the polymers;  silicone tubes;	Not measured;	Low dead volume;  Strong connection;  Cheap;  Simple and fast to produce and use;	Only for polymer microsystems;
Peek tubes are pressed, flanged and housed in cavities preheated to the transition temperature of the tube. All the structure is themal bonded or CYTOP coating is used; RIE was used for PC to increase bonding between PC and CYTOP; [45]	PEEK;  Glass;  Polycarbonate;  PMMA;  CYTOP;	30 psi;	Low dead volume;  Strong connection;  Accuracy of alignment depends on accuracy of bonding;	Several processing steps;
ECDM machine is used to imprint threads. Plastic screws are molded into the glass threads; [46]	Glass; PVDF;	30 psi; (206 Kpa)	Strong connection;  Easy to use;	Long process;  Relatevely big connection;
Fluid inlet are produced by molding with standard plastic fluidic connectors, which can be detached or attached manually. The strenght of the connection depends on the depth of the fluidic port. [47]	PDMS;	8500 Pa	Cheap;  Easy to fabricate;  Low dead volume;	This configuration does not give a strong connection but can be improved;  All the system should be in PDMS;
DRIE is used to fabricate accurately sized cross-sections for connecting capillaries. To circumvent the necessity of gluing the capillaries, a new coupler combining DRIE with injection-molded press fittings has been developed, allowing capillaries to be exchanged [48]	POM;	60 psi (414Kpa); only using a silicone gasket ;	Ease of alignment;	weak connection;  It requires big space;

## Reversible fluidic interconnections: Gaskets

Working principle	Materials	Resistance	Advantages	Drawbacks
PDMS is moulded in an house of PMMA (bottom plate) and holes are drilled in correspondence of inlet and outlet of the system; the bottom plate of PDMS is pressed against the system to ensure sealing; [49]	PDMS;  PMMA;	8000 Pa;	Low dead volume; Integrated electrical interconnections; Safe condition for the microsystems; Versatile and flexible connection; Cheap;	Difficult to fabricate and assembly;  Low pressure resistance;  High external forces required;
The micromachined boss around the port contains a gasket capture channel which mates to a ridge that is molded into the elastomer gasket. When the two parts are compressed, the elastomer is tightly captured in the channel region around each port, and the containment of the gasket is such as to keep it from being squeezed out from under the boss. [50]	PDMS;  Silicon;	Over 500psi;	Strong connection;  Easy to assembly;  Low dead volume;	It requires a system in function of the package;  Disomogenous stresses on the chip;
Fluidic interconnection assembled using flip-chip aligner/bonder. Doubleside adhesive tape is use to attach yhe chip to the package[11]	PMMA; PEEK; Silicone rubber; Ceramic (alternatively to polymers);	20 atm;	Nice design based on electronic packaging technology;  High tolerance during assembly;  Low dead volume;	Tape is not a good solution for sealing;  A lot of passages during fabrication;



## Reversible fluidic interconnections: O-rings

Working principle	Materials	Resistance	Advantages	Drawbacks
Using DRIE a ring shaped house for casting liquid silicon is etched; the silicone is cased and cured in order to make an o-ring, the backside of the connection is etched in order to have a through hole performing a fluidic connection in wich we can insert a capillary that will be kept by the o-ring. The inner diameter of the o-ring is less than the hole in order to permitt deformation of the o-ring during the insertion of the tube for having a tight seal. [51]	Silicone; Silicon; Nitride;	60 psi;	Smart structure;	High dead volume;  Long process;
The connection is made by inserting the tubing through an hollow screw, which is then finger-tightened, compressing the o-ring and forming a seal. [52]	Peek; Ferrules; PMMA; Rubber;	1000 psi; 800 psi (for the o-ring configuration)	Low dead volume; Strong connection;	Several steps for fabricating and assembly it.
Commercial o-rings of rubber are fixed between the external port and the inlet/outlet of the system [53]	Rubber; Polymers;	120 Kpa;	Cheap;	Difficult to hand. Disomogeneous stresses on microsystem;
Custom made rings, housed in a polymer frame , allows plug'n'play functionality between external tubes and the fluidic system [54]	Silastic elastomer	Up to 7 bar;	Fast and easy to fabricate and use; Strong connection; Low dead volume; Auto-sealed connection.	I requires space; not applicable for inlets which are too close each other;
A Teflon tube is inserted into a microstainless tube with heating method. The stainless tube is thread in order to screw it into a board that hold the system. The Teflon tube is pressed against the system ensuring sealing [55]	Teflon; PEEK; Stainless tubes	5MPa	Very strong; Easy to use; Inert to most chemicals; Low dead volume	I requires space; not applicable for inlets which are too close each other;

### **Reversible fluidic interconnections: Silicone tubes**

Working principle	Materials	Resistance	Advantages	Drawbacks
<p>The system uses short pieces of flexible tube that is available in various dimensions and many different materials. These tube-pieces, which are cut from a long tube, are plugged into a hole. In the center of this hole another hole with a smaller diameter is drilled. This establishes the connection to a standard thread that is cut from the backside into the connector. The length of the tube-piece is a bit longer than the hole's depth so that a small part will stick out of the hole. A microsystem with a through-hole that is pressed against the connector will deform the tube. Due to its elasticity the tube will seal the connection. [10]</p>	<p>Silicone; PMMA;</p>	<p>More than 1.2 MPa</p>	<p>Strong connection; Low dead volume;  Cheap;</p>	<p>Difficult to obtain very flat piece of silicone tubes.</p>
<p>A dual-in-line structure, consisted of two 10-channel linear arrays on opposite sides of the chip. Silicone tubes as wetting material, designed to extend 0.5 mm from the edge of the lead guide of the socket[14]</p>	<p>Polymers; Silicone;</p>	<p>0.2 MPa</p>	<p>Fully functioning socket for a microchip; Low dead volume; Flexibility;  Reusability;  Strong connection;</p>	<p>Disomogeneous stresses on microsystem; Difficult to have and keep the right extended length of the tube from the lead guide; difficult to reach an high density;</p>

## **B. List of Optical interconnections**

Interconnection level		Methods	Pros	Cons	Materials	Description	Literature
Interface between fluidic channel and medium driving the light		Optical fibers	Simplified design; Minimized reflecting surfaces;	Difficult alignment; Manual work for assembling required;	PDMS; PMMA; Si;	Fibers are brought directly close to the fluidic channel (detection point)	[69], [70], [71], [72], [16]
		Waveguides	Precise alignment; They can be spaced very close to each other; Facile alignments adding tapers; Flexible design;	More complicate design required; Needs bends or surface coupling to avoid stray light	PMMA; Epoxy; Su-8; PDMS;	The light travels into a core with a specific pattern having trapping properties for the light	[73], [74], [75], [76], [77], [92]
Interface between optical components inside the systems or between systems							
External coupling interface between system and outworld	Transverse coupling	End-butt coupling	Simple; Minimized reflecting surfaces	Difficult alignment; Low efficiency	Glass;	The light is coupled approximating two waveguiding structures or a waveguiding structure to the detection point;	[77], [78], [79]
		Lenses	High efficiency; Alignment easier;	More reflecting surface; More complex design;	Photoresist; PDMS; Glass;	Lenses are used to focus the light source into a waveguiding structure or detection point	[85], [86], [87], [88] [89], [90], [91], [103F104]
	Surface coupling	Gratings	Avoid straight light; Reflecting surface minimized;	Limits to modes propagation; Difficult to integrate; Careful adjustment of input coupling angle;	SiO <sub>2</sub>	The light is coupled into a waveguiding structure through grating or prisms, allowing excitation of specific modes	[92], [93] [94],
		Prism coupling					

## C. List of publications

- Books:** Chapter 9 of the book O. Geschke, H. Klank, P. Telleman, “Microsystem Engineering of Lab on a Chip devices”, entitled “Packaging of Microsystems” . Published by Wiley-VCH, ISBN 3-527-30733-8.
- Journals:**
- G.Keramas, G. Perozziello, O. Geschke, C.B.V. Christensen “Development of a multiplex microarray microsystem”, Lab on a Chip, 2004, 4
- D. Snakenborg, G. Perozziello, H. Klank, O. Geschke, And J. P. Kutter “Direct milling and casting of polymer-based optical waveguides for improved transparency in the visible range” Journals of Micromechanics and MicroEngineering 2006 16 375-381
- Gerardo Perozziello, Frederik Bundgaard, Oliver Geschke “Fluidic Interconnections for Microfluidic systems: A new integrated fluidic interconnection allowing plug´n´play functionality accepted for Sensors&Actuators B, 9.10.06
- Gerardo Perozziello, Zhyu Zhang, Detlef Snakenborg, Jörg P. Kutter, Klavs F. Jensen and Oliver Geschke “Optical connector plugs for multiplexed and simultaneous detection purposes in microfluidic systems”, manuscript prepared
- Detlef Snakenborg, Gerardo Perozziello, Oliver Geschke and Jörg P Kutter ”A fast and reliable way to establish fluidic interconnections to planar microchip ” accepted for J. Micromech. Microeng.
- Frederik Bundgaard, Gerardo Perozziello, Oliver Geschke “Rapid prototyping tools and methods for all-COC/Topas fluidic Microsystems”, Journal of Mechanical Engineering Science 2006, p.1625-1632
- Z.Zhang, P. Boccazzi, H.G. Choi, G. Perozziello, A. J. Sinskey and K. F. Jensen “Micochemostat-microbial continuous culture in a polymer-based, instrumented microbioreactor”, Lab Chip, 2006, 6, 906

**Conferences:**

G. Simone, G. Perozziello, N. Szita, V. Tagliaferri “Synthesis and characterization of tunable highly transparent nanocomposites: an in-depth experimental analysis oriented to the fabrication of waveguides ” accepted at MRS spring conference 2006, Boston

G. Perozziello, D. Snakenborg, Z.Zhang, J.P. Kutter, O. Geschke, K. F. Jensen “A fluidic motherboard including fluidic and optical interconnections, having modular functionality for optical analysis in microfluidic systems” accepted for oral presentation at  $\mu$ TAS 2006, 5-9.11. 06, Tokyo

Gerardo Perozziello, Zhyu Zhang, Detlef Snakenborg, Jörg P. Kutter, Klavs F. Jensen and Oliver Geschke “Optical connector plugs for multiplexed and simultaneous detection purposes in microfluidic systems” Proceedings of  $\mu$ TAS 9-13 October 2005 Boston, MA 1155-1157

Frederik Bundgaard, Gerardo Perozziello and Oliver Geschke “Rapid Prototyping methods for all-COC/Topas® waveguides and Microfluidic systems” Proceedings of  $\mu$ TAS 9-13 October 2005 Boston, MA 1200-1202

D. Snakenborg, G. Perozziello, O. Geschke, and J. P. Kutter ”Novel, fast and flexible methods for fabrication of polymer-based optical waveguides” Proceedings of  $\mu$ TAS 9-13 October 2005 Boston, MA 1224-1226

Zhyu Zhang, Gerardo Perozziello, Nicolas Szita, Paolo Boccazzi, Anthony J. Sinskey, Oliver Geschke and Klavs F. Jensen “Microbioreactor “Cassette” with integrated fluidic and optical plugs for high throughput bioprocessing” Proceedings of  $\mu$ TAS 9-13 October 2005 Boston, MA 1410-1412

Zhyu Zhang, Paolo Boccazzi, Hyung-goo Choi, Gerardo Perozziello, Oliver Geschke, Anthony J. Sinskey, Klavs F Jensen “Design and fabrication of a polymer-based Instrumented microbioreactor for high-throughput continuous microbial cell cultures” Proceedings of AIChE, Annual meeting 2005 30 October- 4 November Cincinnati, OH

Zhiyu Zhang, Paolo Boccazzi, Nicolas Szita, Hyun-Goo Choi, Gerardo Perozziello, Oliver Geschke, Anthony J. Sinskey, Klavs Jensen “A Polymer-based, Instrumented Microbioreactor for High-Throughput Microbial Cell Cultures” Proceedings of Lab Automation 2006 21-25, January, 2006, Palm Springs, California

- A. Johansson, G. Perozziello, O. Geschke, A. Boisen “Fast packaging of polymer cantilever chip by micromilling” Proceedings of 4M 2005 29 June – 1 July 2005, Karlsruhe, Germany 401-403
- F. Bundgaard, G. Perozziello, O. Geschke “Rapid Prototyping of all-COC/Topas® fluidic Microsystems” Proceedings of 4M 2005 29 June – 1 July 2005, Karlsruhe, Germany 405-407
- C.B. Nielsen, G. Perozziello, F. Bundgaard, Bjarne Helbo, T. Tang, O. Geschke “Microfluidic systems in polymers performing chemical analysis” Medical Plastics, November 2004, Copenhagen, Denmark
- O. Geschke, M.F. Jensen, G. Perozziello, F. Bundgaard, C.B. Nielsen, L. H. Christensen “Polymer microstructures - Are they applicable as optical components?” SPIE Optics East 24-28 October 2004 Philadelphia US
- G. Perozziello, M. F. Jensen, J. E. McCormack, F. Bundgaard, and O. Geschke “Plug’n’pump fluidic interconnection”, Proceedings of MicroTAS 26-30 September 2004 Malmö, Sweden 575-577 (oral presentation)
- F. Bundgaard, T. Nielsen, D. Nilsson, P. Shi, G. Perozziello, A. Kristensen, O. Geschke, “Cyclic Olefin Copolymer (COC/Topas®)-an exceptional material for exceptional Lab on a Chip systems“ Proceedings of MicroTAS 26-30 September 2004 Malmö, Sweden 372-374
- G. Perozziello, O. Geschke “A novel reversible packaging for microfluidic systems” CIRP seminar November 2003, Copenhagen, Denmark
- G. Danieli, G. Fragomeni, G. Perozziello “An iterative solution to establish a correspondence between points image and actual coordinates in space for application to real time virtual reality representation of surgical procedures”. ESDA2002: 6th Biennial Conference on Engineering System Design and Analysis. July 2002, Istanbul, Turkey (Copyright © by ASME)

---

## Bibliography

---

- [1] Klavs F. Jensen “Microreaction engineering – is small better?” *Chemical Engineering Science* 56 (2001) 293-303
- [2] Carlos H. Mastrangelo, Mark A. Burns and David T. Burke “Microfabricated Devices for genetic Diagnostics” *Proceedings of the IEEE*, Vol. 86, No.8, August 1998
- [3] Carl Hansen and Stephen R. Quake “Microfluidics in structural biology: smaller, faster...better” *Current Opinion in Structural Biology* 2003, 13: 538-544
- [4] Jan Lichtenberg, Nico F. de Rooij, Elisabeth Verpoorte “Sample pre-treatment on microfabricated devices” *Talanta* 56 (2002) 233-266
- [5] Elisabeth Verpoorte and Nico F. de Rooij “Microfluidics meets MEMS” *Proceedings of the IEEE*, Vol.91, No.6, June 2003
- [6] Klaus B. Mogensen, Henning Klank, and Jörg P. Kutter “Recent developments in detection for microfluidic systems” *Electrophoresis – An International Journal*, 25(21):3498-3512, 2004
- [7] S. Krawczyk, “Discussion on optical integration in lab-on-a-chip Microsystems for medical diagnostics” *Physica Status Solidi C*, 0(3):998-1012, 2003
- [8] K. B. Mogensen, N. J. Petersen, J. Hübner, and J. P. Kutter “Monolithic integration of optical waveguides for absorbance detection in microfabricated electrophoresis devices” *Electrophoresis*, 22:3930-3938, 2001
- [9] Holger Becker and Laurie E. Locascio “Polymer microfluidic devices” *Talanta*, 56(2):267-287, 2002
- [10] Zhen Yang and Ryutaro Maeda “A world-to-chip socket for microfluidic prototype development”, *Electrophoresis* 2002, 23, 3474-3478
- [11] Paul Galambos, Gilbert L. Benavides, Murat Okandan, Mark W. Jenkins and Dale Hetherington “Precision alignment packaging for microsystems with multiple fluid connections” *proceedings of 2001 ASME: International Mechanical Engineering conference and Exposition*, November 11-16, 2001 New York, NY.
- [12] C. Gonzalez, S.D. Collins, R.L. Smith “Fluidic interconnects for modular assembly of chemical microsystems”, *Sensors and Actuators B* 49 1998, 40-45.
- [13] Bonnie L. Gray, Scott D. Collins, Rosemary L. Smith “Interlocking mechanical and fluidic interconnections fabricated by deep reactive ion etching”, *Sensors and Actuators A* 112 (2004) 18-24



- 
- [14] T.S.J.Lammerink, V.L. Spiering, M.Elwenspoek, J.H.J. Fluitman and A.van den Berg “Modular concept for fluidic handling systems”, IEEE 1996, 0-7803-2985-6
- [15] P.F. Man, D.K. Jones, and C.H. Mastrangelo “Microfluidic Plastic interconnects For Multi-bioanalysis Chip modules” SPIE Vol.3224, 0277-786X/97
- [16] Makoto Hikita, Naoki Ooba, Ryoko Yoshimura, Mitsuo Usui, Takashi Yoshida, and Saburo Inamura “Polymeric Optical Waveguide Films for Short-Distance Optical Interconnects” IEEE Journal of Selected Topics in Quantum Electronics, Vol.5 No.5, September/Octobe 1999
- [17] Seung-Jin Cho, Satoshi Sasaki, Kazunori Ikebukuro, Isao Karube “A fluorescnt nitrate sending system using a reaction cartridge and titanium trichloride” Talanta 54(5):903-911, 2001
- [18] Christof Debaes, Michael Vervaeske, Valérie Baukens, Heidi Ottevaerre, Pedro Vynck, Patrik Tuteleers, Bart Volckaerts, Wim Meeus, Marnik Brunfaut, Jan Van Campenhout, Alex Hermanne, and Hugo Thienpont “Low-Cost Microoptical Modules for MCM Level Optical Interconnections” IEEE Journal of Selected Topics In Quantum Electronics, VOI.9, No.2, (2003)
- [19] Oliver Geschke, Henning Klank, Pieter Telleman “Microsystem Engineering of Lab-on-a-chip Devices” © 2004 Wiley-VCH ISBN: 3-527-30733-8
- [20] Zhyu Zhang, Paolo Boccazzi, Hyung-goo Choi, Gerardo Perozziello, Oliver Geschke, Anthony J. Sinskey, Klavs F Jensen “Design and fabrication of a polymer-based Instrumented Microbioreactor for High-throughput Continuous Microbial Cell Cultures” AICHE’05
- [21] Gerardo Perozziello, Zhyu Zhang, Detlef Snakenborg, Jörg P. Kutter, Klavs F. Jensen and Oliver Geschke “A microfluidic motherboard including fluidic and optical interconnections for modular, multiplexed or simultaneous optical analysis in microfluidicsystems”, in preparation
- [22] Zhyu Zhang, Gerardo Perozziello, Nicolas Szita, Paolo Boccazzi, Anthony J. Sinskey, Oliver Geschke and Klavs F. Jensen “Microbioreactor “Cassette” with integrated fluidic and optical plugs for high throughput bioprocessing” proceedings of  $\mu$ TAS 2005 Conference 1410-1412
- [23] Henning Klank, Jörg P. Kutter and Oliver Geschke ”CO<sub>2</sub>-laser micromachining and back-end processing for rapid production of PMMA-based microfluidic systems” Lab on a Chip, 2002, 1
- [24] F. Bundgaard, T. Nielsen, D. Nilsson, P. Shi, G. Perozziello, A. Kristensen, O. Geschke, “Cyclic Olefin Copolymer (COC/Topas®)-an exceptional material for exceptional Lab on a Chip systems“ Proceedings of MicroTAS 26-30 September 2004 Malmö.

- 
- [25] El-Ali; Gaudet S, Gunther A., Sorger P K, Jensen K F ” Cell Stimulus and Lysis in a Microfluidic Device with Segmented Gas-Liquid Flow” Analytical Chemistry Vol.77 3629-3636 2005
- [26] Kwang W Oh, Arum Han, Shekhar Bhansali and Chong H Ahn “A low-temperature bonding technique using spin-on fluorocarbon polymers to assemble Microsystems” J. Micromech. Microeng. 12 (2202) 187-191
- [27] F.Niklaus, H. Andersson, P.Enoksson, G. Stemme “Low temperature full wafer adhesive bonding of structured wafers” Sensors and Actuators A 92 (2001) 235-241
- [28] Liwei Lin “MEMS Post-Packaging by Localized Heating and Bonding” IEEE Transactions on Advanced Packaging, Vol.23, No.4, November 2000
- [29] Philippe Arquint, Peter D. van der Wl, Bart H. van der Schoot, Nico F. de Rooij ”Flexible Polysiloxane interconnection between two substrates for microsystem assembly” Transducers '95 Eurosensors IX Stockholm, Sweden, June 25-29, 1995
- [30] W K Schomburg, D Maas, W Bacher, B Büstgens, J Fahrenberg, W Menz and D Seidel „Assembly for micromechanics and LIGA“ J. Micromech. Microeng.5 (1995) 57-63
- [31] Yu-Chuan Su, and Liwei Lin “Localized Plastic bonding for micro assembly, packaging and liquid encapsulation” 0-7803-5998-4/01/ ©2001 IEEE
- [32] Vincent L.Spiering, J.W.Bernschot, Miko Elwenspoek, and Jan H. J. Fluitman “Sacrificial wafer Bonding for Planarization after very deep etching” Journal of Microelectromechanical systems, Vol. 4, No.3, September 1995
- [33] A. Brask, Jörg P Kutter, H Bruus, “Long-term stable electrosmotic pump with ion exchange membrane” Lab Chip 2005, 5, 730-738
- [34] G.Keramas, G. Perozziello, O. Geschke, C.B.V. Christensen “Development of a multiplex microarray microsystem”, Lab on a Chip, 2004, 4
- [35] Henrik Bruus ”Theoretical microfluidics” Lecture notes 2005 of the course of Microfluidic at DTU, Denmark
- [36] Allan W. Snyder, John D. Love ”Optical Waveguide Theory” © 1983 Chapman & Hall ISBN 0-412-09950-0
- [37] Bahaa E. A. Saleh, Malvin Carl Teich ”Fundamentals of Photonics © 1991 John Wiley & Sons 0-471-83965-5

- 
- [38] Kristian P Larsen “Micro-Electro-Mechanical Devices for Controlling light” Ph.D. Thesis MIC- Department of Micro and Nano Technology of DTU (Technical University of Denmark)
- [39] Christof Debaes, Valérie Baukens, Pedro Vybck, Patrik Tuteleers, Bart Volkaerts, Wim Meeus, Marnik Brunfaut, Jan Van Campenhout, Alex Hermanne and Hugo Thienpont ”Low-Cost Microoptical Modules for MCM Level Optical Interconnections” © 2003 IEEE Journal of Selected Topics in Quantum Electronics, Vol.9 No.2 March/April 2003
- [40] Ashish V Pattekar and Mayuresh V Kothare “Novel microfluidic interconnectors for high temperature and pressure applications”, J.Miromech.Microeng. 13 (2003) 337-345, printed in UK
- [41] Jr-Hung Tsai and Liwei Lin “Micro-to-Macro fluidic interconnectors with an integrated polymer sealent”, J.Micromech.Microeng. 11 (2001) 577-581, printed in UK
- [42] Sheng LI, Carl B Freidhoff, Robert M young “ Fabrication of micronozzles using low-temperature wafer-level bonding with SU-8”, J. Micromech.Microeng. 13 (2003) 732-738, Printed in the UK
- [43] Helene Andersson, Wouter van der Wijngaart, Peter Enoksson, Goran Stemme “Micromachined flow-through filter-chamber for chemical reactions beads”, Sensors and Actuators B 67 (200) 203-208
- [44] B.L. Gray, D.Jaeggi, N.J. Moulras, B.P. van Driehuisen, K.R. Williams, N.I. Maluf, G.T.A. Kovacs “Novel interconnection technologies for integrated microfluidic systems, Sensors and Actuators 77 (1999) 57-65
- [45] Carl K. Fredrikson and Z. Hugh Fan ”Macro-to-micro interfaces for microfluidic devices” Lab Chip, 2004, 4, 526-533
- [46] Aniruddha Puntambekar and Chong H Ahn “Self-aligning microfluidic interconnects for glass- and plastic- based microfluidic systems” J.Micromech.Microeng. 12 (2002) 35-40;
- [47] Eunice S Lee, Dwight Howard, Enzhu Liang, Scott Collins and Rosemary L Smith “Removable tubing interconnects for glass-based microfluidic systems made using ECDM”, J. Micromech. Microeng. 14 (2004) 535-541, printed in UK
- [48] Deniz Armani, Chang Liu and Narayan Aluru “ Re-configurable fluid circuits by PDMS elastomer Micromachining”, 0-7803-5194-0/99 ©1999 IEEE
- [49] Gerardo Perozziello and Oliver Geshcke, “A novel reversible packaging for microfluidic system”, CIRP seminar, Copenhagen, November 2003

- 
- [50] Robert B. Darling “Development of a high Density, Planar, Modular Microfluidic Interconnect system”, Transducers '01, Eurosensors XV, Munich, Germany, June 10-14, 2001
- [51] Tze-Jung Yao, Sangwook Lee, Weileun Fang, Yu-Chong Tai “Micromachined Rubber O-ring Micro-fluidic Couplers”, 0-7803-5273-4/00 ©2000 IEEE
- [52] P. Krulevitch, W. Benett, J. Hamilton, M. Maaghribi, and K. Rose “Polymer-Based Packaging Platform for Hybrid Microfluidic Systems”, Biomedical Microdevices 4, 301-308, 2002
- [53] Nicolas Boalth, Jesper Wandrup, Lasse Larsson, Peter A. Frischauf, Finn C. Lundsgaard, Willy L. Andersen, Niels-Henrik Jensen, Rolf Singer, Carl P. Trolborg, Gitte Lunding “Blood gases and oximetry: calibration-free new dry-chemistry and optical technology for near-patient testing” Clinica Chimica Acta 307 (2001) 225-233
- [54] Gerardo Perozziello, Martin F. Jensen, John E. Mc Cormack, Frederik Bundgaard, Oliver Geschke “Plug'n'pump fluidic interconnection” Proceedings of  $\mu$ Tas, Malmö, 26-30 September 2004 575-577
- [55] Keisuke Morishima, Yoshikazu Yoshida and Takehiko Kitamori “One touch fluidic tube connector for micro fluidic devices” Proceedings of *m*Tas, Malmö, 26-30 September 2004 171-173
- [56] Wen H. Ko “Packaging of microfabricated devices and systems” Materials Chemistry and Physics 42 (1995) 169-175
- [57] Daniela Staiculescu, Kyutae Lim, Albert Sutono, Hongwei Liang “Flip-chip vs. wirebonding” Printed Circuit Design, San Francisco, June 2002, Vol.19, 12-16
- [58] E. Veerpoorte, A. Manz, H. Ludi, A.E. Bruno, F. Maystre, B. Krattiger, H.M. Widmer, B.H. van der shoot and N.F. de Rooij “A silicon flow cell for optical detection in miniaturized total analysis systems” Sens. Actuators B, Chem., vol. 6 pp. 66-70, 1992
- [59] Z. Liang, N. Chiem, G. Ocvirk, T. Tang, K. Fluri, and D.J. Harrison “Microfabrication of a planar absorbance and fluorescence cell for integrated capillary electrophoresis devices” Anal. Chem., vol. 68, pp. 1040-1046, 1996
- [60] H. Salimi-Moosavi, Y. Jiang, L. Lester, G. McKinnon, and D.J. Harrison “A multireflection cell for enhanced absorbance detection in microchip-based capillary electrophoresis devices” Electrophoresis, vol.21, pp. 1291-1299, 2000
- [61] N. Burgraf, B. Krattiger, A. J. De Mello, N. F. De Rooij, and a. Manz, “Holographic refractive index detector for application in microchip-based capillary separation systems” Analyst, vol. 123, pp. 1443-1447, 1998

- 
- [62] G.Ocvirk, T.Tang, and D. J. Harrison, "Optimization of confocal epifluorescence microscopy for microchip-based miniaturized total analysis systems" , *Anayst*, vol.123, pp. 1429-1434, 1998
- [63] G. Jiang, S. Attiya, G. Ocvirk, W. E. Lee, and D.J Harrison " Red diode laser induced fluorescence detection with a confocal microscope on a microchip for capillary electrophoresis" *Biosens. Bioelectron.*, vol 14, pp. 244-248, 1990
- [64] E. Verpoorte "Chip vision – optics for microchips" *Lab on a chip*, 203, 3, 22-27
- [65] M. Kufner, S.Kufner "Microoptics for optical interconnects. *Int. Journal of Optoelectronics* 12 (1998), 119-126
- [66] S. Ura and S. J. Sheard, " A configuration for guided-wave excitation into a disposable integrated-optic head" *Opt. Commun.*, 1998, 146, 85-89.
- [67] D. Nilsson, S. Balslev, M. M. Gregersen, and A. Kristensen "Micro-fabricated solid state dye lasers based on a photo-definable polymer" *Applied Optics*, Vol. 44, pp. 4965-4971 (2005)
- [68] Michael L. Chabynec, Daniel T. Chiu, J. Cooper McDonald, Abraham, D. Stroock, James F. Christian, Arieh M. Karger and George M. Whitesides "An integrated Fluorescence Detection System in Poly(dimethylsiloxane) for Microfluidic Applications, *Anal. Chem.* 2001, 73, 4491-4498
- [69] Shize Qi, Xuezhu Liu, Sean Ford, Jmaes Barrows, Gloria Thomas, Kevin Kelly, Andrew McCandless, Kun Lian, Jost Goettert and Steven A. Soper "Microfluidic devices fabricated in poly(methyl methacrylate) using hot.embossing with integrated sampling capillary and fiber optics for fluorescence detection" *Lab Chip*, 2002, 2, 88-95
- [70] C G J Schabmueller, J R Pollard, A G R Evans, J S Wilkinson, G Ensell and A BrunnSchweiler "Integrated diode detector and optical fibres for in situ detection within micromachined polymerase chain reaction chips" *J. Micormech. Microeng.* 11 (2001) 329-333
- [71] P. Boyle, D.F. Moore, R.R.A. Syms "Micropackaging Using Thin Films as Mechanical Components" 0-7803-7430-4/02/ ©2002 IEEE
- [72] Zhenua LIang, Nghia Chiem, Gregor Ocvirk, Thompson Tang, Karl Fluri, and D. Jed Harrison "Microfabrication of a Planar Absorbance and Fluorescence Cell for Integrated Capillary Electrophoresis Devices" *Anal. Chem.* 1996, 68, 1040-1046
- [73] Koji Enbutsu, Makoto Hikita, Satoru Tomaru, Mitsuo Usui, Saburo Imamura and Tohru Maruno "Multimode Optical Waveguide Fabricated by UV Cured Epoxy Resin for Optical Interconnection" *Proceedings of APCC/OECC'99 - 5th Asia Pacific Conference*

- 
- on Communications/4th Optoelectronics and Communications Conference 1648 -1651 vol.2 (1999)
- [74] Z. Wang, J. El-Ali, M. Englund, T. Gotsæd, I. R. Perch-Nielsen, K. B. Mogensen, D. Snakenborg, J. P. Kutter and A. Wolff “ Measurements of scattered light on a microchip flow cytometer with integrated polymer based optical elements” , *Lab Chip*, 2004, 4, 372-377
- [75] Bryan G. Splawn, Fred E. Lytle “ On-chip absorption measurements using an integrated waveguide” *Anal. Bioanal. Chem.* (2002) 373: 519-525
- [76] Shin’Ichi Iwano, Etsuji Sugita, Kazunori Kanayama, Ryyo Nagase and Kenichi Nakano “Design and Performance of Single-Mode Plug-in Type Optical-Fiber Connectors” *Journal of Lightwave Technology*, Vol.8 No.11 November 1990
- [77] W. Hunziker “Ways to Cost Effective Packaging: Waveguide Tapers and Passive Self-Alignment” 0-7803-4947-4/98/ ©1998 IEEE
- [78] U. Wallrabe, H. Dittrich, G. Friedsam, Th. Hanemann, J. Mohr, K. Müller, V. Piotter, P. Ruther, Th. Schaller, W. Zibler “ Micromolded easy-assembly multi fiber connector: RibCon® „ *Microsystem Technologies* 8 (2002) 83-87 2002
- [79] Stefan Sinzinger, Jurgen Jahns ”Microoptics” 3-527-40355-8 - Wiley-VCH, Berlin (2003)
- [80] Bryan G. Splawn, Fred E. Lytle “ On-chip absorption measurements using an integrated waveguide” *Anal. Bioanal. Chem.* (2002) 373: 519-525
- [81] U. Wallrabe, H. Dittrich, G. Friedsam, Th. Hanemann, J. Mohr, K. Müller, V. Piotter, P. Ruther, Th. Schaller, W. Zibler “ Micromolded easy-assembly multi fiber connector: RibCon® „ *Microsystem Technologies* 8 (2002) 83-87 2002
- [82] Shin’Ichi Iwano, Etsuji Sugita, Kazunori Kanayama, Ryyo Nagase and Kenichi Nakano “Design and Performance of Single-Mode Plug-in Type Optical-Fiber Connectors” *Journal of Lightwave Technology*, Vol.8 No.11 November 1990
- [83] J. C. Roulet, E. Verpoorte, R. Volkel, H. P. Herzig, N.F. de Rooij, and R. Dandliker, “Microlens systems for fluorescence detection in chemical microsystems” *Opt. Eng.*, vol. 40, no.5, 2001
- [84] Jean-Christophe Roulet, Reinhard Völkl, Hans Peter Herzig, Elisabeth Verpoorte, Nico F. de Rooij „Fabrication of Multilayer Systems Combining Microfluidic and Microoptical Elements for Fluorescence detection“ *Journal of Microelectromechanical Systems*, Vol. 10, No. 4, December 2001

- 
- [85] Jeonggi Seo and Luke P. Lee “Fluorescence amplification by self-aligned integrated microfluidic optical systems” 0-7803-7731-1/03 ©2003 IEEE
- [86] Jackie Chen, Weisong Wang, Ji Fang and Kody Varahramyan “Variable-focusing microlens with microfluidic chip” *J. Micromech. Microeng.* 14 (2004) 675-680
- [87] M Agarwal, R A Gunasekaran, P Coane and K Varahraman “ Polymer-based variable focal length microlens system” *J. Micromech. Microeng.* 14 (2004) 1665-1673
- [88] Yong-qi Fu and Ngoi Kok Ann Bryan “Hybrid microdiffractive-microrefractive lens with a continuous relief fabricated by use of focused-ion-beam milling for single-mode fiber coupling” *Applied Optics / Vol.40 No.32 / 10 November 2001*
- [89] S. Camou, H. Fujita and T. Fujii “ PDMS 2D optical lens integrated with microfluidic channels: principle and characterization” *Lab Chip*, 2003, 3, 40-45
- [90] Marc P. Christensen, Predrag Milojkovic, Michael J. McFadden and Michael W. Haney “Mutliscala Optical Design for Global Chip-to-Chip Optical Interconnections and Misalignment Tolerant Packaging” *IEEE Journal on selected Topics in Quantum Electronics*, Vol.9, No.2, March/April 2003
- [91] Shogo Ura and Hiroshi Nishihara “Integreted-Optic Grating Devices for Optical Interconnects” 2003 IEEE Annual meeting Conferece procededing Vol.1 177-178
- [92] Chris Maims, John Hulme, Peter R. Fielden, Nicholas J. Goddard, “ Grating coupled leaky waveguide micro channel sensor chips for optical analysis” *Sensors and Actuators B* 7 (2001) 671-678
- [93] Tobias Kraus, Axel Günther, Nuria de Mas, Martin A. Schmidt, Klavs, F. Jensen “An integrated multiphase flow sensor for microchannels“ *Experiments in Fluids* 36 (2004) 819-832
- [94] Gerardo Perozziello, Detlef Snakenborg, Frederik Bundgaard, Jörg P. Kutter, and Oliver Geschke “Plug’n’pump fluidic interconnection for microfluidic systems”, in preparation
- [95] J.E. Shiley and C.R. Mischke “Mechanical Engineering design” 7<sup>th</sup> edition, McGrawHill, ISBN:0071006079
- [96] G.A.C.M. Spierings, J. Haisma and F.J.H.M. van der Kruis “Direct bonding of organic polymeric materials” *Philips Journal of Research* Vol. 49 No. 1/2 1995
- [97] J.Mizuno, T. Harada, T.Glinsner, M. Ishizuka, T. Edura, K. Tsutsui, H. Ishida, S. Shoji, Y. Wada “Fabrications of Micro/Channel Device by hot emboss and Direct bonding of PMMA” *Proceedings of ICMENS’04* 2004

- [98] Gerardo Perozziello, Zhyu Zhang, Detlef Snakenborg, Jörg P. Kutter, Klavs F. Jensen and Oliver Geschke “Optical connector plugs for multiplexed and simultaneous detection purposes in microfluidic systems”, in preparation
- [99] Peter Fris “Integrated Optical Detection for Biochemical Microsystems” Ph.D. Thesis, November 201, Mikroelektronik Centret
- [100] Andrea Rainelli, Richard Stratz, Karin Schweizer, Peter C. Hauser „Miniature flow-injection analysis manifold created by micromilling”, *Talanta* 61 (2003) 659-665
- [101] D. Snakenborg, G. Perozziello, H. Klank, O. Geschke, And J. P. Kutter “Direct milling and casting of polymer-based optical waveguides for improved transparency in the visible range” *Journals of Micromechanics and MicroEngineering* 2006 16 375-381
- [102] H.L.T. Lee, R.J. Ram ”Integrated fluid Injectors and mixers for pH control in miniature bioreactor arrays” *Proceedings of  $\mu$ TAS 2005 Conference* (2005) 34-36
- [103] Gerardo Perozziello, Zhyu Zhang, Detlef Snakenborg, Jörg P. Kutter, Klavs F. Jensen and Oliver Geschke “Optical connector plugs for multiplexed and simultaneous detection purposes in microfluidic systems” *proceedings of  $\mu$ TAS 2005 Conference* (2005) 1155-1157
- [104] Mohammed Zourob, Stephan Mohr, Peter R. Fielden, Nicholas J. Goddard “Small volume refractive index and fluorescence sensor for micro toal analysis systems ( $\mu$ TAS) applications” *Sensors and Actuators B* 94 (2003) 304-312